# Temporal gating of attosecond pulse trains

Lund Reports on Atomic Physics, LRAP-403

Erik P. Månsson

February 24, 2009

Master's Thesis
Lund University
Faculty of Engineering, LTH


LUND UNIVERSITY

# Sammanfattning

*Hög övertonsgenerering* är en process där en grupp väldigt korta ljuspulser skapas av att man lyser med en intensiv laser genom en gas. Även lasern som driver processen är pulsad och för att skilja pulserna åt kommer ordet ”blixt” att används här för de korta utbrott av ljus som skapas i gasen medan ”puls” oftast syftar på den drivande laserpulsen.

Elektroner som slits loss från och återvänder till gasatomer skapar ljusblixtar kring varje riktningsbyte hos laserns elektriska fält, alltså två gånger per optisk cykel. Eftersom laserpulsen vanligen varar flera optiska cykler skapas många ljusblixtar. Detta kallas ibland ett *attosekundspulståg*, för vid rätt förhållanden kan varje ljusblixt vara kortare än 100 as $= 100 \times 10^{-18}$ s. Diagram 1(a) illustrerar det drivande laserpulsens fält och de två blixtarna per cykel. Det tillhörande spektrumet som kan observeras i experiment har diskreta övertoner på udda multiplar av laserpulsens frekvens.

Det främsta användningsområdet för så här korta ljuspulser är att undersöka och styra processer i atomer och molekyler. Ljusblixtarna är kortare än vissa kemiska reaktioner och bara ett par gånger längre än den klassiska omloppstiden för elektronen i en väteatom.

Trots att mycket intressant forskning har gjorts med dessa tåg av pulser på attosekundskalan under ett drygt decennium har det också funnits en strävan mot att använda *ensamma attosekundspulser*. För att starta, stanna eller undersöka en snabb atomär process framstår det som betydligt mer praktiskt med en ensam ljusblixt än med ett helt tåg som kommer att störa atomen före och efter den starkaste blixten.

Metoder som hindrar de flesta blixtarna från att skapas och bara släpper fram en eller två blixtar kommer att kallas *tidsgrindar;* bara under det tidsintervall då grinden är ”öppen” kommer ljusblixtar att skapas. Det finns flera sätt att uppnå detta, till exempel kan ett par dubbelbrytande plattor av kvarts få polarisationstillståndet att variera mellan cirkulärt och linjärt inom den drivande pulsen. Bara när polarisationen är linjär återvänder elektronerna till atomerna som de avlägsnats från, vid cirkulär polarisation skapas därför inga ljusblixtar.

Det är även känt att användandet av blått ljus kan förhindra uppkomsten av varannan ljusblixt, vilket visas i Diagram 1(b). En utgångspunkt för arbetet var att med hjälp av blått ljus ytterligare förkorta den tidsgrind som kvartsplattorna skapar. Målet var att minska antalet ljusblixtar och helst få en ensam blixt, vars spektrum är kontinuerligt som i Diagram 1(c) och inte längre uppvisar några diskreta övertoner.

Ett datorprogram skapades för att simulera elektronernas beteende, enligt en halvklassisk modell med vissa tillägg. Utifrån simuleringsprogrammets resultat bedömdes det inte vara praktiskt genomförbart att komma nära en ensam ljusblixt med de drivande pulser på 35 fs $= 35 \times 10^{-15}$ s som det använda lasersystemet ger. Experimentellt stämde det med att det knappt gick att urskilja någon signifikant förbättring på grund av plattorna med dessa pulser, blått ljus gav dock den förväntade halveringen av antal blixtar. Diagram 2(a) visar hur ett spektrum utan blått ljus och utan försök till tidsgrind såg ut.

Att efterkomprimera pulserna till 10 fs verkade lämpligt i simuleringsprogrammet för att tillsammans med blått ljus få en helt ensam blixt, och en så gott som ensam blixt även utan blått. Med pulser någonstans mellan 7.8 och 14 fs, utan blått ljus, erhölls experimentella spektrum som i Diagram 2(b), där det knappt går att urskilja några övertoner.

Intensiteten i dessa lyckade spektrum var dock låg och trots medelvärdesbildning över mer än $10^5$ laserpulser var bruset betydande. Kombinerat med att lasersystemet ännu inte kunde ge pulser med stabil enveloppfas[1] och att egenskaper i spektrumet kan påverkas av denna fas, innebär det att det inte med säkerhet går att avgöra hur få blixtar som skapades. Utifrån ett resonemang om när dessa störningar kan inträffa bedöms att mellan en och tre blixtar skapades för de flesta laserpulser vid den bästa inställningen.

Inga experimentella resultat erhölls för blått ljus i kombination med efterkomprimerade pulser, men enligt simuleringarna är det värt att försöka igen eftersom en någorlunda ensam ljusblixt bör kunna skapas även utan kvartsplattorna då, vilket skulle ge högre intensitet.

[1] Svängningarnas (bärvågens) läge i förhållande till tidpunkten där pulsen har maximal amplitud.

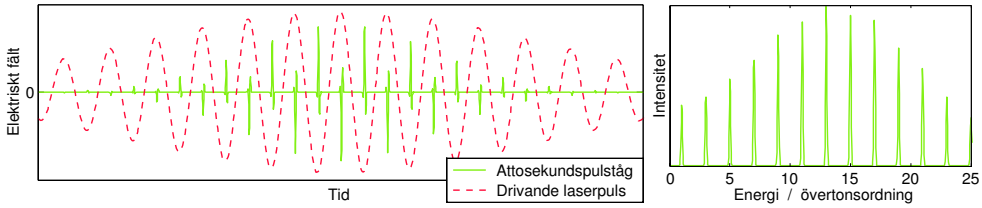


(a) Skiss av ett typiskt attosekundspulståg. Dess spektrum har smala toppar vid udda övertonsordningar.

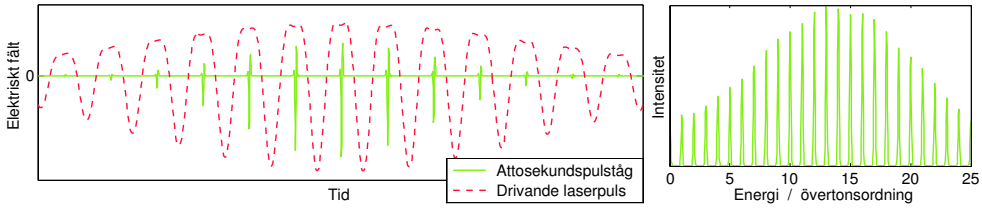


(b) Med blått ljus tillfört försvinner varannan blixt och spektrumet får dubbelt så många toppar, var och en något bredare än förut.

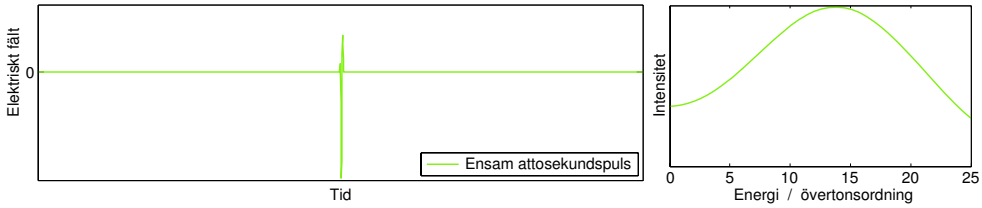


(c) Ju färre blixtar desto bredare blir topparna i spektrumet. En ensam blixt, som i detta fall, ger ett kontinuerligt spektrum.

Diagram 1: Principskisser för hur antalet blixtar påverkar spektrumet.

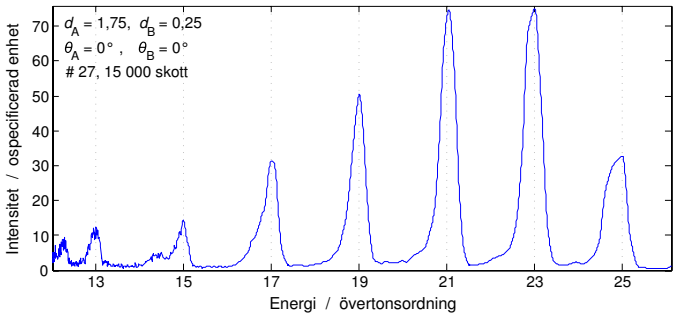


(a) Spektrum utan någon tidsgrind, med 35 fs drivpuls. Eftersom övertonerna är tydligt avgränsade motsvarar detta ett stort antal blixtar.

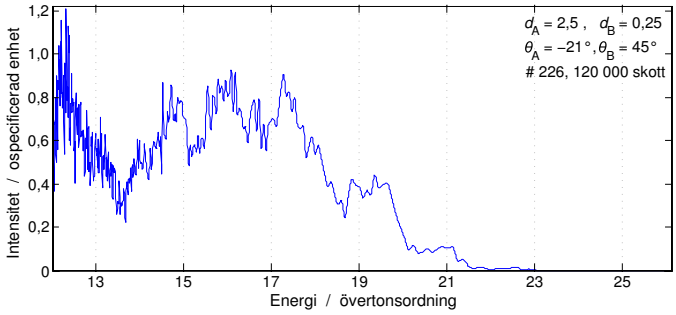


(b) Det resultat som troligen motsvarar minst antal blixtar. Med kvartsplattor riktade enligt $\theta_A = -21°$, $\theta_B = 45°$ och efterkomprimering av drivpulsen till mellan 7.8 fs och 14 fs.

Diagram 2: Experimentella spektrum.

# Contents

Lund, February 24, 2009.
Supervisor: Johan Mauritsson

# Introduction

High harmonic generation is a process where a group of very short pulses of light are generated when shining a very intense laser through a gas. As the laser that drives the process is also pulsed, a diversified terminology is introduced; the word "burst" refers to a short pulse generated in the gas while "pulse" is mainly used for the driving laser.

One burst of light is generated at every turn of the electric field of the laser, which means two bursts per optical cycle. As the laser pulse usually has a duration of many optical cycles, many bursts will be emitted. This is sometimes called an *attosecond pulse train*, because under the right circumstances each short burst can have a duration of less than 100 as $= 100 \times 10^{-18}$ s. Figure 3(a) illustrates the oscillations of the driving laser field and the short bursts created twice per cycle.

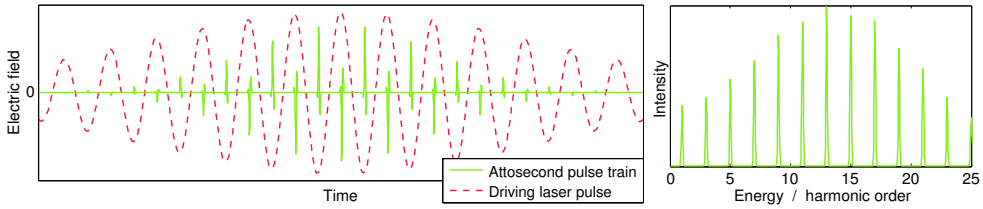


(a) A schematic, typical pulse train. The spectrum has narrow peaks at odd harmonic orders.

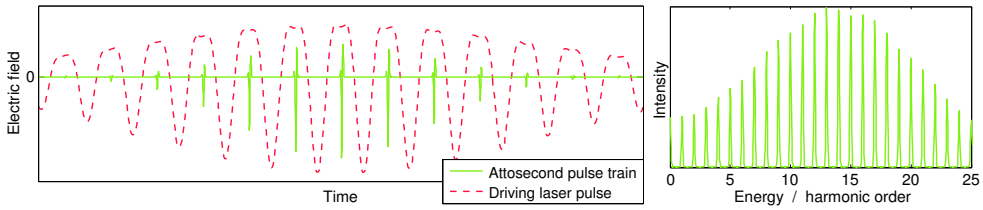


(b) With blue light added every second burst disappears while the spectrum gets twice as many peaks, each somewhat wider.

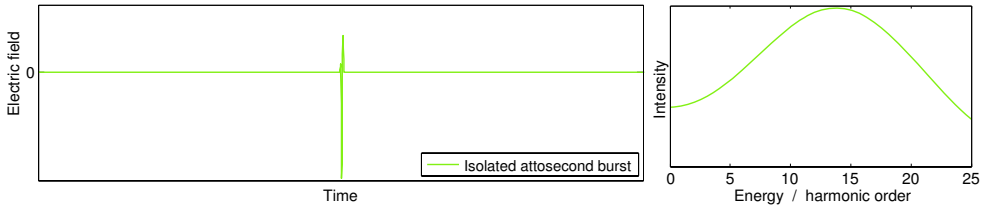


(c) The fewer bursts, the wider peaks in the spectrum. A single burst gives a continuous spectrum.

Figure 3: Illustration of a regular attosecond pulse train and the influence of adding blue, compared to a single burst.

Typical uses of attosecond pulses are to learn more about processes in molecules or atoms, as these pulses are shorter than some chemical reactions and only a few times longer than the classical "orbit time" of an electron in a hydrogen atom.

While interesting research has been done with trains of pulses during the last decade or two, there has also been a desire to use a *isolated attosecond burst*. To start, stop or probe a fast atomic process it seems a lot more practical with a single burst than an entire train which will disturb the atom before and after the most intense burst.

A scheme that prevents most of the attosecond bursts from being generated, and only lets through one or a few bursts will be called a *temporal gate*. Only during an interval when the gate is "open" will bursts be generated. There are several ways of achieving this, as described on page 12. In this project a method with varying polarization state of the laser pulse will be combined with addition of blue light to the input. The use of some blue light is known to remove every second attosecond burst, illustrated in Figure 3(b), so it should help make the temporal gate produced by the varying polarization even shorter. The spectrum that we are hoping to get is that of a single burst, which is shown in Figure 3(c).

# Chapter 1

# Background

The concepts of *polarization state* and *nonlinear optics* are essential in this thesis. Nonlinear optics gives the understanding and nomenclature of the process of high order harmonics, which is to be confined to a shorter time interval. Customization of the polarization state is the main tool that was utilized for that aim.

## 1.1 Polarization

Light is the name of electromagnetic waves (or photons) in the wavelength range visible to our eyes. Electromagnetic waves are variations of the electric and magnetic vector fields, in time and space. For simple kinds of waves, the electric and magnetic fields are closely related, so that it is sufficient to describe how one of the fields varies to know the other. The research presented here covers effects that depend on how electrons are accelerated by light, which for non-relativistic electron velocities is mainly[1] dependent on the electric part of the electromagnetic field. Thus it is natural to base the description of polarization on the *electric* vector rather than on the magnetic.

At a fixed position $\vec{r}$, the time evolution of the electric field vector $\vec{E}(t) = \vec{E}(\vec{r}, t)$ defines the *polarization state* of the field. For complicated fields the polarization state may vary over time, but in the case of a monochromatic wave it is constant and the tip of the electric field vector traces a generalized ellipse over time. The evolution of $\vec{E}(t)$ is classified into one of three cases [1, ch. 6.1] [2, ch. 3.6]:

**Linear polarization:** $\vec{E}(t)$ is proportional to a fix vector. Geometrically it means $\vec{E}(t)$ only varies back and forth along a line in space; the ellipse reduces to a line.

**Right-handed elliptic polarization:** $\vec{E}(t)$, at the fixed position, moves clockwise as time passes, when viewed by an observer that the wave is is approaching.[2]

**Left-handed elliptic polarization:** $\vec{E}(t)$ moves counterclockwise.

A more fine grained description is given by the *ellipticity* $\varepsilon$, which is a number in the range $-1 \leq \varepsilon \leq 1$. $|\varepsilon|$ is the ratio between the minor and major axes of the ellipse, having the extreme values $\varepsilon = 0$ for linear polarization (LP) and $|\varepsilon| = 1$ when the polarization ellipse is a circle. The sign gives the left- or right-handedness, particularly *left circular polarization* (LCP) has $\varepsilon = -1$ and *right circular polarization* (RCP) has $\varepsilon = 1$.

[1] See section 2.3.2 on page 24 for the full motivation.

[2] It should be noted that this is the definition of right and left ellipticity often used in optics texts, while electrical engineering texts often use the opposite classification [2, ch. 3.6].

With the complex electric field vector in the $xy$-plane [3] Saleh & Teich [1, ch. 6.1] define

$$\varepsilon = \tan\theta_\varepsilon, \quad E_\mathrm{x} = \vec{e}_\mathrm{x} \cdot \vec{E}, \quad E_\mathrm{y} = \vec{e}_\mathrm{y} \cdot \vec{E}$$
$$\sin 2\theta_\varepsilon = \frac{2|E_\mathrm{x}||E_\mathrm{y}|\sin(\varphi)}{|E_\mathrm{x}|^2 + |E_\mathrm{y}|^2}$$
$$|E_\mathrm{x}||E_\mathrm{y}|\sin(\varphi) = |E_\mathrm{x}||E_\mathrm{y}|\sin(\arg E_\mathrm{y} - \arg E_\mathrm{x}) = \mathfrak{Im}\left(E_\mathrm{x}^* E_\mathrm{y}\right)$$

which gives the instantaneous ellipticity

$$\varepsilon(\vec{r},t) = \tan\left(\frac{1}{2}\sin^{-1}\left(2\,\mathfrak{Im}\frac{E_\mathrm{x}^*(\vec{r},t)E_\mathrm{y}(\vec{r},t)}{\left\|\vec{E}(\vec{r},t)\right\|^2}\right)\right) \tag{1.1}$$

## 1.2 Nonlinear optics

The propagation of light is, like all electromagnetic waves, described by Maxwell's equations. A full understanding of them is not necessary here, it suffices to discuss the electric field and note what happens when the waves propagate inside a homogeneous, isotropic and spatially nondispersive material. The electrons (and nuclei) of the atoms are affected by the field and start to vibrate; vibrating charged particles in turn emit electromagnetic waves.

Usually one separates the electric field into two terms, the original field $\vec{E}$ and the additional field $\vec{P}$ created by the material[4]. $\vec{P}$ is related to $\vec{E}$ (and possibly the magnetic field) in ways dependent on the material, described by some material model.

Simple material models are based on *linear*, time invariant systems of equations. A property of these is that if the incoming wave is sinusoidal at a certain frequency, the output is also sinusoidal and at the same frequency. The only changes that the material may cause are constant delays and attenuations of the signal. We further assume a dispersion-free medium, which means the delay between $\vec{E}$ and $\vec{P}$ is zero. With the constant $u$ describing the interaction strength, a simple linear expression for one scalar component is

$$P(\vec{r},t) = u\,E(\vec{r},t). \tag{1.2}$$

Some ways of expressing $u$ are $u = \epsilon_0\chi = (\epsilon_\mathrm{r} - 1)\epsilon_0 = (n^2 - 1)\epsilon_0$, where $\epsilon_0$ is the electric permittivity of free space, $\epsilon_r$ is the relative permittivity[5] and $n$ the refractive index of the medium.

Real materials are usually more complicated, perhaps with a nonlinear relation between input and output. Usually the linear equation still is a useful approximation at low input field strengths, but gradually gives the wrong results at higher strengths. While still neglecting dispersion, a nonlinear relation can be expressed as a Taylor polynomial of sufficiently high order $N$. In such a nonlinear model, (1.2) is changed into

$$P(\vec{r},t) = u_1E(\vec{r},t) + u_2E^2(\vec{r},t) + u_2E^3(\vec{r},t) + \cdots + u_NE^N(\vec{r},t) \tag{1.3}$$

### 1.2.1 Second order harmonic generation

In the nonlinear regime, a sinusoidal input can give non-sinusoidal output. Using Fourier series, the result can be expressed as a sum of harmonic signals at multiple frequencies. Typically the strength of terms drops quickly with increasing $N$, so that the first few terms dominate in equation (1.3). Then the dominating frequencies are low multiples of the input (*e.g.* 0, 1, 2 and 3 times the input frequency).

[3] In the models it will be assumed that the electric field vector lies in the $xy$-plane while the wave propagates along the $z$-axis. This orthogonality is true for a monochromatic wave in an isotropic material [2]. We thus define the physical electric field $\vec{\mathcal{E}} = \mathfrak{Re}\,\vec{E}$ as the real part of the complex electric field variable $\vec{E}(\vec{r},t) = E_\mathrm{x}(\vec{r},t)\vec{e}_\mathrm{x} + E_\mathrm{y}(\vec{r},t)\vec{e}_\mathrm{y}$.

[4] The field $\vec{P}$, created by the material, is confusingly called *polarization density*, which is hardly related to the *polarization state* defined in section 1.1.

[5] Unfortunately both ellipticity and permittivity are usually denoted by the same Greek letter. In this report only $\epsilon_0$ and $\epsilon_r$ refer to permittivity while all other uses of $\varepsilon$ refer to ellipticity.

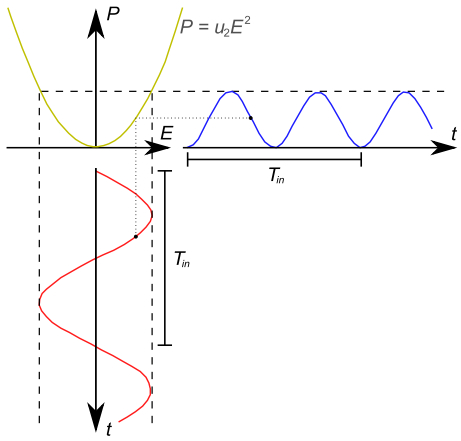


Figure 1.1: Illustration of how the $E^2$-term gives a term in $P$ at the double frequency and a constant offset. The green parabola shows the relation stated in equation (1.4) with $u_1 = 0$. The red, vertical diagram shows the input $E(t)$ and the blue diagram on the right hand side shows $P(t)$. The period time of $E(t)$ is marked as $T_{\text{in}}$ and $P(t)$ clearly has the double frequency. Based on [1, figure 21.2-1].

Second order harmonic generation (SHG) deals with the output term that has twice the input frequency. Taking only the first and second order in (1.3), $N = 2$, and using $E = E_0 \cos(\omega t)$ as input we have

$$\begin{aligned} P &= u_1 E + u_2 E^2 = u_1 E_0 \cos(\omega t) + u_2 E_0^2 \cos^2(\omega t) \\ P &= u_1 E_0 \cos(\omega t) + u_2 E_0^2 \left(\tfrac{1}{2} + \tfrac{1}{2}\cos(2\omega t)\right) \\ P &= \tfrac{1}{2} u_2 E_0^2 + u_1 E_0 \cos(\omega t) + \tfrac{1}{2} u_2 E_0^2 \cos(2\omega t). \end{aligned} \tag{1.4}$$

We note that the resulting polarization density contains the original frequency, the double frequency (called *second order harmonic*) and a constant offset – signals at two non-original frequencies have been created by the material. A nice illustration of this effect is given in Figure 1.1.

The second order harmonic generation efficiency $\eta_{\text{SHG}}$, turns out proportional to the square of the original field strength amplitude, causing second order effects to be negligible at low field strengths.

$$\eta_{\text{SHG}} = \frac{I_{2\omega}}{I_\omega} \propto \frac{P_{2\omega}^2}{(\epsilon_0 E_0)^2} \propto \frac{(u_2 E_0^2)^2}{E_0^2} \propto E_0^2. \tag{1.5}$$

## 1.3 High-order harmonic generation

### 1.3.1 Introduction

Just as a second order term in the material model gave a signal at twice the input frequency, higher order terms may give signals at higher multiples of the input frequency. For an input at angular frequency $\omega_1$, a signal at $\omega_H = H\omega_1$ is called the harmonic of order $H$.

Using equation (1.3) with higher $N$ and similar steps that gave equation (1.4) suggests that the strength of harmonics decrease with increasing $H$ for a given $E$, but also that increasing $E$ favors harmonics at high orders more than at the low orders. The details of the sequence of $u_H$-coefficients will determine a spectral profile of harmonic intensities for a given input intensity (irradiance) $I = nc_0\epsilon_0|E_0|^2/2$.

A different perspective is to start from the quantization of light into photons, and express the harmonic generation as absorption of $H$ photons of energy $\hbar\omega_1$ followed by emission of a single photon of energy $\hbar\omega_H$. The probability of such a process can be approximated using quantum mechanical perturbation theory.

Studies of spectra from the interaction between high laser intensities and atomic gases in the late 1980s did not mach the predictions made using perturbative models. The models

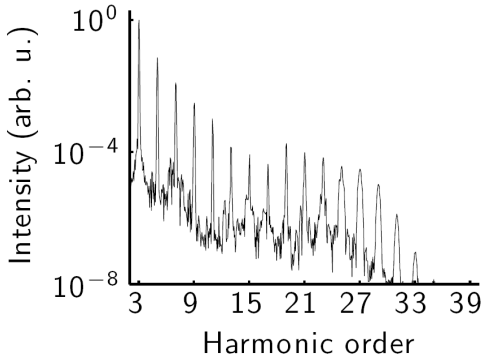


Figure 1.2: Calculated spectrum from high-order harmonic generation in argon, showing a plateau in intensity between orders 13 and 27. [3, figure 1.2]

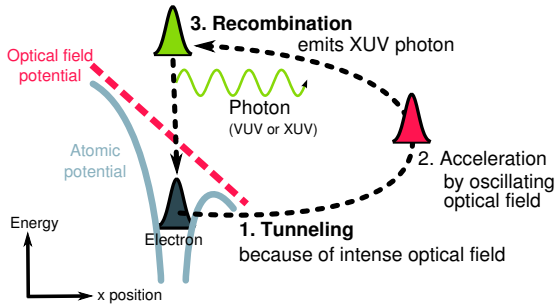


Figure 1.3: An illustration of the three-step model for High order harmonic generation.

used at that time predicted the intensity would drop exponentially with harmonic order, while experiments revealed a plateau of almost constant intensity over several harmonic orders. In the 1990s the phenomenon known as *High-order Harmonic Generation* was explained, both semi-classically (the *three-step model*) and quantum mechanically [3, ch 1.1] [4]. A calculated diagram that matches experimental results is presented in Figure 1.2 for illustration. With helium as medium, a plateau of harmonics up to 700 eV ($H \approx 440$) was observed in 2004 [5].

### 1.3.2 The three-step model

Chapter 2.3 contains a more detailed explanation of the model that is used in the presented simulations of the interaction between the intense laser pulse and the gas, but it is essential with a basic understanding already here. The semi-classical three-step model is the main part of the model used, and it has been shown to give very similar results [6] to a more rigorous, quantum mechanical treatment.

The medium can be an atomic gas (*e.g.* noble gas) and the electric field of the light source is called the *optical field* to separate it from the field of the atom or ion. The optical field is assumed to be comparable in amplitude to the atomic field (thus in the highly nonlinear regime) and as an approximation the atomic field is neglected. The three steps, illustrated in Figure 1.3, are: [6, 7, 8]

1. With some probability, the optical field (tunnel-)ionizes the atom, releasing an electron wave packet.

2. The electron is treated as a classical particle, starting at rest near the nucleus and accelerated by the oscillating laser field. A linear polarization state means that the electron moves back and forth along a line as in the left half of Figure 1.4.

3. Depending on the time of ionization and the nature of the optical field, the electron may or may not pass through the ion at later times, Figure 1.4 illustrates two cases. Some probability of recombination per near-passage of the ion is assumed, and upon

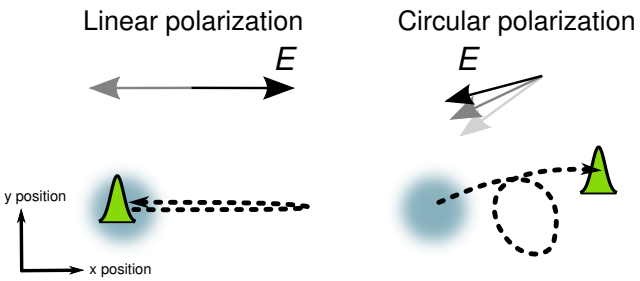


Figure 1.4: Circular polarization typically means that the electron does not return, as opposed to linear polarization where the electron is likely to return to the atom.

recombination into the ion a photon is emitted. Usually it suffices to consider the first passage, as the later are less probable. The energy of the photon is the ionization energy plus the kinetic energy that the electron obtained from the optical field.

Intuitively, the recombination probability would depend on how close the electron got to the nucleus during the passage. The tolerance for near-passages is affected by the quantum mechanical broadening of the electronic wave packet (approximated to occur only transversally to its velocity). A quantum mechanical calculation of the probability also relies on that the returning electron wave packet interacts *coherently*[6] with the fraction of the electron wave function that never was ionized in step 1.

The cut-off at the high-order side of the plateau in Figure 1.2 is explained by the fact that the electron can only gain a limited amount of energy from the oscillating field. The higher intensity at the lowest orders, to the left of the plateau, and the very weak intensities above the cut-off, follow the previously expected exponential weakening with harmonic order and the three-step model only adds the plateau part of the spectrum.[7] A more detailed treatment of the three-step model is given in chapter 2.3.

### 1.3.3 Modulated spectrum – a train of pulses

Because of the many different (a continuum of) electron trajectories happening with comparable probability and virtually simultaneously during the *burst*, photons are emitted with a continuum of wavelengths, typically in the *extreme ultraviolet* (XUV) regime. If there was only one such burst it would give a smooth curve, covering several harmonic orders in the spectrum as sketched in Figure 3(c).

After some filtering[9], the very short pulse allowed by such a spectrum can be realized, below 100 as in duration. But observed spectra are usually modulated, with more or less narrow peaks at odd harmonic orders, corresponding to there being a train of bursts, with alternating sign, instead of just one burst.

Actually, the fact that only odd numbered harmonics appear under common circumstances has been explained in several ways:

**Atomic potential symmetry:** a medium with inversion symmetry for each atom has coefficients $u_H = 0$ for even integers $H$. Via the dipole matrix element this in turn makes the intensity at even harmonic orders be zero. [10]

**Selection rule for conservation of angular momentum:** Assume $H$ photons transferring energy to the electron and one XUV-photon being emitted, each with a spin angular momentum of $m = -1$ or $m = +1$ in units of $\hbar$ when projected on a fixed axis. As the spin projection, $m_H\hbar$, of all absorbed photons is equal to that of the single emitted photon, $m_H$ is an odd number. Finally, $m_H$ is the sum of $H$ odd numbers (each photon has $|m| = 1$) which means also $H$ must be odd. An underlying assumption is that no angular momentum is transferred to other particles, such as the ion.

**Temporal:** The second half the optical cycle is identical to the first half, with the only exception that the field has been reversed. All steps of the three-step model work equivalently in the second half of the cycle, causing the period time of the recombination

events to be half the optical cycle. A transform from temporal to spectral domain tells that a halved temporal period means a doubling of the frequency period (spacing).

If the phase of many harmonics are locked together, the result is a pulse train, just as in a mode-locked laser. The repetition rate, $T/2 = \lambda/(2c)$, is typically a few femtoseconds while the pulses of the high order harmonic pulse train can be less than 100 as long, thus called *attosecond pulse train*. In this perspective the original emission may contain a continuous frequency band, because it it the $T/2$-periodic repetition that gives the discrete structure of harmonics.

The first two perspectives do not appear to explain the continuum spectrum that can be reached with an isolated attosecond pulse, at least the selection rule perspective does not, so the temporal perspective is used in this report.

Sometimes an asymmetry is introduced so that the harmonic generation only occurs once per carrier cycle of the input laser, which results in the spectra containing both odd and even harmonics. This can be achieved by adding light at the double frequency (half the period time), sometimes referred to as *blue* while the fundamental frequency is in the infra*red* (800 nm). The carrier phase of the blue light should be such that the two colors interfere constructively in one of the (fundamental) half-cycles and destructive in the other half-cycle and thus only give strong harmonic generation once per cycle.

To get the single, short pulse that the broad spectral range allows for, it is necessary to get rid of the repetition of the generation process and confine it to a time interval of about half an optical cycle. This will be explained further in section 1.5.

## 1.4 Highly intense light sources

As previously noted, highly nonlinear effects such as HHG can only be observed in very strong electric fields. The field strength is proportional to the square root of the intensity, which is power per unit area. For a given power, the highest intensity is reached at the focus, where the effective beam area is minimal.

It is easier to make a high powered laser if it only emits the high power during short pulses, and no light most of the time, so that the average power you need to pump into it can remain low. A mode-locked laser gives this kind of short pulses through the coherent interference of oscillator modes at slightly different wavelengths. The pulse duration is inversely proportional to the width of the frequency band that can be amplified and mode locked in the laser.

A high powered laser system will be used for the experimental studies. The first stage is a titanium-sapphire[6] based mode-locked laser with oscillator modes centered around 800 nm (called the *carrier wavelength*) and a pulse duration of about 12 fs.

The laser pulse itself is not powerful enough; it is amplified in a *chirped pulse amplifier*. After passing a grating used as positive chirp-filter, the pulse energy has been spread over a much longer duration (some $10^4$ times) so that the power is manageable by the amplifier. It is then amplified by repeatedly passing crystals pumped into population inversion, and a negative chirp filter compresses it back to a short duration, nominally $t_{\mathrm{FWHM}} = 35$ fs, while keeping the high energy. This is the pulse used in the experiments are compressed further as described in section 3.3.1.

## 1.5 Temporal gating techniques

### 1.5.1 What does “gating” mean?

The flux of emitted photons from the HHG process is high only for nearly linear polarization states, as introduced in Figure 1.4 and shown experimentally in Figure 2.5 on page 26.

Designing the electric field so that it is near-linearly polarized only during a short interval, or multiple separate intervals if desired, is called *gating* because it makes photons be emitted mainly during these intervals when the gate is “open”. Most of the effort, both in previous works and in this project, has been on making a gate with a single open interval, and to

[6] Ti:$Al_2O_3$

make that interval as short as possible. The ideal result would then be a *single burst*, *i.e.* only one strong burst of photons emitted during a half-cycle of the fundamental field.

Some properties of a gate are

**Contrast:** High contrast means that the gate quickly changes between open and closed, so the photon flux is low except in the main burst. High contrast is thus desirable.

**Energy distribution:** Within the gate, even if it gives a single burst, you have a continuum of trajectories. Each trajectory in the simulation program has a specific return time, return energy and probability. The details of the field will affect these distributions. Physically this is expected to affect the chirp and duration of the ultra short pulse (sub-femtosecond) that with suitable treatment could be formed by the main burst.

**Efficiency:** As the energy of the driving pulse is limited by the laser system, it is often desirable that a high amount of energy goes "through the gate" to get a sufficient photon yield, rather than use energy for the "gate part" which does not contribute to the useful output.

### 1.5.2 Previous work

In scientific literature, several methods to temporally confine the high harmonic generation have been proposed and used. Typically one or more of the following tools are used

**Short input pulse:** If the driving pulse is short, then naturally the generation is confined to an even shorter interval. 5 fs input pulses have been used to generate single bursts.[11]

**Static field:** When a static electric field, or light of comparably low frequency, is added to a somewhat short driving pulse, a constant acceleration is added to the electrons. This will limit their ability to return to the ion after they were ionized by the driving pulse, and was recently suggested as a way of temporal confinement and to raise the cutoff energy [12].

**Polarization state:** As sketched in Figure 1.4, and experimentally in Figure 2.5 on page 26, the high harmonic generation almost exclusively occurs when the driving field is linearly polarized. Thus any method to make the ellipticity change rapidly and be zero for a short while should be useful to confine the generation. Some methods that have been proposed and used are:

- **Polarization retarding plates:** A rather common method involves two polarization retarder plates to create a pulse which is circularly polarized at the start and the end, but linear in the middle [13]. It will be explained in detail in the next chapter, see Figure 2.4 on page 23. It is this kind of gate that has been used in this project, which some variations.
- **Combination of linearly polarized fields:** Instead of two retarder plates, Tzallas *et. al.* [14] used only one to create two circularly polarized pulses, then a separate linear polarized field was added to act as driving field in the open part of the gate. The output is similar to the above version, but as interferometers were used to create each of the pulses some additional flexibility is achieved, as if the retarder plate thickness could be varied continuously.
- **Chirped pulses and ionization:** Another scheme recently proposed uses the interference between two chirped pulses to produce a time-varying ellipticity that will work as a gate [15]. As the gate will recur a few times during the envelope the ionization during the main pulse is intended to reduce the number of remaining electrons so that the second opening in the gate should not cause much high harmonic generation.

**Two colors:** When light at the double frequency is added together with a fundamental pulse, every second burst can be eliminated [16]. While not in itself a temporal confinement, the initial idea for this project was to combine it with a polarization gate and hopefully be able to get few bursts without requiring a few-cycle driving pulse. This combination has been called *Double Optical Gate* [17].

### 1.5.3 Spectral characteristics of an isolated pulse

As the number of bursts giving the pulse train decreases, the harmonic peaks in the spectrum will grow wider. One way to reach this conclusion is that when the pulses are so few that they hardly could be seen as a train, we lose the interference effects that produced the discrete harmonics. Another way is to remember a property of the Fourier transform; if a structure in the temporal domain is made shorter its representation in the spectral domain will become wider, loosely speaking.

At about three bursts you should note clearly that the peaks in the spectrum are wider and the valleys are not as deep; compare Figure 3.4(a) on page 33 with Figure 3(a) on page 6. Two bursts should give a distinctively different spectrum, where the modulation of the continuum profile is more sinusoidal. Finally, a single burst gives a continuum rather than any peak structure, as in Figure 3(c).

If the method of reducing the number of bursts works better for high or low energies, harmonic peaks could appear in the other energy regime where there would be significant emission during more than one half-cycle.

With a reduced number of bursts the spectrum is not expected to become wider than allowed by the range of return energies in the three-step model, however the cutoff harmonic order (and thus the total spectrum width) depends on the peak field strength[4] which is likely to be lower in a gated setup than with a fully linearly polarized field. One reason for this is the fact that we use parts of the laser pulse to cancel other parts so that the end result should be linearly polarized over a shorter time. One can also expect some losses due to more optics (two or three quartz plates) which give reflections and dispersion.

## 1.6 Aim and limits

The aim of the project at hand was to theoretically and experimentally investigate possibilities of temporal confinement of the high harmonic generation process. Ideally, only a single or two bursts should be generated, using the present laser system which gives 35 fs pulses. The kind of gating was restricted to some kind of polarization gating together with the two-color technique, and harmonics were to be generated in argon.

If possible, it was also desirable to have the nature of the gate easily adjustable, *e.g.* being able to select whether one, two or three pulses should be produced, and maybe their separation. It was assumed that such control could be useful in applications where fast processes then could be started by the first burst and investigated through its interaction with the second burst.

An initial limitation was that I should not work on making the input laser pulse shorter, only how to manipulate the polarization state and let it vary in time in a useful way. There were however other people in the group working on making shorter laser pulse and eventually, based on the simulations in this project, it was decide to use shorter pulses too.

# Chapter 2

# Modeling

## 2.1 Simulation program overview

To theoretically investigate different gating techniques and eventually select suitable parameters to use in the experiments, computer simulations were performed with a set of Matlab programs. The main program consists of several functions which fit together in a single simulation chain:

**Plate simulation:** The electric field that will reach the generation gas chamber is determined at this stage. Initially the field was specified as a sum of one or several rather arbitrary pulses[1], but when the choice of gating technique was settled on two retarder plates a specialized function was created to use plate parameters and initial laser pulse properties as input.

**Electron simulation:** Here, the high-order harmonic generation is simulated semiclassically using electron trajectories which are determined by the electric field and the three-step model described below. The main results are recombination times $t_\mathrm{r}$, recombination energies $U_\mathrm{r}$ and relative probability (photon flux $\Phi_\mathrm{r}$) of the trajectories, which will be defined later.

**Analysis:** Various diagrams can be drawn, to illustrate at what time, energy and relative probability that photons are emitted by the recombining electrons. Some minor attempts of reconstructing the electric field of the resulting attosecond bursts were made, but the semiclassical three-step model is not well suited to describe the emitted photons, specifically their polarization and phase. A pseudo-spectrum was attempted but not used, instead diagrams of ellipticity, flux and the spectrogram were mostly used to visualize the effects of a certain gating pulse.

### 2.1.1 Pulse shape

The pulses are Gaussian in time, with full width half max durations $t_{\mathrm{FWHM},p} = \tau_p\sqrt{2_e \log 2}$ and central frequency $\omega_p$, where $p$ is the integer label of the pulse. No spatial properties of the pulses are considered, thus all atoms are assumed to be at the center of the focal plane and propagation effects in the gas are neglected.

The electric field of a Gaussian pulse $p$ at time $t$ is defined as the *real* part of the complex wavefunction

$$\vec{E}_p(t) = \vec{J}_p \underbrace{\mathrm{e}^{i\omega_p(t-o_p+\Delta_{\mathrm{CEP},p})}}_{C_p(t)} \mathrm{e}^{-(1-ia_p)(t-o_p)^2/\tau_p^2} \tag{2.1}$$

where $a_p$ is the *chirp parameter*, $o_p$ is a time offset (delay) and the *Jones vector* or *complex amplitude* $\vec{J}_p$ gives the polarization state[2] and amplitude of the pulse. The purpose of $o_p$

[1] Each input pulse term has a Gaussian temporal envelope and is monochromatic except for the short duration and possible chirp. Frequency, chirp, polarization state, delay and Carrier-Envelope phase can be set individually for each pulse term.

[2] See page 7 for polarization states.

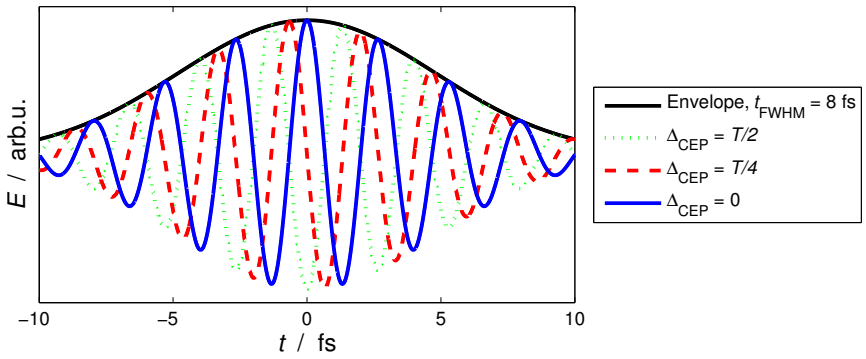


Figure 2.1: Electric field of Gaussian pulses with different carrier-envelope offsets.

is to be able to offset the pulses in time to design the field, experimentally it could mean a change in an the interferometer arm length. For a chirped pulse it is necessary to distinguish between the transform limit duration $t_{\mathrm{TL},p}$ which is related to the spectral width, and the actual pulse duration $t_{\mathrm{FWHM},p} = t_{\mathrm{TL},p}\sqrt{1+a_p^2}$.

The factor $C_p(t)$ is called the *carrier* or phase factor, and the rest is the complex envelope which also contributes to the total complex phase. $\Delta_{\mathrm{CEP},p}$ expresses the *carrier-envelope offset phase* in units of time, defined as illustrated in Figure 2.1. The maximum pulse envelope occurs at time $t = o_p$, while the phase factor has a maximum at $t = o_p - \Delta_{\mathrm{CEP},p}$ if the pulse has not passed through any plate. The dispersive quartz plates (and practically any material) will give further carrier-envelope offsets, as treated in equation (2.9).

There is also a different version of (2.1) implemented, where the chirp is not of the regular, linear kind, but intended intended to emulate the chirp of a pulse compressed by *Self Phase Modulation*, SPM. Specifically, the phase term $\varphi_{\mathrm{linear}} = +ia_p(t-o_p)^2/\tau_p^2$ in (2.1) is replaced by $\varphi_{\mathrm{SPM}} = -i\frac{1}{2}a_p \mathrm{e}^{-2(t-o_p)^2/\tau_p^2}$. The factor $\frac{1}{2}a_p$ was selected[3] to keep the same chirp rate at the pulse center as in the case of linear chirp.

As no detailed expression for the a SPM pulse from our capillary waveguide setup was used, I consider this chirp formula to be a rough approximation. Additionally, the appropriate $a_p$ is not known and the capillary used for SPM makes the output fluctuated a lot so no single pulse formula is expected to be able to reproduce the experimental spectra which are averaged over many different pulses. The correlations between simulations and experiments were later examined and in general the variables expected to be correlated were not notably better with SPM than with linear chirp. The SPM kind of chirp is left as an option in the program which is disabled by default, and it is not used in the rest of this report.

When using the plate-simulation program, the total input intensity (as it would be in the focus) is specified, along with the ratio between intensity that should be used for the frequency doubled pulse term and the fundamental pulse. How the plate simulator works is described in section 2.2.5. However, a Gaussian pulse expression similar to equation (2.1) is still used for the field before the plates.

## 2.2 Polarization retarders

### 2.2.1 Introduction

Polarization retarders are devices where different polarization states of light propagate with different speed, as described by different refractive indices in a birefringent material. The most common kind of retarder uses the linear birefringence of an uniaxial material, where the modes that have different speed are linearly polarized. It is possible, using optical activity or the Faraday effect, to have circularly polarized modes. A quick investigation suggested

[3] Equation (22.5-11) on page 988 of [1] gives $n_2 L k_0 = a/(2I(0))$, which is inserted into eq. (22.5-8) $\varphi_{\mathrm{SPM}} = -n_2 L k_0 I(t) = a\frac{1}{2}\exp(-2t^2/\tau^2)$.

that those effects would be too weak or more complicated experimentally, so I have focused on uniaxial materials.

The optical retarder plates (also called waveplates) used here are made of an uniaxial material, quartz, with the optical axis in the $xy$-plane while the propagation direction is $\vec{e}_z$. Light linearly polarized along the optical axis propagates slower (can be faster in other materials), than light polarized along other directions. The highest propagation speed occurs for light polarized orthogonally to the optical axis. These two orthogonal axes in the $xy$-plane are labeled "slow" and "fast", with the refractive indices $n_S$ and $n_F$ respectively.

For a quantitative understanding of the retarder, the effect on an input electric field $\vec{E}_{in}(t)$ propagating along the $z$-axis is examined here. First the vectorial consequences are treated in a monochromatic fashion, then additional dispersion effects which become important for short pulses are considered. The center wavelength of the fundamental pulse, $p = 1$, has been set to the nominal vacuum wavelength value $\lambda_1 = 800$ nm.

### 2.2.2 Retardation of phase

If the fast and slow axes form a coordinate system $(F, S)$ rotated an angle $\theta$ from the $(x, y)$-system, the basis coordinate vectors expressed in the $(x, y)$-system are

$$\left[\hat{\mathbf{e}}_F, \hat{\mathbf{e}}_S\right] = \mathbf{R}\left[\hat{\mathbf{e}}_x, \hat{\mathbf{e}}_y\right] = \mathbf{R}\begin{bmatrix}1 & 0\\ 0 & 1\end{bmatrix} = \begin{bmatrix}\cos\theta & -\sin\theta\\ \sin\theta & \cos\theta\end{bmatrix}. \tag{2.2}$$

In the $(F, S)$ system, the passage time through a plate of thickness $L$ is

$$\begin{aligned} \tau_F &= n_F(\lambda_p)L/c_0 && \text{for the F-component}\\ \tau_S &= n_S(\lambda_p)L/c_0 = \tau_F + \delta > \tau_F && \text{for the S-component}\\ \text{where } \delta &= \tau_S - \tau_F = \big(n_S(\lambda_p) - n_F(\lambda_p)\big)\frac{L}{c_0} = Td \end{aligned} \tag{2.3}$$

is the phase retardation time, which expresses the retardation as the time separation between the fast and slow component after the plate. Two other representations are the length $l = \delta c_0 = \lambda_p d$ and the the dimensionless number $d$. In this report $d$, which expresses the retardation in units of the vacuum wavelength $\lambda_p$ or its period time, will be preferred as the period time is a suitable unit when designing a few-cycle polarization gate.

A plate where $d = m + 1/4$ (or $d = m + 3/4$) for some integer $m$ is called a quarter-wave plate of order $m$, and can be used to change linearly polarized light into circularly polarized light and vice versa. Correspondingly, the case $d = m + 1/2$ is called a half-wave plate. Actually, these linear $\leftrightarrow$ circular polarization state transforms are only exact for monochromatic light. Expressions with better validity for short pulses will be derived in the following sections.

First, the incident field is expressed using the $(F, S)$-basis,

$$\vec{E}_{in}(t) = \vec{e}_F\left(\vec{e}_F \cdot \vec{E}_{in}(t)\right) + \vec{e}_S\left(\vec{e}_S \cdot \vec{E}_{in}(t)\right)$$

then each component is delayed by its passage time. The resulting physical vector $\vec{E}_{out}$ is expressed in the $(x, y)$-basis as the coordinate vector $\boldsymbol{E}_{out}(t)$:

$$\begin{aligned} \vec{E}_{out}(t) &= \vec{e}_F\left(\vec{e}_F \cdot \vec{E}_{in}(t-\tau_F)\right) + \vec{e}_S\left(\vec{e}_S \cdot \vec{E}_{in}(t-\tau_S)\right)\\ \boldsymbol{E}_{out}(t) &= \begin{bmatrix}\cos\theta\\ \sin\theta\end{bmatrix}\left[\cos\theta, \sin\theta\right]\boldsymbol{E}_{in}(t-\tau_F) + \begin{bmatrix}-\sin\theta\\ \cos\theta\end{bmatrix}\left[-\sin\theta, \cos\theta\right]\boldsymbol{E}_{in}(t-\tau_S)\\ \boldsymbol{E}_{out}(t) &= \mathbf{M}_F(\theta)\,\boldsymbol{E}_{in}(t-\tau_F) + \mathbf{M}_S(\theta)\,\boldsymbol{E}_{in}(t-\tau_S) \end{aligned} \tag{2.4}$$

where time delays from (2.3) are used, and the following "mode projection" matrices are introduced

$$\mathbf{M}_F(\theta) = \begin{bmatrix}\cos^2\theta, & \cos\theta\sin\theta\\ \cos\theta\sin\theta, & \sin^2\theta\end{bmatrix} \qquad \mathbf{M}_S(\theta) = \begin{bmatrix}\sin^2\theta, & -\cos\theta\sin\theta\\ -\cos\theta\sin\theta, & \cos^2\theta\end{bmatrix} \tag{2.5}$$

### 2.2.3 Propagation through a dispersive plate

The issue for pulsed (broadband) light in dispersive media, such as quartz, are that $\tau_\mathrm{F}$ and $\tau_\mathrm{S}$ depend on the wavelength via the refractive index in (2.3). Thus all wavelengths will not be retarded equally by a quartz plate. By sandwiching different materials it is possible to create more achromatic retarders, but only to some limit and at a higher price. Such retarders have not been used or analyzed in detail.

The refractive index also affects the reflectivity $R(\lambda)$, experienced when entering and leaving the plate, typically in conjunction with an anti-reflection coating. The manufacturer of the used plates specified that $R(800\mathrm{nm}) < 0.1\%$ and $R(\lambda) < 1\%$, $750\mathrm{nm} \leq \lambda \leq 850\mathrm{nm}$. Although a 10 fs pulse has significant power outside the given wavelength range[4] it was assumed that the reflectivity would not increase rapidly outside that range and neither reflectivity nor coating was included in the simulations.

The program handles the fundamental pulse and a possible pulse with double frequency as independent Gaussian pulse terms, and adds them after passing all plates to get the electric field that is considered to reach the generation gas. Refractive index functions $n(\lambda_p)$ for several materials are supported by the program, given by Sellmeier coefficients from references [1, p. 180], [18] and [19]. Numeric differentiation gives the group refractive index $N(\lambda_p) = n(\lambda_p) - \lambda_p \frac{\mathrm{d}n}{\mathrm{d}\lambda_p}$ and the chirp coefficient defined below.

The two lowest orders of dispersion are the wavelength-dependent variation in passage time and the *group velocity dispersion* (GVD) which together can be expressed as a group delay $\tau_\mathrm{e}$ of the pulse envelope and a chirp filter with chirp coefficient $b_p$ [1, ch. 22.3]. To get the correct absolute phase (carrier-envelope offset), a phase delay $\tau_\mathrm{c}$ is applied to the carrier. Both delays are given directly by the propagation speed for carrier and envelope respectively

$$\tau_\mathrm{c} = n(\lambda_p)\, L/c_0 \qquad \text{and} \qquad \tau_\mathrm{e} = N(\lambda_p)\, L/c_0 \tag{2.6}$$

In order to apply separate envelope- and carrier delays and the chirp, the Gaussian pulse definition in equation (2.1) is expanded into

$$\begin{aligned}
\vec{E}_p(t, \tau_\mathrm{c}, \tau_\mathrm{e}, b_p) &= \vec{J}_p \underbrace{\mathrm{e}^{i\omega_p(t-o_p-\tau_\mathrm{c}+\Delta_{\mathrm{CEP},p})}}_{C_p(t,\tau_\mathrm{c})} \mathrm{e}^{-\left(1-ia_p(b_p)\right)(t-o_p-\tau_\mathrm{e})^2/\tau_p^2(b_p)}, \qquad (2.7)\\
a_p(b_p) &= a_p + (1+a_p)^2 b_p/\tau_p^2\\
\tau_p(b_p) &= \tau_p \sqrt{1 + 2a_p b_p/\tau_p^2 + (1+a_p^2) b_p^2/\tau_p^4}
\end{aligned}$$

The plate effectively increases the carrier-envelope offset by $\tau_\mathrm{e} - \tau_\mathrm{c}$, so the value specified by $\Delta_{\mathrm{CEP},p}$ does not apply after the plate. Similarly, the chirp parameter $a_p$ and duration parameter $\tau_p$ that the pulse was defined with are changed by the chirp coefficient $b_p$, which depends on the GVD coefficient $D_\nu$ and plate thickness $L$:

$$b_p = \frac{LD_\nu}{\pi} = \frac{L\lambda_p^3}{c_0^2}\frac{\mathrm{d}^2 n}{\mathrm{d}\lambda_p^2} \qquad \text{from [1, ch. 22.3]} \tag{2.8}$$

#### Pulse duration as function of plate thickness

The consequences of equation (2.7) will be illustrated here for the plate thicknesses used experimentally. The chirp coefficient given by (2.8) for the fast component is 2% above that of the slow component, but in the following discussion their average will be used.

When using all three plates, their total dispersion is approximated by a single plate of retardation $d_\mathrm{tot} = 1.75 + 2.5 + 0.25 = 4.5$ which gives the chirp coefficient $b = 34\ \mathrm{fs}^2$. The dispersion-induced lengthening for some pulses, assumed to be typical for the long and short experimental setups, is shown in Figure 2.2 as a function of total plate thickness.

If the pulse was transform limited or positively chirped initially it will be longer and positively chirped after the plate, because $b > 0$ for quartz. A negatively chirped input pulse will become shorter instead, towards its transform limit, which is not shown in the figure.

[4] For an unchirped Gaussian pulse of duration $t_{\mathrm{FWHM},p} = 10$ fs, the wavelength width is approximately $\lambda_{\mathrm{FWHM},p} \approx 0.441\lambda_p^2/(c_0 t_{\mathrm{FWHM},p}) \approx 94$ nm. Thus its spectral intensities at 753 nm and 847 nm are roughly half the peak value.

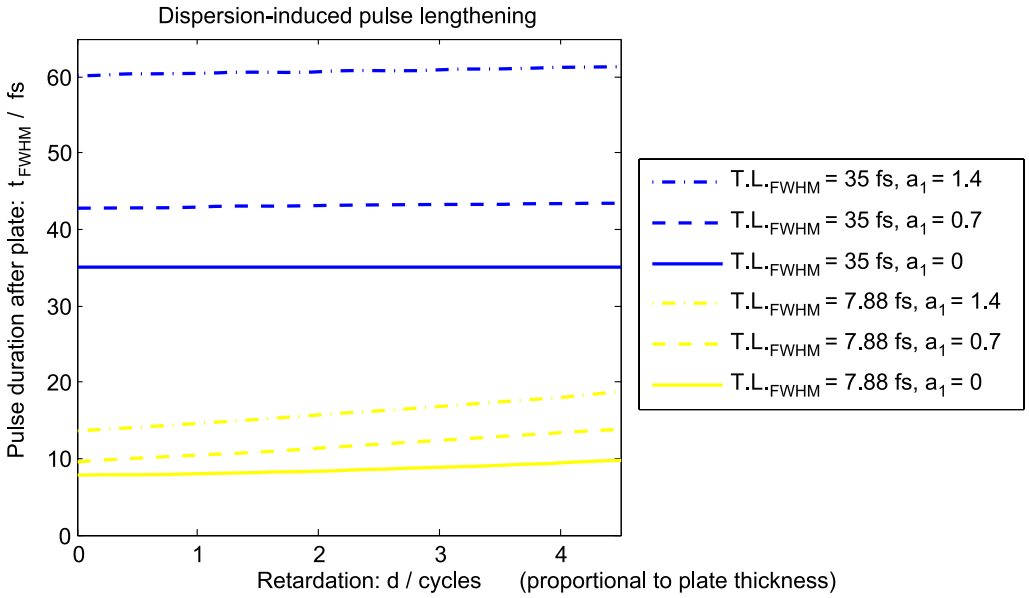


Figure 2.2: The pulse duration is increased when passing through quartz plates, as given by equations (2.7) and (2.8). Pulses of transform limit 35 fs (directly from the laser system) and 7.88 fs (estimated for SPM at 803 mbar from Figure 4.2) are displayed, for three different chirp parameters.

### 2.2.4 Retardation by a dispersive plate

As previously mentioned, a birefringent plate has different refractive indices for the fast and slow modes. The suffix $_{\mathrm{F}}$ or $_{\mathrm{S}}$ will be used to tell which refractive index to use for $b$, $\tau_{\mathrm{e}}$ and $\tau_{\mathrm{e}}$ in equations (2.6) and (2.8), *e.g.* the envelope delay for the fast mode is $\tau_{\mathrm{e,F}} = N_{\mathrm{F}}(\lambda_p)\, L/c_0$. To keep the variable names short, the $p$-index is not always included, anywhere a wavelength is used implicitly it should of course be $\lambda_p$ with the $p$-index of the appropriate pulse.

If the input pulse is Gaussian, $\vec{E}_{\mathrm{in}}(t) = \vec{E}_p(t, 0, 0, 0)$, equation (2.7) for passage through a dispersive medium can be incorporated into equation (2.4) to get

$$\boldsymbol{E}_{\mathrm{out},p}(t) = \mathbf{M}_{\mathrm{F}}(\theta)\, \boldsymbol{E}_p(t,\, \tau_{\mathrm{c,F}},\, \tau_{\mathrm{e,F}},\, b_{\mathrm{F}}) + \mathbf{M}_{\mathrm{F}}(\theta)\, \boldsymbol{E}_p(t,\, \tau_{\mathrm{c,S}},\, \tau_{\mathrm{e,S}},\, b_{\mathrm{S}}) \tag{2.9}$$

The boldface $\boldsymbol{E}_p$ just means that the $(x, y)$-coordinate representation is used for all vectors, *i.e.* $\boldsymbol{J}_p$ rather than $\vec{J}_p$ which was used in (2.7).

### 2.2.5 Gating applications

In section 1.5.1, several ways of obtaining a polarization gate were presented. Here, the electric field output from the setup that uses retarder plates will be derived. It involves two plates, called A and B, with thickness $L_{\mathrm{A}}$ and $L_{\mathrm{B}}$.

From now on, it will be assumed that there are one or two linearly polarized, approximately Gaussian, input pulses reaching the plates; the *fundamental* (infrared) pulse with index $p = 1$ and possibly a *frequency doubled* (blue) pulse which is given index $p = 2$. When there is no doubled pulse its Jones vector is simply set to zero, $\vec{J}_2 = \vec{0}$. The fundamental pulse is considered to have the vacuum wavelength $\lambda_1 = 800$ nm, which gives the period time that will be used as time unit through much of the report, and some basic pulse properties:

$$T = 800\,\mathrm{nm}/c_0 \approx 2.67\,\mathrm{fs} \qquad \omega_1 = 2\pi/T \qquad \lambda_2 = \lambda_1/2 \qquad \omega_2 = 2\omega_1$$

The plate thicknesses are selected to give the phase retardations $d_{\mathrm{A}}$ and $d_{\mathrm{B}}$ at $\lambda_1$. Obviously the retardation will be different at at other wavelengths. Equation (2.3) gives

$$\begin{aligned} L_{\mathrm{A}} &= \lambda_1\, d_{\mathrm{A}} / \big(n_{\mathrm{S}}(\lambda_1) - n_{\mathrm{F}}(\lambda_1)\big) \\ L_{\mathrm{B}} &= \lambda_1\, d_{\mathrm{B}} / \big(n_{\mathrm{S}}(\lambda_1) - n_{\mathrm{F}}(\lambda_1)\big) \end{aligned} \tag{2.10}$$

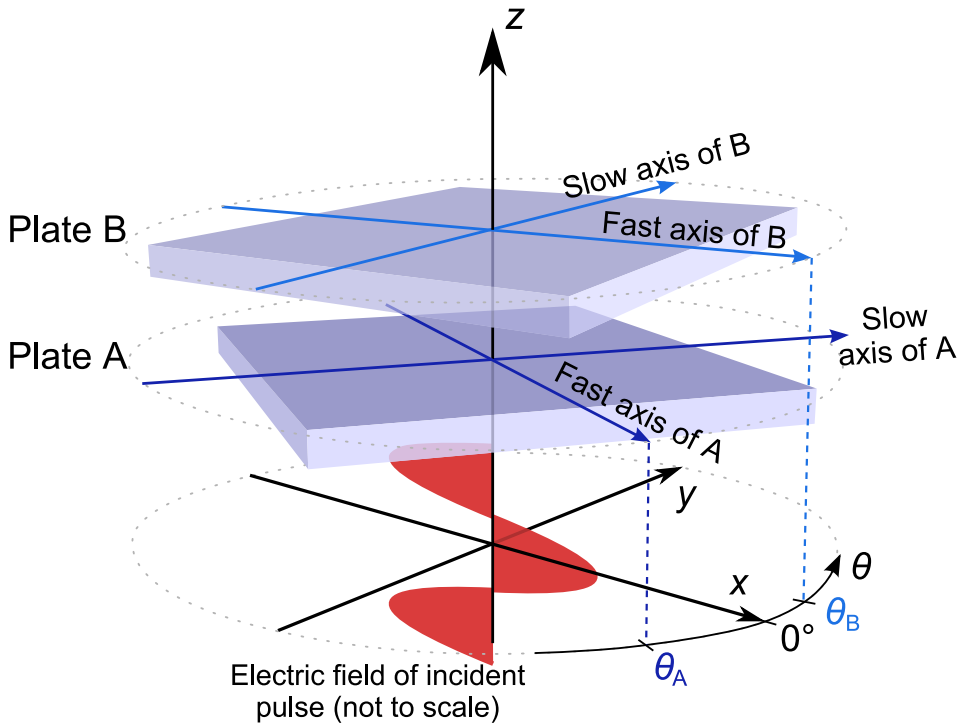


Figure 2.3: Two polarization retarder plates, with their fast axes rotated $\theta_\mathrm{A}$ and $\theta_\mathrm{B}$ from the $x$-axis.

Further, the $x$-axis is defined to be the polarization axis of the fundamental pulse, so $\boldsymbol{J}_1 = \boldsymbol{e}_\mathrm{x} J_1 = \left[\begin{smallmatrix}1\\0\end{smallmatrix}\right] J_1$, and both pulses propagate in the positive $z$-direction. The fast axes of plates A and B are rotated in the positive direction from the $x$-axis by the angles $\theta_\mathrm{A}$ and $\theta_\mathrm{B}$ respectively, as illustrated in Figure 2.3. The "standard setup", used by [20] and many others, has[5] $\theta_\mathrm{A} = -45°$, $\theta_\mathrm{B} = 0°$ and both plates as quarter-wave plates, but I have used other angles and retardations too.

Equation (2.9)[6] gives the optical field after plate A, expressed in $(x, y)$-coordinates for the pulse with the arbitrary index $p$,

$$\begin{aligned}\boldsymbol{E}_{\mathrm{A},p}(t) = {} & \mathbf{M}_{\mathrm{A,F}}(\theta_\mathrm{A})\, \boldsymbol{E}_p(t,\, \tau_{\mathrm{c,A,F}},\, \tau_{\mathrm{e,A,F}},\, b_{\mathrm{A,F}}) \\ & + \mathbf{M}_{\mathrm{A,S}}(\theta_\mathrm{A})\, \boldsymbol{E}_p(t,\, \tau_{\mathrm{c,A,S}},\, \tau_{\mathrm{e,A,S}},\, b_{\mathrm{A,S}})\end{aligned} \tag{2.11}$$

The second plate should be a zero order quarter-wave retarder, $\delta_\mathrm{B} = T/4$, but the expressions below will be derived for arbitrary $\delta_\mathrm{B}$. A zero-order plate is better than one of higher order (thickness) because all kinds of dispersion increase with the plate thickness. In the standard setup mentioned previously the A-plate is thought of as causing an two orthogonally, linearly polarized pulses with some time offset, and then the B-plate turns them into circularly polarized pulses (which give no HHG) except in the middle where they should interfere to form a linearly polarized field. Figure 2.4 illustrates the field produced. Dispersion may reduce envelope overlap (beyond the desired time offset) and when the two terms cannot cancel each other perfectly, the gating effect is reduced.

For the second plate, $\boldsymbol{E}_{\mathrm{A},p}(t)$ is the input field and each of its two terms is still a Gaussian pulse. As seen for plate A, a single input term gives two output terms, so after plate B there will be four terms expressing the field caused by one pulse before A.[7] As the light is not tightly focused when passing through the plates, non-linear effects in the material are neglected. In a linear material electric fields follow the superposition principle and, it is justified to treat them as independent terms in B.

[5] With $\theta_\mathrm{B} = 0°$ and no blue pulse, the sign of with $\theta_\mathrm{A}$ does not matter in simulations since it just causes an inversion of $y$-coordinates. In experiments there may be some asymmetry that makes the sign matter.

[6] Naturally with the thickness $L_\mathrm{A}$ substituted for $L$ in earlier definitions.

[7] When the frequency doubled pulse is present, there are eight terms in total after the plates.

As the following equation will be obtained by taking several simultaneous steps, a motivation is given first by reasoning about the vectorial and scalar factors in $\boldsymbol{E}$:

- Concerning the polarization direction, just as in (2.9) the Jones vector of the input pulse term is multiplied from the left by the appropriate matrix $\mathbf{M}_{\mathrm{B,F}}$ or $\mathbf{M}_{\mathrm{B,S}}$.
- The scalar part, the chirped Gaussian wavefunction, will be handled by adding the delays and chirp coefficients of plate B to the values already obtained when the pulse term passed plate A. It can be seen as if each term experiences a single plate with an optical path length $L\,n = L_{\mathrm{A}}\,n_{\text{“S or F in A”}} + L_{\mathrm{B}}\,n_{\text{“S or F in B”}}$. Since we do not model anything happening in the air or at plate surfaces, only this optical path matters, which motivates that chirp coefficients and delays are additive.[8]

All in all, the general expression for retardation through two plates is:

$$\begin{aligned}\boldsymbol{E}_{\mathrm{B},p}(t) = {} & \mathbf{M}_{\mathrm{B,F}}(\theta_{\mathrm{B}})\mathbf{M}_{\mathrm{A,F}}(\theta_{\mathrm{A}})\,\boldsymbol{E}_p(t,\ \tau_{\mathrm{c,A,F}}+\tau_{\mathrm{c,B,F}},\ \tau_{\mathrm{e,A,F}}+\tau_{\mathrm{e,B,F}},\ b_{\mathrm{A,F}}+b_{\mathrm{B,F}}) \\ & + \mathbf{M}_{\mathrm{B,F}}(\theta_{\mathrm{B}})\mathbf{M}_{\mathrm{A,S}}(\theta_{\mathrm{A}})\,\boldsymbol{E}_p(t,\ \tau_{\mathrm{c,A,S}}+\tau_{\mathrm{c,B,F}},\ \tau_{\mathrm{e,A,S}}+\tau_{\mathrm{e,B,F}},\ b_{\mathrm{A,S}}+b_{\mathrm{B,F}}) \\ & + \mathbf{M}_{\mathrm{B,S}}(\theta_{\mathrm{B}})\mathbf{M}_{\mathrm{A,F}}(\theta_{\mathrm{A}})\,\boldsymbol{E}_p(t,\ \tau_{\mathrm{c,A,F}}+\tau_{\mathrm{c,B,S}},\ \tau_{\mathrm{e,A,F}}+\tau_{\mathrm{e,B,S}},\ b_{\mathrm{A,F}}+b_{\mathrm{B,S}}) \\ & + \mathbf{M}_{\mathrm{B,S}}(\theta_{\mathrm{B}})\mathbf{M}_{\mathrm{A,S}}(\theta_{\mathrm{A}})\,\boldsymbol{E}_p(t,\ \tau_{\mathrm{c,A,S}}+\tau_{\mathrm{c,B,S}},\ \tau_{\mathrm{e,A,S}}+\tau_{\mathrm{e,B,S}},\ b_{\mathrm{A,S}}+b_{\mathrm{B,S}})\end{aligned} \tag{2.12}$$

The field reaching the generation gas chamber is considered to be

$$\boldsymbol{E}_{\mathrm{gen}}(t) = \sum_p \boldsymbol{E}_{\mathrm{B},p}(t_{\mathrm{ref},p} + t), \tag{2.13}$$

where the time coordinate of each pulse has been shifted by the reference time

$$t_{\mathrm{ref},p} = \tau_{\mathrm{e,A,F}}(\lambda_p) \;+\; \tau_{\mathrm{e,B,F}}(\lambda_p) = N_{\mathrm{F}}(\lambda_p)\,\big(L_{\mathrm{A}} + L_{\mathrm{B}}\big)/c_0\,. \tag{2.14}$$

This reference time is the envelope delay for the pulse, which means that if you use offsets $o_p = 0$ for all pulses, their envelopes will overlap in time *after* the plates rather than before. This definition of the pulse offsets is a lot more useful, as it is in the gas that the overlap matters. It also means that the time axes of diagrams can remain centered at $t \approx 0$ regardless of which plate thickness is used.

Experimentally, the time offset before the plates is not that meaningful to measure. If an interferometer is used so that the offset can be adjusted by changing the length of one interferometer arm, then it is no more difficult to monitor the time overlap after the plates than before them. In a setup where the time offset is known *before* the plates, one should let $o_2 - o_1 = \Delta t_{\text{before plates}} + \Delta t_{\text{by plates}}$ to get correct simulations, with eq. (2.10) giving

$$\begin{aligned}\Delta t_{\text{by plates}} &= t_{\mathrm{ref},2} - t_{\mathrm{ref},1} = \big(N_{\mathrm{F}}(\lambda_2) - N_{\mathrm{F}}(\lambda_1)\big)\frac{L_{\mathrm{A}} + L_{\mathrm{B}}}{c_0} \\ &= \big(d_{\mathrm{A}} + d_{\mathrm{B}}\big)\,T\,\frac{\big(N_{\mathrm{F}}(\lambda_2) - N_{\mathrm{F}}(\lambda_1)\big)}{\big(n_{\mathrm{S}}(\lambda_1) - n_{\mathrm{F}}(\lambda_1)\big)} \approx 16.04\text{ fs} \times \big(d_{\mathrm{A}} + d_{\mathrm{B}}\big)\,.\end{aligned} \tag{2.15}$$

The numerical value shows that the offset induced even by the thinnest choice of plates is about 12 period times, which is more than an order of magnitude above the time that the gate is supposed to be “open” to get a single burst of light out. Therefore it is important that the pulses have an offset of the same order of magnitude, with opposite sign, before the plates to overlap after the plates. However, in all experiments made in this project $\Delta t_{\text{before plates}}$ was either unknown or tunable via interferometer arms, so offsets were only expressed after the plates.

When using an interferometer, there is also an experimental option to put the plates in an interferometer arm so that only one of the pulses goes through them, preferably the blue is the one that skips the plates as it does not need to be circularly polarized at any time. This option is supported by the program. Just as otherwise, the offset $o_2$ applies when the pulses are added together in the gas chamber, “after” the plates although the blue never went through any plate.

[8] The phase delay is proportional to the optical path length. The motivation for group delay and chirp coefficient may also need the fact that differentiation is a linear operator: it is permitted to differentiate the path length $L\,n$ to get $N$ and $b_p$ rather than differentiate the individual refractive indices first.

### 2.2.6 Simplified picture

An approximative, specialized version of the general equation (2.12) will be presented here, for the "standard case" $\theta_{\mathrm{A}} = -45°$, $\theta_{\mathrm{B}} = 0°$, $\boldsymbol{J}_1 = J_1\boldsymbol{e}_{\mathrm{x}}$ with only the fundamental pulse $p = 1$. This will make it easier to understand why the polarization state can be changed by retarder plates.

As first approximation, all dispersion corrections are dropped and only a single delay used, directly in (2.1). Evaluation of the **M**-matrices in (2.11) then yields

$$\boldsymbol{E}_{\mathrm{A}}(t) \approx \begin{bmatrix} 1 \\ -1 \end{bmatrix} \frac{1}{2} E_1(t - \tau_{\mathrm{A,F}}) + \begin{bmatrix} 1 \\ 1 \end{bmatrix} \frac{1}{2} E_1(t - \tau_{\mathrm{A,F}} - \delta_{\mathrm{A}}) \tag{2.16}$$

The optical field after plate A clearly consists of two different, linearly polarized terms where one is delayed by $\delta_{\mathrm{A}}$ with respect to the other.

With $\theta_{\mathrm{B}} = 0°$ and $d_{\mathrm{B}} = 1/4$, setting $\tau_{\mathrm{AB}} = \tau_{\mathrm{A,F}} + \tau_{\mathrm{B,F}}$ allows the output of the second plate to be written

$$\begin{aligned} \boldsymbol{E}_{\mathrm{B}}(t) &\approx \begin{bmatrix} 1 & 0 \\ 0 & 0 \end{bmatrix} \boldsymbol{E}_{\mathrm{A}}(t - \tau_{\mathrm{B,F}}) + \begin{bmatrix} 0 & 0 \\ 0 & 1 \end{bmatrix} \boldsymbol{E}_{\mathrm{A}}(t - \tau_{\mathrm{B,F}} - T/4) \\ \boldsymbol{E}_{\mathrm{B}}(t) &\approx \frac{1}{2} \begin{bmatrix} E_1(t - \tau_{\mathrm{AB}}) & + E_1(t - \tau_{\mathrm{AB}} - \delta_{\mathrm{A}}) \\ -E_1(t - \tau_{\mathrm{AB}} - T/4) & + E_1(t - \tau_{\mathrm{AB}} - \delta_{\mathrm{A}} - T/4) \end{bmatrix} \end{aligned} \tag{2.17}$$

For monochromatic input of constant amplitude, *i.e.* not a pulse but only the carrier $E_1(t) = J_1 C_1(t) = J_1 \mathrm{e}^{i\omega_1 t}$, equation (2.17) can be simplified further via the relation

$$E_1(t - \tau_{\mathrm{AB}} - T/4) = J_1 \mathrm{e}^{i\omega t - i\omega\tau_{\mathrm{AB}} - i\omega T/4)} = -i\mathrm{e}^{-i\omega\tau_{\mathrm{AB}}} E_1(t)$$

Actually, the constant amplitude-requirement will be relaxed to allow a slowly varying envelope. More precisely, $\max\{\delta_{\mathrm{A}}, T/4\} \ll t_{\mathrm{FWHM}}$, where $t_{\mathrm{FWHM}}$ is the duration of the pulse. Equation (2.17) is then approximated by

$$\begin{aligned} \boldsymbol{E}_{\mathrm{B}}(t) &\approx \frac{1}{2}\mathrm{e}^{-i\omega\tau_{\mathrm{AB}}} \begin{bmatrix} E_1(t) & + E_1(t - \delta_{\mathrm{A}}) \\ -(-i)E_1(t) & + -iE_1(t - \delta_{\mathrm{A}}) \end{bmatrix} \\ \boldsymbol{E}_{\mathrm{B}}(t) &\approx \frac{\mathrm{e}^{-i\omega\tau_{\mathrm{AB}}}}{2} \underbrace{\begin{bmatrix} 1 \\ i \end{bmatrix}}_{\hat{\mathbf{e}}_{\mathrm{RCP}}} E_1(t) + \frac{\mathrm{e}^{-i\omega\tau_{\mathrm{AB}}}}{2} \underbrace{\begin{bmatrix} 1 \\ -i \end{bmatrix}}_{\hat{\mathbf{e}}_{\mathrm{LCP}}} E_1(t - \delta_{\mathrm{A}}) \end{aligned} \tag{2.18}$$

Now one concludes that the "standard" kind of gate can be understood as separating the input into two circularly polarized terms. One of the terms is delayed in proportion to the retardation of the first plate, $d_{\mathrm{A}}$. When using $\theta_{\mathrm{A}} = -45°$ the LCP term is delayed.

As the experiments will involve rather short pulses instead of continuous light, this separation is only an approximation. For 35 fs input, $T/4/t_{\mathrm{FWHM}} \approx 0.25/13 \approx 2\%$ means that $\delta_{\mathrm{A}}$ will be the limiting term. If 15% of $t_{\mathrm{FWHM}}$ used as limit, approximation (2.18) can be considered useful up to $d_{\mathrm{A}} \lesssim 2$, but higher retardations were often used.

For 10 fs input $\delta_{\mathrm{B}}$ is 7% and still acceptable, but since all suitable values for plate A have $\delta_{\mathrm{A}} \gtrsim 0.6 \cdot T$ equation (2.18) will *not* be valid for the short input pulses.

The field caused by a "standard gate" is illustrated in Figure 2.4. The pulse duration 7.88 fs and $d_{\mathrm{A}} = 2.75$ are arbitrarily selected to make the important aspects of the illustration easy to distinguish. The right diagram shows the total field after the plates, calculated using the original equation (2.12)[9], while the left part of the figure shows the fast and delayed terms of equation (2.18).

Comparing the helix directions of the RCP and the LCP terms with the sum, one observes that when the fast RCP component initially dominates in amplitude the sum is RCP. The sum gradually turns more linearly polarized and finally as the delayed LCP component arrives it becomes LCP. The dashed blue line shows $|\varepsilon|$, the absolute value of the ellipticity, having a zero where the polarization switches sign from right ($\varepsilon > 0$) to left ($\varepsilon < 0$).

[9] Using the approximative (2.18) gives the same general characteristics but a different carrier-envelope phase and changes the precise shape of the central part.

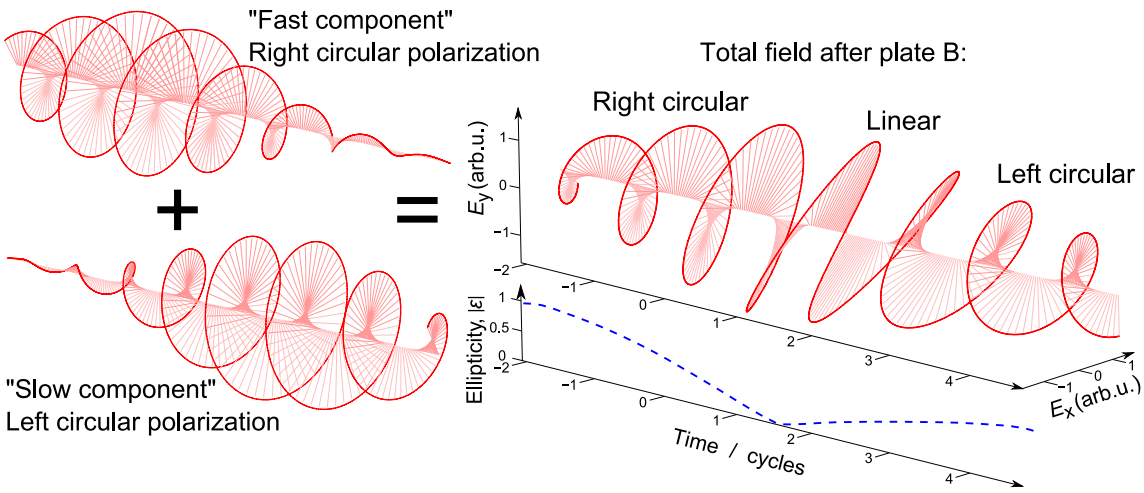


Figure 2.4: The field created by the standard kind of polarization gate, with a short pulse. On the left side, the fast and slow circularly polarized components of equation (2.18) are drawn separately. The rightmost diagram shows the total field $\boldsymbol{E}_{\mathrm{B}}(t)$, which is approximately their sum. The dashed blue line is the absolute value of the ellipticity.

The near-linearly polarized part in the middle, where the electric field vector changes along an almost straight line as time passes is the "open" part of the gate, where high harmonics can be generated by electrons driven forward and back by this straight field section. Compare with the sketch in Figure 1.4; when the field is not linearly polarized the electrons typically do not return.

The retardation of the first plate, $d_{\mathrm{A}}$ determines the delay between the fast and slow component: the higher $d_{\mathrm{A}}$, the further apart they come. In relation to the pulse duration $t_{\mathrm{FWHM}}$ it also determines the narrowness of the gate and the intensity where the gate is open. For small values of $d_{\mathrm{A}}/t_{\mathrm{FWHM}}$, the ellipticity changes slowly with time, so the gate is not very sharp. Higher values can increase $|\frac{\mathrm{d}\varepsilon}{\mathrm{d}t}|$ $|\mathrm{d}\varepsilon/\mathrm{d}t|$, making the gate more narrow. This comes at the cost of a decreased intensity in the linearly polarized part, because the two pulse components get too far apart. Eventually the overlap is so small that the weak linearly polarized part does not generate any harmonics.

The fractional part of $d_{\mathrm{A}}$ determines along what direction the open part of the gate is polarized. Integer $d_{\mathrm{A}}$ makes it polarized along the $x$-axis and quarter-wave plates give directions $\pm 45°$ from the $x$-axis and if $d_{\mathrm{A}}$ was increased gradually then the right part of Figure 2.4 would seem to rotate clockwise, when viewed from the positive time-side as in the figure.

## 2.3 Single atom-response simulation

Only the response of a single atom to the optical electric field is modeled, thus phase matching effects in the gas and spatial characteristics of the laser beams are not considered. The current simulation program is not intended to give an absolute measure of the emission strength, only a relative or qualitative understanding of how the emission is distributed in time and energy. The theoretical framework is the three-step model which was introduced on page 10.

### 2.3.1 Step one – Ionization

The instantaneous ionization flux, $\Phi_{\mathrm{i}}(t)$ $[\mathrm{s}^{-1}\mathrm{m}^{-2}]$, is the number[10] of electrons that are tunnel-ionized per unit time per incident beam area. For these simulations it was defined from the ionization rate $w$ $[\mathrm{s}^{-1}]$ and the probability for an electron to remain in a bound

[10] Rather the *expectation value of* number of electrons, as we are discussing a stochastic process.

state $P_\mathrm{b}(t)$ as follows.

$$\begin{aligned}\Phi_\mathrm{i}(t) =& - w(t)P_\mathrm{b}(t)\rho_\mathrm{s} = \rho_\mathrm{s}\frac{\mathrm{d}P_\mathrm{b}(t)}{\mathrm{d}t} \\ P_\mathrm{b}(t) =& \exp\left(-\int_0^t w(t)\,\mathrm{d}\tau\right), \quad P_\mathrm{b}(0) = 1, \\ \rho\mathrm{s} =& N_\mathrm{Ar}\, l_\mathrm{gen} \approx 2.6\times 10^{21}\ \mathrm{m}^{-2}\end{aligned} \tag{2.19}$$

The $\rho_\mathrm{s}$-value is rather arbitrary, an area density was necessary to get the correct dimension for $\Phi_\mathrm{i}(t)$, but the selected value is by no means assumed to have any significant digits to represent our experimental conditions. This value was based on $l_\mathrm{gen} = 3.5$ mm [11, in the supporting on-line material] and an argon pressure of 3000 mbar [20] in the volume where harmonics are generated.

Qualitatively, ionization is more likely at high instantaneous electric field[21], but the quantitative relation is non-trivial. An expression from Tong & Lin [22] for ionization rate $w_\mathrm{TBI}$ that is applicable up to the barrier-suppression regime where the laser field may be stronger than the atomic field is used. The parameter $C_l = 2.44$ was taken from [23] and an electronic state with $l = 1, m = 0$ was assumed. Two other articles that were used in the process of understanding and implementing an expression for ionization rate are [21] and [24].

### 2.3.2 Step two – Trajectory

The simulation program starts electron trajectories at regular time intervals, usually a few hundred times per cycle, and determines the ionization flux at the start of these trajectories. The ionization flux multiplied by a return probability for the trajectory are considered to determine the flux of emitted photons from that trajectory.

Assuming the optical field is much stronger than the atomic attraction of outer electrons, we can use the model of a free electron accelerated only by the Lorentz force of the optical electromagnetic field, $\vec{F} = q\,\mathfrak{Re}\vec{E} + q\vec{v}\times\mathfrak{Re}\vec{B}$. The magnetic term in the Lorentz force is proportional to velocity $\vec{v}$ and considering the ratio between magnetic flux density $\vec{B}$ and electric field, it turns out[11] that the magnetic force is negligible compared at non-relativistic speeds. Based on this argument, no magnetic force was used in the simulations. An electron emitted by ionization at time $t_\mathrm{i}$ starts at origin and then follows the simulated trajectory

$$\vec{r}_{t_\mathrm{i}}(t) = \iint_{t_\mathrm{i}}^{t} \frac{q}{m_\mathrm{e}}\mathfrak{Re}\,\vec{E}(t')dt', \quad t \geq t_\mathrm{i}. \tag{2.20}$$

The trajectory is simulated until either the global simulation time interval ends or the electron trajectory reaches a preset maximum duration. The MATLAB program that evaluates equation (2.20) defaults to use `cumsum` (Riemann sum) for both integrals. Optionally, the more accurate but also time consuming differential equation solver `ode45` (explicit Runge-Kutta 4,5) can be used for the first integral, but that does not make any notable difference with the short sampling times used, usually between 4 and 7 as.

For each $t_\mathrm{i}$, all local minima of $|\vec{r} - \vec{0}|$ are determined as candidates for electron recombination with the ion (which has been approximated as stationary). A minima at $t = t_\mathrm{r}$ defines the *trajectory*

$$\vec{\mathbb{r}}_{t_\mathrm{i},\,t_\mathrm{r}} = \{\vec{r}_{t_\mathrm{i}}(t) : t_\mathrm{i} \leq t \leq t_\mathrm{r}\} \tag{2.21}$$

with the *excursion time* $t_\mathrm{excursion} = t_\mathrm{r} - t_\mathrm{i}$. Multiple trajectories may share the same ionization time.

[11] For a harmonic field in free space, the maximum ratio between the magnetic and the electric force terms is $\frac{qvB_0}{qE_0} = \frac{v\mu_0 H_0}{E_0} = \frac{v\mu_0}{\eta_0} = v\sqrt{\mu_0\epsilon_0} = v/c_0$. This is assumed to be approximately true also in more general cases, so that the non-relativistic criterion $v/c_0 \ll 1$ gives $\vec{F} \approx q\,\mathfrak{Re}\vec{E}$. This approximation was also used by Dahlström [25, p. 11].

For each trajectory, the distance to the ion and the non-relativistic kinetic energy of the electron are known from the simulation when it is at minimum distance from the ion:

$$r_\mathrm{r} = |\vec{r}_{t_\mathrm{i}}(t_\mathrm{r})| \tag{2.22}$$

$$U_\mathrm{r} = \frac{m_\mathrm{e}}{2}\left|\dot{\vec{r}}_{t_\mathrm{i}}(t_\mathrm{r})\right|^2. \tag{2.23}$$

### 2.3.3 Step three – Recombination

The recombination probability $\eta$ is defined as the probability of an electron recombining with the ion, given that it does follow a certain trajectory. In case it recombines, a photon is emitted with energy $H_\mathrm{r}\hbar\omega_1 = U_\mathrm{r} + U_\mathrm{ion}$, where $U_\mathrm{ion}$ is the ionization potential and $H_\mathrm{r}$ the energy expressed as harmonic order of the fundamental IR frequency $\omega_1$. Otherwise, no further record is kept of the electron. The possibility of returning at a later local minimum is referred to as a different trajectory.

Using the ionization flux defined in equation (2.19), the flux of recombining electrons is defined as

$$\Phi_\mathrm{r}(t) = \Phi_\mathrm{i}(t)\eta\big(\vec{r}(t_\mathrm{r}),\, t_\mathrm{excursion}\big) \tag{2.24}$$

This is also the *flux of emitted photons*, as each returning electron is considered to emit a single photon. When multiplied by the photon energy, an intensity $I_\mathrm{r}$ per trajectory is obtained from the simulation.

$$I_{\mathrm{r},\,t_\mathrm{i}}(t_\mathrm{r}) = \Phi_\mathrm{r}(t) H_\mathrm{r}\hbar\omega_1, \tag{2.25}$$

The sum of these intensities,

$$I_\mathrm{r}(t_\mathrm{r}) = \sum_{t_\mathrm{i}} I_{\mathrm{r},\,\mathrm{t_i}}(t_\mathrm{r}). \tag{2.26}$$

should have some correlation to the experimental momentaneous intensity of emitted photons, if the simulation works.

If the sum is taken aver all times, for photon energies grouped into a set of narrow energy bins, *i.e.* a histogram over $I_{\mathrm{r},\,t_\mathrm{i}}(t_\mathrm{r})$ is made[12], then you end up with something like an intensity spectrum, which at first thought would have similarities to experimental spectra. As such a simulated spectrum did not include the phase of the emitted photon fields, it will fail to model their interference which is critical to get the modulations or discrete harmonic peaks in the spectrum. But there are probably other issues too, particularly the high energies dominate in the simulated histogram-spectrum if the trajectories are defined as stated above, which does not match experimental spectra.

### 2.3.4 Models for recombination probability

There are multiple models implemented for estimating the recombination probability $\eta$, which will be described below. Generally they ignore an unknown scaling factor so that they give $\eta = 1$ under the best conditions, which is too high and yet a reason for $I_\mathrm{r}$ to be considered qualitatively, not quantitatively.

#### Ellipticity mean during trajectory

Multiple investigations of the ellipticity-dependence of high harmonic generation [26, 6, 27] show approximately Gaussian relations between the ellipticity $\varepsilon$ defined in eq. (1.1), and the photon count of generated harmonics. Figure 2.5 shows a typical example. I assume that $\eta$ is the factor in eq. (2.25) that should contain such a dependence.

The derivation in [27] puts $\eta = \mathbf{d}_+(\varepsilon)/\mathbf{d}_+(0)$, where $\mathbf{d}_+(\varepsilon)$ is the dipole operator matrix element between the ground state and a continuum state with a certain kinetic energy when the optical field has ellipticity $\varepsilon$. The expression is evaluated at $t_\mathrm{r}$, using Gaussian-like matrix elements from [4]. Since their simulation is based on the Shrödinger equation, it incorporates the average *diffusion effect* where the electron packet grows wider with time because of the non-zero initial velocity variance.

[12] Think of it as an integration along the time axis in Figure 3.1 on page 29.

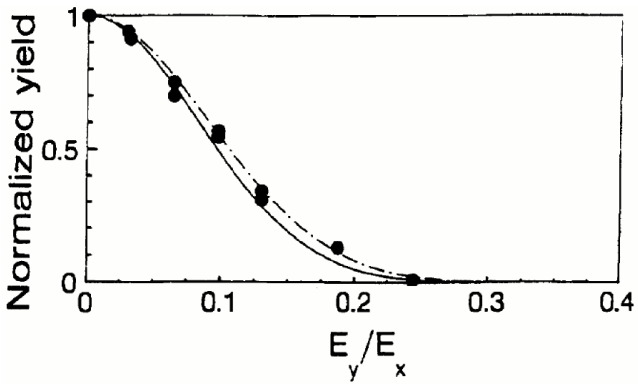


Figure 2.5: Dependence of the 41st harmonic intensity ("yield") in neon on ellipticity ($E_y/E_x$). Circles are experimental results with $\lambda = 775\,\mathrm{nm}$, pulse duration $\sim 200$ fs and peak intensity $\sim 8 \times 10^{18}\,\mathrm{W\,m^{-2}}$. The curves show theoretical results for $8 \times 10^{18}\,\mathrm{W\,m^{-2}}$ (solid) and $5 \times 10^{18}\,\mathrm{W\,m^{-2}}$ (dashed). [27, figure 1(a)].

The *threshold ellipticity* $\varepsilon_{\mathrm{th}}$, at which $\eta$ drops to half its maximum value, varies with harmonic order and medium, but typical values are about 0.08 to 0.18 [20][13]. My simulations use $\varepsilon_{\mathrm{th}} = 0.15$ where nothing else is specified.

As the simulation program presented here does not use a full quantum mechanical model it cannot use the expressions from [27]. Instead it uses a simple Gaussian relation, with the *average* ellipticity during the trajectory as input,

$$\eta_{\mathrm{ellipticity}} = \frac{1}{2^{\varepsilon^2_{\mathrm{avg}}/\varepsilon^2_{\mathrm{th}}}}\,, \quad \varepsilon_{\mathrm{avg}} = \frac{1}{t_{\mathrm{r}} - t_{\mathrm{i}}} \int_{t_{\mathrm{i}}}^{t_{\mathrm{r}}} |\varepsilon(t)|dt \tag{2.27}$$

### Distance

The *distance model* is based on the ad hoc assumption about $\eta$ being a Gaussian function of $r_{\mathrm{r}}$. Probably, the same assumption is made in [8, p. 1995].

$$\eta_{\mathrm{distance}} = \frac{1}{2^{r^2_{\mathrm{r}}/r^2_{\mathrm{th}}}} \tag{2.28}$$

The distance parameter $r_{\mathrm{th}}$, called the *threshold distance*, is used by most remaining models in some way. It is somewhat related to the threshold ellipticity or to the electronic wave packet size. By running simulations with various constant ellipticities, $r_{\mathrm{th}}$ was calibrated to make the Distance method approximate the Ellipticity method, which is valid at constant ellipticity according to [27]. As $\eta_{\mathrm{distance}}$ will vary during the optical cycle no exact agreement can be found, but an approximate averaging $\eta_{\mathrm{distance}} \sim \eta_{\mathrm{ellipticity}}$ landed in the empiric relation

$$r_{\mathrm{th}} = 1.77\ \mathrm{nm} \times \sqrt{I_{\mathrm{in}}/10^{19}\ \mathrm{W\,m^{-2}}}; \tag{2.29}$$

$I_{\mathrm{in}}$ is the sum of the peak optical intensity for all incident pulses. When the long pulse is simulated with $I_{\mathrm{in}} = 1.27 \times 10^{18}\ \mathrm{W\,m^{-2}}$, the formula gives $r_{\mathrm{th}} = 0.631$ nm.

### Gaussian diffusion

Initiated by the recommendation of Marcus Dahlström, this method is an attempt to account for the diffusion effect when an electronic wave packet broadens with time, on top of the distance model. It is based on the time evolution of a Gaussian probability distribution under the Shrödinger equation with total energy = potential energy (no source term or dampening), which becomes a diffusion equation. The analytic solution used here was taken

[13] The lower value is reached at harmonic order $H = 73$ in neon, while the higher value is reached at $H = 13$ in argon.

from [1, eq. 3.1-7] (a different subject, but the same kind of equation).

$$\eta_{\text{diffusion}} = \frac{1}{\zeta \, 2^{r_{\text{r}}^2/\left(r_{\text{th}}^2 \zeta\right)}} \,, \quad \zeta = 1 + \frac{t_{\text{excursion}}^2}{\left(\frac{m_{\text{e}} r_{\text{th}}^2}{\hbar \log 2}\right)^2} \tag{2.30}$$

The initial half-width at half max (HWHM) radius of the electron wave packet is set to $r_{\text{th}}$. It can be motivated by comparing the resulting equation (2.30) to the distance model (2.28), as this choice makes them equal for zero excursion time, $t_{\text{excursion}} = 0 \Rightarrow \zeta = 1$, where no diffusion would have occurred. The approximate calibration of $r_{\text{th}}$ against $\eta_{\text{ellipticity}}$ at constant ellipticity is still used.

The rate at which $\eta_{\text{diffusion}}$ decreases as function of excursion time is determined by the denominator in $\zeta$. At page 30 it is remarked that the return flux seems a little high for long trajectories. Decreasing the nominator can give some redistribution of flux from long trajectories to short trajectories. Most of the dynamics in flux values come from the ionization rate which varies several orders of magnitudes during an optical cycle, while the decay in $\eta$ usually contributes one or two orders of magnitude. Reducing the value of $r_{\text{th}}$ can increase the decay rate and dynamics of $\eta_{\text{diffusion}}$ and it could also be motivated by the "atomic radius" of argon being at most 0.2 nm [28], a third of the current $r_{\text{th}}$ value. As no value of $r_{\text{th}}$ that would keep agreement with both the empirically known $\eta_{\text{ellipticity}}$ at constant $\varepsilon$ and give a faster decay of $\eta_{\text{diffusion}}$ has been found, the definition in equation (2.29) is still used.

$\eta_{\text{diffusion}}$ is the default model in the simulation program and it is used for all simulations presented here.

# Chapter 3

# Design and methods

## 3.1 Choice of gating technique

After an initial literature study, a simulation program was developed where the result of using an arbitrary electric field to generate harmonics could be estimated. One idea was to use the approach with two interferometers from Tzallas *et al.* [14]. But it seemed too complex to build two interferometers, and attempts to theoretically achieve the desired delays in a single glass piece were made, which would remove the flexibility that was one of the points with the interferometer setup. If polarization retarder plates were used instead then their angles would be easy to change and allow some flexibility in the field design.

As presented in the Results chapter, starting in section 4.3.1, the polarization gating ability of the approaches considered here is dependent on the envelope of the pulse. It would be advantageous with shorter pulses and based on these simulation-aided conclusions it did not seem likely to get down to one or two bursts with reasonable energy efficiency using long pulses. Then the scope restrictions where changed to allow the use of shorter pulses from SPM-compression, on which work was in progress anyway. Miguel Miranda, Marko Swoboda and Thomas Fordell all worked on the pulse compression that turned out essential for this project.

The gate design was settled to use polarization retarder plates and the simulation program was developed further to provide specialized functions to simulate the field that such plates would cause. It was assumed that input pulse would be 10–15 fs, and after simulating many different configurations, three retarder plates were bought. As only two plates are necessary this would enable the retardation in "plate A" to be switched or two plates to be used together to get the sum of their retardations.

An interferometer is available that gives blue light with the same polarization direction, $\theta_2 = 0°$, as the fundamental pulse. Using the crystal for generation of blue without the interferometer it should also be possible to get $\theta_2 = 90°$. If plate A is a quarter-wave plate then it seemed best to let the blue light be input at $\theta_2 \sim 0°$s, while if A is a half-wave plate then $\theta_2 \sim \pm 90°$ was found to be better. This is probably related to the remark on page 23 about the fractional part of $d_\mathrm{A}$ determining the direction of the linear polarized field of the gate.

Further comments on the gate design process are given in the chapter 4.3 where some simulations are presented.

## 3.2 Simulation implementation

### 3.2.1 Limitation of excursion time

For the numerical computations, some finite limitation is necessary on the excursion times that should be considered. In section 2.3.4 it was shown that the probability that an electron will return decreases with excursion time. Additionally, phase matching effects which are not modeled in this work may play a role for which trajectories contribute to light that can be observed under normal experimental circumstances.

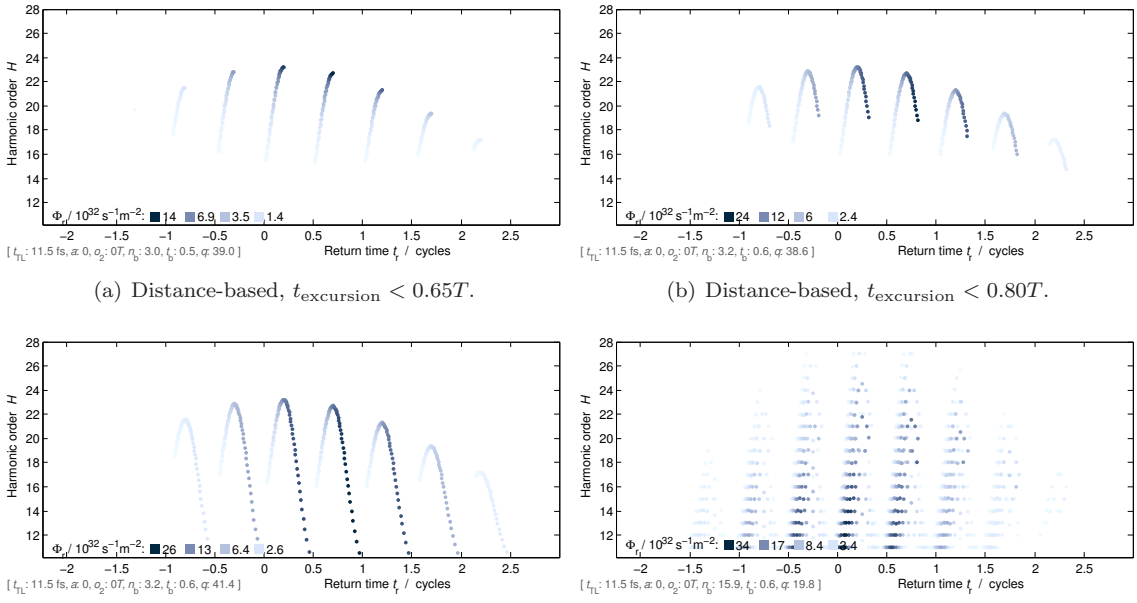


(a) Distance-based, $t_{\text{excursion}} < 0.65T$.

(b) Distance-based, $t_{\text{excursion}} < 0.80T$.

(c) Distance-based, $t_{\text{excursion}} < 1.0T$.

(d) Energy-based, $t_{\text{excursion}} < 0.80T$.

Figure 3.1: Simulated spectrograms with different trajectory selections. The distance-based return selector is shown for three different excursion time limits. (d) uses the energy based return selector described in section 3.2.2. All figures were made with a 11.5 fs pulse without plates, described more in depth in section 4.3.4.

Particularly, it has been claimed [29] that it is a sufficient approximation to only include the shortest excursion time for each return energy, which would mean limiting to the *short trajectory* [25, p. 12] having $t_{\text{excursion}} < 0.65T$. On the other hand, such a limitation is not always used [30, Figure 3.5] and it is not obvious that such a limitation is valid when the ellipticity varies with time and the trajectories will be different from the linearly polarized case. The limitation $t_{\text{excursion}} < 0.8T$ will be used as a trade-off in the simulations presented here. A comparison to shorter and longer limitations is made in Figure 3.1(a)–(c).

### 3.2.2 Selection of return trajectories

The upper limit on excursion time is not the only sieve for trajectories in the simulation program. As there is a continuum of possible trajectories the amount would still be infinite unless some discretization is used. The program first uses a limited time resolution, typically 200–600 samples per optical cycle, when integrating the electric field to get the trajectory of the electron.

Secondly, it would be very memory consuming to treat every sample as a possible recombination with the ion (end of trajectory), therefore only samples where the electron is at a local minimum distance to the ion were used in section 2.3.3. This method is called the *distance based return selector*, as it uses return times $t_r$ where the electron passes close to the ion and thus should have a high $\eta_{\text{distance}}$[1]. The return energy $H_r$ is determined based on what velocity the electron had at that time.

An alternative method for selecting return times was also implemented. The approach of this *energy-based return selector* is to select $t_r$ such that $H_r$ is an integer harmonic order, or the sample time closest to give an integer. As the electron may be very far from the ion at the $t_r$ selected, the return probability corresponding to the selected $t_r$ may be very low. Even after filtering away trajectories with $\eta \approx 0$, the remaining number of trajectories is much higher with this approach than with the distance-based selector. A smaller energy spacing than one harmonic order could be used to get higher resolution, but as that would increase the memory and computation time further it was not done.

[1] See page 26

The distance-based return selector roughly gives one energy per return time, so it resembles a curve in a spectrogram, as Figure 3.1 (a)-(c) shows. The energy based selector gives a wide range of energies above and below that curve, of which the ones at higher energy have lower return flux $\Phi_r$ than the points on the curve while the lowest energies are favored in flux (darker in the figure). Figure 3.1(d) shows the spectrogram made with the same conditions and maximum excursion time as in Figure (b).

In the distance-based version it is rather the long excursion times, between 0.6 and 1.0 cycles that have the highest return flux – which does not seem to agree very well with the statements about long trajectories being negligible. Possibly this shows the limitations of the semiclassical three-step model that has been used. A spectrogram in Ref. [30, Figure 3.5] which was obtained from a more quantum mechanical treatment[4] shows higher intensity for the shorter excursion times. Similarities to the energy-based selector in my program are the high flux at short excursions and low energies, and that there is some intensity at more than one energy per return time. The similarity to the distance-based selector is mainly that one energy per time is rather dominant in intensity, so that a curve is formed per burst.

The number of bursts is the same in both methods, and to check the reduction in burst count caused by various gates is the main purpose of the simulation program, therefore it seems possible to use either version. Also the maximum energy, the maximum flux and the general shape are related between methods, though not the distribution of flux among trajectories.

As the energy based diagram is harder to read and takes longer time to simulate, because of the many points in it, it was judged that the gating quality could be distinguished based on simulations with the simpler distance-based return selector. When reading the simulated spectrograms in the results section one should keep in mind that the flux of the rightmost return times may be overestimated.

However, if a simulated histogram-spectrum should be displayed, it seems the energy-based selector gives a flux (or intensity) distribution more like the experimental one, where low or middle harmonic orders dominate.

## 3.3 Experimental setup

### 3.3.1 Post compression

When shorter pulses than 35 fs were used, they were created by post-compression from self phase modulation (SPM) and chirped mirrors. The self phase modulation occurs when the light propagates through a gas filled chamber while focused to form a very narrow and thus intense beam. The light propagates inside a hollow fiber, about one meter long, acting as a waveguide to maintain the tight beam, seen on the left side of Figure 3.2(a). The pressure in the chamber is referred to as the *capillary pressure*, higher pressure gives more SPM and a wider spectrum of the output light.

Then an appropriate amount of chirp compensation, achieved by chirped mirrors, is necessary to make the pulse have zero chirp and thus be as short as possible with the spectral width given by SPM – "transform limited". As we used the same chirped mirrors at all pressures this process was probably not optimal, but some fine tuning was possible by changing the chirp and focusing mirror for the input pulse.

As the light must hit the narrow hollow fiber, the laser beam must not change direction very much. A camera with a feedback loop was monitoring a reflection of the beam to correct for drift. The sample rate and feedback was not at a level where stabilization between the laser shots every millisecond could be maintained, only long term drift was compensated.

### 3.3.2 Generation of blue light

The blue light, or more precisely the second harmonic, was generated in a KDP crystal of type-I that gives the second harmonic with orthogonal polarization to the fundamental.

Via dichroic beam-splitters and mirrors in an interferometer, shown in Figure 3.2(b), the polarization axis is turned so that the red and blue are both polarized along the $x$-axis ($\theta_1 = \theta_2 = 0°$. Because of the interferometric setup where a micrometer screw controls

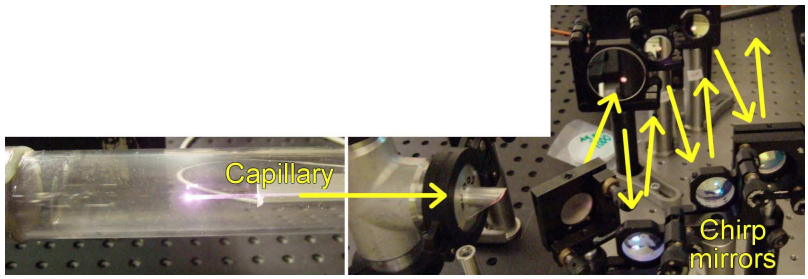


(a) The capillary and five chirped mirrors that are used for post compression of the laser pulse. The principal beam direction is indicated by the arrows.

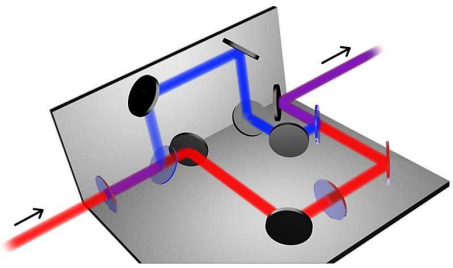

(b) Illustration of the red-blue interferometer. Places where the red and blue beams overlap are colored purple.

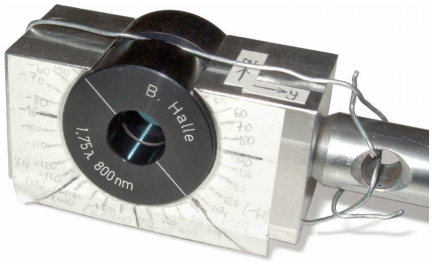


(c) Two quartz plates in their holder. The plate with $d_A = 1.75$ is seen with its fast axis oriented at $\theta_A = -45°$.

Figure 3.2: Details of the experimental setup.

the blue path length, the temporal offset between the blue and red pulses, $o_2 - o_1$, can be adjusted. Scans over sub-femtosecond delays could be made by letting a motor rotate a thin glass sheet in the red path.

### 3.3.3 Plate holder

The polarization retarder plates are mounted in cylindrical housings. These housings were slid into a hole through an aluminium block, where a segment of the hole was outside the block so a part of the plate housings was sticking out as shown in Figure 3.2(c). The purpose of this was to be able to rotate the plates while in place even when the holder was put in the interferometer where there was not much space to access the plates from the sides. On each side of the aluminium block, a paper with angular markings was used as reference when positioning the plates, probably with an accuracy of $\pm 3°$.

Three quartz plates were bought, having retardations $d = 0.25$, $d = 1.75$ and $d = 2.5$. The zero-order quarter wave retarder, $d = 0.25$, was always used as plate B while plate A could be either $d = 1.75$, $d = 2.5$ or both combined to give $d = 4.25$.

### 3.3.4 Generation and detection

A sketch of the main components just before and inside the vacuum chambers is given in Figure 3.3. Between the plates and the chamber for harmonics generation there was a plane mirror, a focusing mirror and an entry window at Brewster angle. The focusing mirror had a focal length of 50 cm when the long pulse was used and 30 cm when post-compressed pulses were used. The shorter focal length was used to counteract the loss of pulse intensity in the post-compression setup, by giving a smaller spot size it should increase the intensity at focus, but also reduce the depth of focus [1, ch. 3.2].

The argon gas for both generation and detection was emitted by small pulsed nozzles to keep the ambient concentration low. The average pressure in the generation chamber was measured as $P_{\text{gen}}$ and approximately kept in the range $4 \times 10^{-6}$ bar $\lesssim P_{\text{gen}} \lesssim 4.9 \times 10^{-6}$ bar. After the harmonics have been generated, an aluminium sheet filters away the wavelengths of the strong fundamental pulse. There is also a toroidal mirror that focuses the light into the detection gas jet.

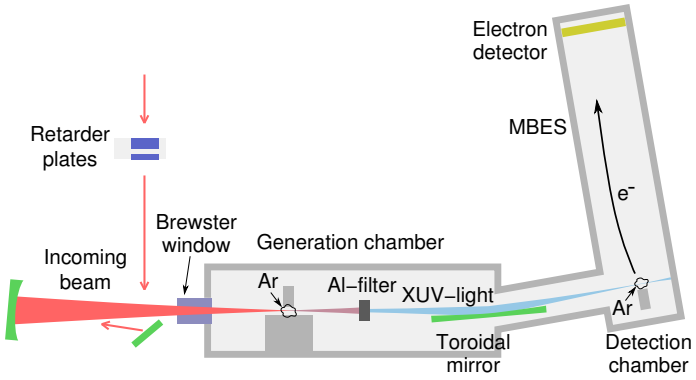


Figure 3.3: Sketch of some components in and just before the generation and detection chambers. The sloped part on the right side is the MBES spectrometer, containing a time-of-flight resolving electron detector.

The spectrum of the generated high harmonics was measured by first letting the light ionize electrons from argon in a second chamber and then detecting the velocities of these electrons to get their energies. This is referred to as a *magnetic bottle electron spectrometer* (MBES), because a magnetic field directs the ionized electrons to the detector. The pressure in the detection gas chamber was $2 \times 10^{-7}$ bar $\lesssim P_{\text{det}} \lesssim 3 \times 10^{-7}$ bar. A program called `ScanAnalysis` was used to rescale the raw velocity-spectra to spectra with an energy axis in units of the laser photon energy (harmonic order).

## 3.4 Averaging

### 3.4.1 The importance of carrier-envelope phase

In a long pulse of light, the envelope intensity does not change much during an optical cycle, but as the pulse gets shorter the envelope becomes steeper. In a 35 fs pulse the maximum intensities of the central peak and the adjacent peak differ only by 0.4% while in a 8 fs pulse the adjacent peak has 8% lower intensity, assuming zero carrier-envelope offset $\Delta_{\text{CEP},1} = 0$ in both cases. If $\Delta_{\text{CEP},1} = \pm T/4$ then there is not one central peak but two peaks of equal intensity, which means the difference between them is 0%.

As the electric field determines the ionization probability and the electron trajectories, an intensity difference in the central part of the pulse, where a standard gate is open, can be assumed to make some difference to the generated harmonics or XUV-bursts. For instance the electron's recombination time, its return energy and the carrier-envelope phase difference[2] $\Delta\varphi_{\text{b}}$ could be affected. For short pulses the value of $\Delta_{\text{CEP},1}$ which could make the intensity ratio vary between 0 and several percent, will be important for the properties of the generated bursts and the photon spectrum that can be observed.

The simulation program based on the three-step model can not calculate the phase of emitted photons or the spectrum they generate, so it can not be used to analyze this effect. Calculations by Baltuška *et. al.* for a 5 fs driving laser pulse in Neon show that a change in $\Delta_{\text{CEP},1}$ will affect $\Delta\varphi_{\text{b}}$ and shift the observed spectrum up or down in energy. [31] For some $\Delta_{\text{CEP},1}$-values, even harmonic orders ($\Delta\varphi_{\text{b}} = 0$) are observed instead of the usual odd harmonics ($\Delta\varphi_{\text{b}} = \pi$). Spectra corresponding to three different $\Delta\varphi_{\text{b}}$-values are shown in Figure 3.4, calculated for a completely artificial pulse train with three bursts of 70 as duration.

Baltuška *et. al.* mainly analyzed the near-cutoff energies but it was mentioned that below 40% of the cutoff energy the peak positions were affected less by $\Delta_{\text{CEP},1}$-variations. As the cutoff order depends on the input intensity and the medium it is not obvious if the same

[2] $\Delta\varphi_{\text{b}}$ is here defined as the *increment* in carrier-envelope phase *angle* between adjacent XUV-bursts, which seems to be the convention. This definition differs from the carrier-envelope offset $\Delta_{\text{CEP},1}$ used for the driving pulse, which is not an increment between two pulses and which was defined with the dimension time.

relation will hold in our experiments which use argon. Presumably similar CEP effects do occur also when a polarization gate is used to limit the number of generated bursts if the driving laser pulse is short enough to make the number of bursts low.

When the polarization state is designed to make a gate, the electric field is more irregular and although unreliable in this sense, the simulation program suggests that the spacing between average return times if trajectories can deviate a little from the normal $T/2$. With a short driving pulse and few bursts, a slight distribution of electron return flux that could possibly change the burst offsets uniformly enough to change the spacing between peaks in the spectrum. The same thing would happen if the wavelength of the fundamental pulse was changed slightly which could occur with fluctuations in the post-compression capillary. Such a change would stretch or compress the spectrum along the energy axis rather than just move it, but especially for high harmonic orders the result would be that peaks moved and the same averaging consequences would occur.

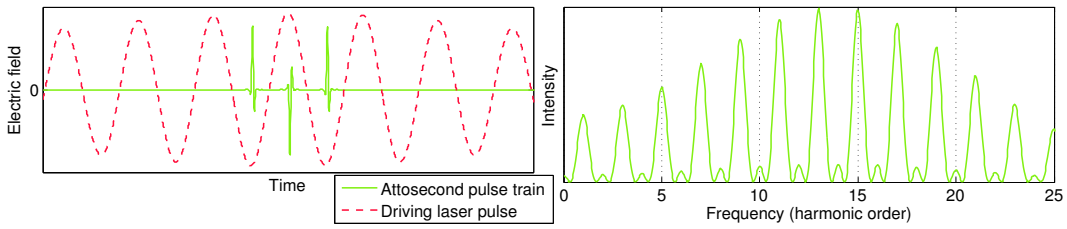


(a) $\Delta\varphi_\mathrm{b} = \pi$

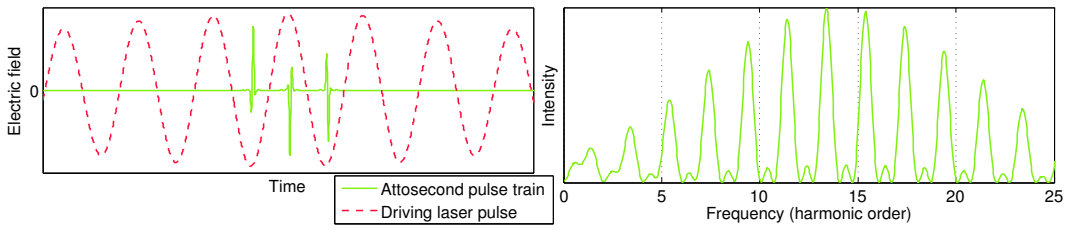


(b) $\Delta\varphi_\mathrm{b} = 0.6\,\pi$

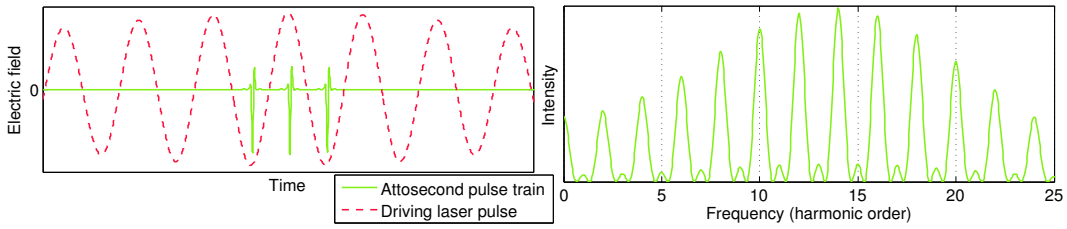


(c) $\Delta\varphi_\mathrm{b} = 0$

Figure 3.4: Temporal and spectral illustrations of a pulse train with three bursts, shown for different values of the inter-burst change in carrier-envelope phase, $\Delta\varphi_\mathrm{b}$. The normal case for long pulses is (a), where odd harmonics are observed in the spectrum.

### 3.4.2 Phase-unstable laser

Although the laser that drives the high harmonic generation process is very intense, the XUV-output is weak. With the polarization gating in use, the number of emitting cycles and to some degree also the amplitude within these cycles is reduced further, lowering the output signal. As a result, a spectrum corresponding to a single shot with the laser would be too weak and only spectra accumulated over $9 \times 10^3$ to $2 \times 10^5$ shots were used. As the laser system makes 1000 shots per second, the maximum acquisition time was 3 minutes and 20 seconds.

A phase-stable laser, where $\Delta_{\mathrm{CEP},1}$ is the same in every shot, would give peaks at the same positions every time and averaging over several shots would only reduce noise. Despite some efforts by the department, the laser system did not have a constant carrier-envelope phase, so the carrier-envelope phase $\Delta_{\mathrm{CEP},1}$ changes randomly between shots. As explained in the previous section this would give spectral peaks at different positions during different shots if the number of cycles in each pulse was low. When measuring the average over many shots, the peaks will be smeared out. The averaged spectrum will have wider peaks than any real, single-shot spectrum and may even look like the continuum spectra expected for an isolated burst.

Another consequence regarding the aim of generating a single attosecond burst, is that while $\Delta_{\mathrm{CEP}} = 0$ makes one of the cycles dominate in intensity, there are two equally strong cycles when $\Delta_{\mathrm{CEP}} = T/4$. Without a phase-stable laser it seems highly unlikely that the polarization gating, while keeping reasonable signal strength, could provide a single (dominating) attosecond burst from every laser shot. There will most likely be at least two bursts of comparable intensity for some $\Delta_{\mathrm{CEP}}$-values, which means that it is unrealistic to expect fully continuous spectra to be obtained. However, if the number of bursts only varies between one and two, the peaks of the spectrum should be very wide and look more like a modulation on top of a smooth continuum-spectrum than discrete peaks.

The result is that with the laser system used it is unlikely that the observed spectra will be fully continuous and even if the peaks look wide it is not possible to conclude exactly how few bursts were generated, as an unknown amount of additional broadening and background is expected to occur when the number of bursts is low. The extra broadening effect is only large when few bursts are generated, maybe 2–3, so it should still be possible to conclude whether we have reached at least that low.

## 3.5 Variables used to describe the results

The following definitions will be used in the presentation and analysis of results.

#### Simulated spectrograms

The fundamental simulation result consists of the variables defined in section 2.3. To describe the narrowness of gates, *standard deviation* in return time $t_{\mathrm{b}}$ and the *weighted burst count* $n_{\mathrm{b}}$ are defined. Both these quantities will be small for a narrow temporal gate.

Introducing $\Phi_{\mathrm{r},\Sigma}$ for the total photon flux, the standard deviation is

$$t_{\mathrm{b}} = \Big( \sum_t (t_{\mathrm{r}} - \mu_{\mathrm{r}})^2 \, \Phi_{\mathrm{r}}(t_{\mathrm{r}}) \,/\, \Phi_{\mathrm{r},\Sigma} \Big)^{1/2}, \quad \mu_{\mathrm{r}} = \sum_{t_{\mathrm{r}}} t_{\mathrm{r}} \, \Phi_{\mathrm{r}}(t_{\mathrm{r}}) \,/\, \Phi_{\mathrm{r},\Sigma}\,, \quad \Phi_{\mathrm{r},\Sigma} = \sum_{t_{\mathrm{r}}} \Phi_{\mathrm{r}}(t_{\mathrm{r}}) \tag{3.1}$$

To define the weighted burst count the spectrogram is first split into one "bin" per burst, separated so that burst number $k$ has return times in the range $t_{k-1} \le t_{\mathrm{r}} < t_k$ where $k$ is an integer. The algorithm for selecting the separation times $t_k$ is complicated and not given here but it mainly looks for gaps among the found return times, after rejecting trajectories with very low flux. Using the separation of the spectrogram into bursts, the weighted burst count is simply the total flux divided by the maximum flux within any single burst:

$$n_{\mathrm{b}} = \Phi_{\mathrm{r},\Sigma} \big/ \big( \max_k \Phi_{\mathrm{r},k} \big)\,, \quad \Phi_{\mathrm{r},k} = \sum_{t_{k-1} \le t_{\mathrm{r}} < t_k} \Phi_{\mathrm{r}}(t_{\mathrm{r}}) \tag{3.2}$$

Many different properties of the simulated spectrogram are weighted together in a heuristic way to form a single "quality" value, named $q$ and printed below each spectrogram. Apart from the above variables it involves the photon energy, the total intensity and the range of energies (if any) that are only emitted in single burst. As the definition is very long and without any theoretical motivation for the weight coefficients, it is not used in this report.

**Experimental spectra**

The experimental spectral intensity is defined as $S(H)$, where $H$ is energy expressed as harmonic order, $H = U/\hbar\omega_1$. A noise-robust quantity intended to represent the cutoff-order is the 90% quantile $H_{90\%}$, defined through the relation

$$\int_0^{H_{90\%}} S(H)\,\mathrm{d}H = 0.90 \int_0^{\infty} S(H)\,\mathrm{d}H \tag{3.3}$$

To define additional quantities describing the peaks and background level, the spectrum is split into one "bin" per peak, by separators $h_l$ placed halfway between the peak positions. Peaks are indexed by an integer $l$, starting at 1 and each bin can be expressed as the range of energies $\mathbb{H}_l = \{H : h_{l-1} \leq H < h_l\}$, where $h_0 = 0$.

A refined peak position $H'_l$, weighted by $S^2(H)$ within each bin is calculated, and its offset from the expected harmonic order $\hat{H}_l$ is defined as $\xi_l = H'_l - \hat{H}_l$. Where blue light is used the expected order is an integer, while an odd integer is expected without blue.

The full width at half maximum (FWHM) of each peak is called $\gamma_l$ and has the dimension energy. The spectrum-wide average $\Gamma$ is obtained by weighting the $\gamma_l$-values by the maximum spectral intensity within each peak bin:

$$\Gamma = \sum_l \gamma_l \hat{S}_l \Big/ \sum_l \hat{S}_l\,, \quad \hat{S}_l = \max_{H\in\mathbb{H}_l} S(H) \tag{3.4}$$

The *background level* $\beta_{\mathrm{v},l}$ of peak number $l$ is the intensity ratio between valley and peak within the bin. The spectrum-wide average $B_\mathrm{v}$ is weighted by intensity $S_l$ within each bin

$$B_\mathrm{v} = \sum_l \beta_{\mathrm{v},l}\, S_l \Big/ \sum_H S(H)\,, \quad \beta_{\mathrm{v},l} = \min_{H\in\mathbb{H}_l} S(H)/\hat{S}_l\,, \quad S_l = \sum_{H\in\mathbb{H}_l} S(H) \tag{3.5}$$

Another expression intended to describe the background level is the histogram ratio $B_\mathrm{h}$, defined using the `hist`-function in MATLAB. The histogram of the spectrum is treated as a ten-dimensional column vector $\boldsymbol{S} = \mathtt{hist}(S)^\top$ and the ratio is calculated as

$$B_\mathrm{h} = [0\,,0\,,0.1\,,0.4\,,1\,,1\,,1\,,1\,,1\,,1]\boldsymbol{S} \,\big/\, \big([1\,,1\,,0\,,0\,,0\,,0\,,0\,,0\,,0\,,0]\boldsymbol{S}\big) \tag{3.6}$$

The ideal continuum-spectrum of a single attosecond burst would have high values for $\Gamma$, $B_\mathrm{v}$ and $B_\mathrm{h}$. These quantities are combined in a heuristic way to a dimensionless quality-value $s$, also called the *singleness value*,

$$s = B_\mathrm{v} + 0.4B_\mathrm{h} + 0.25\,(\Gamma/\hbar\omega_1)^2 \tag{3.7}$$

# Chapter 4

# Results

## 4.1 Overview

Experimental measurements were mainly done with pulses of three different durations; the 35 fs pulses directly from the laser system and pulses post-compressed using self phase modulation at the capillary pressures 549 mbar and 803 mbar. The durations of the post-compressed pulses are estimated in the following section.

Section 4.3 presents simulations of harmonic generation with these pulses sent through different configurations of plates, with and without the second harmonic. Finally, experimental results are presented, including results without plates, the best gate setting and other spectra selected to represent how the parameters plate thickness, plate angles, blue light and pulse duration influence the result.

## 4.2 Post-compressed pulses

Figure 4.1(a) and (b) show spectra of the SPM output from the capillary at the pressures for which short pulse measurements are presented. The fast modulation in (b) is not noise but caused by the use of a thin beam splitter when SPM-spectra were measured in connection to the measurements of harmonics. Smoother but similar spectra of SPM were collected another day for these pressures, but as none of the smooth spectra for 803 mbar had the precise shape of that in (b) the modulated version was kept. The modulated version for 549 mbar is very similar to (a) in general shape, but has the central wavelength 783 nm rather than 776 nm, which is considered to be a minor difference.

Measurements of harmonics without plates were made at a few more pressures up to 1217 mbar, which reduced the intensity without giving wider peaks. Attempts to characterize the capillary output pulses at higher pressures, included in Figure 4.2, suggest that they do not get much shorter than at 850–900 mbar either. No plates were tested at pressures above 803 mbar. The pulse characterization was made with a SPIDER [32] setup, which gives the transform limit duration, the spectral phase and the pulse duration. These measurements fluctuated a lot and sometimes even disappeared temporarily. Fluctuations were visible in the capillary output so the problems are not believed to be pure measurement errors.

Many of the SPIDER-points in Figure 4.2 are the result of saving a handful of measurements from the SPIDER analyzer in rapid succession and then taking their average, sometimes with increased weight on results that were more robust to variation in parameters of the analysis program, or had a common shape of the spectral phase. As the variation is rather high even with the averaged values, any attempt to fit a curve will involve a large uncertainty. The equations of the fitted curves for transform limit and chirp as functions of pressure are given in the figure. These functions are used to get nominal pulse properties for all results with post-compressed pulses and in simulations corresponding to such experiments.

The way the chirp parameter $a = \sqrt{t_{\mathrm{FWHM}}^2/t_{\mathrm{TL}}^2 - 1}$ was obtained, via transform limit $t_{\mathrm{TL}}$ and pulse duration $t_{\mathrm{FWHM}}$, means that the information of its sign was not preserved. But even the sign varied in measurements so to get any simple estimate of the pulse properties this rough approximation was used. Simulations with the opposite sign and zero chirp have also been made for comparison.

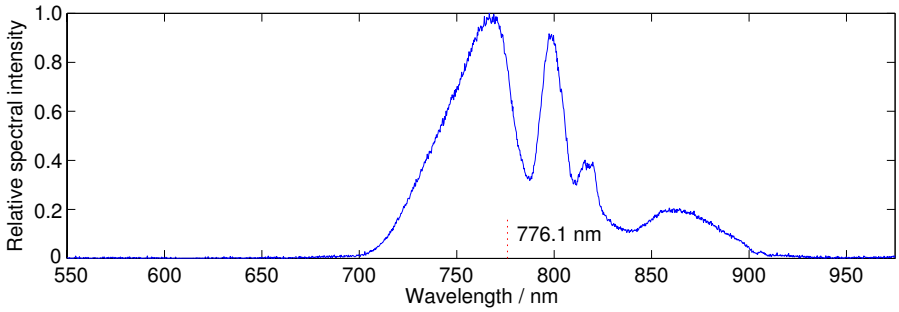


(a) 549 mbar pressure.

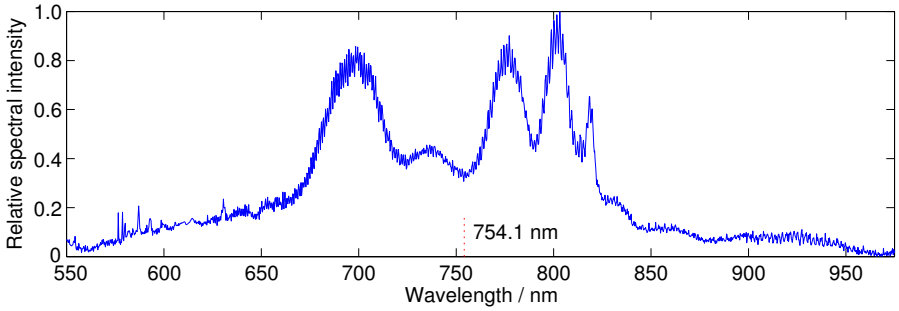


(b) 803 mbar pressure. The fast modulation that makes the lines look wide is not relevant.

Figure 4.1: Spectrum of the post-compressed pulses at two capillary pressures.

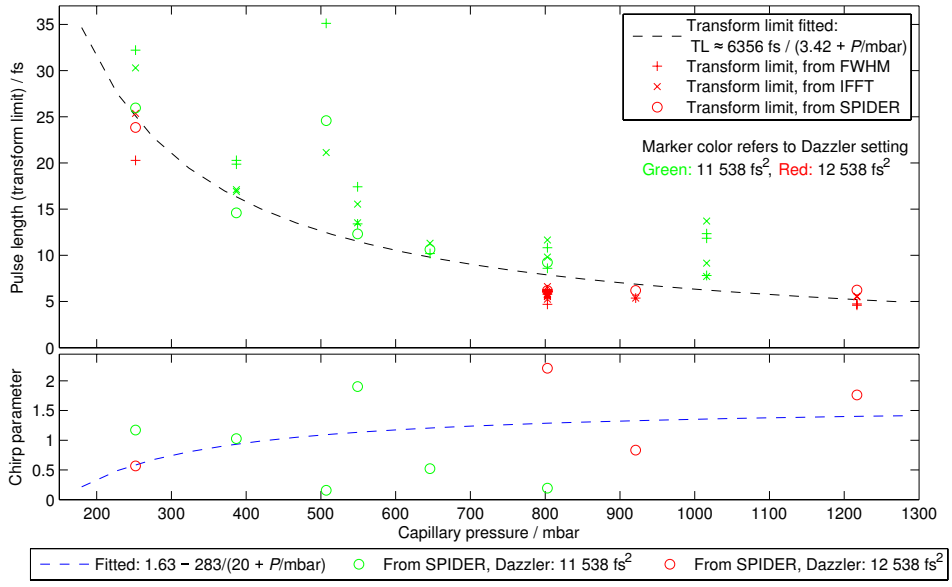


Figure 4.2: Approximative measurements of pulse length and chirp parameter, as functions of pressure. FWHM means that only the spectral width at half max was used together with the rough approximation of a Gaussian profile. IFFT denotes a duration obtained via inverse Fourier transformation of the spectrum, without any spectral phase. The algorithm of the SPIDER analyzer's transform limit was not checked, but it is assumed to be most accurate.

## 4.3 From simulations

### 4.3.1 Basic gating of long pulse

The simulation of harmonic generation with a 35 fs transform-limited pulse, without plates, is presented in Figure 4.3(a). It can also represent the case where plates are present but turned to not alter the polarization ($\theta_A = \theta_B = 0°$). The only change would be dispersion which affects the pulse duration, a negligible effect for the long pulse.

Note that all simulation results are presented as *spectrograms* where the darkness in color gives the photon flux $\Phi_r$ at each point in the (time, energy)-plane. Due to the simulation implementation and sampling, discussed in section 3.2.2, only a small number of points in the plane are actually displayed. The quantities $n_b$ and $t_b$, printed in a small font below each spectrogram, were defined in section 3.5 to describe numerically how long the gate is "open".

The simulations are made with 401.2 samples per optical cycle and the excursion time for electrons is limited to 0.8 optical cycles. The space between points in spectrograms is just a result of the finite sampling; a shorter sampling time would give more continuous lines. The peak optical intensity[1] is $1.27 \times 10^{18}$ W/m$^2$, which gives a cutoff harmonic order near 25, similar to the experimentally observed cutoff order.

In Figure 4.3(b) the standard gate with $d_A = 4.25$ is used. It does not confine the

[1]The simulation only concerns a single atom (*e.g.* in focus) so no spatial intensity profile is used.

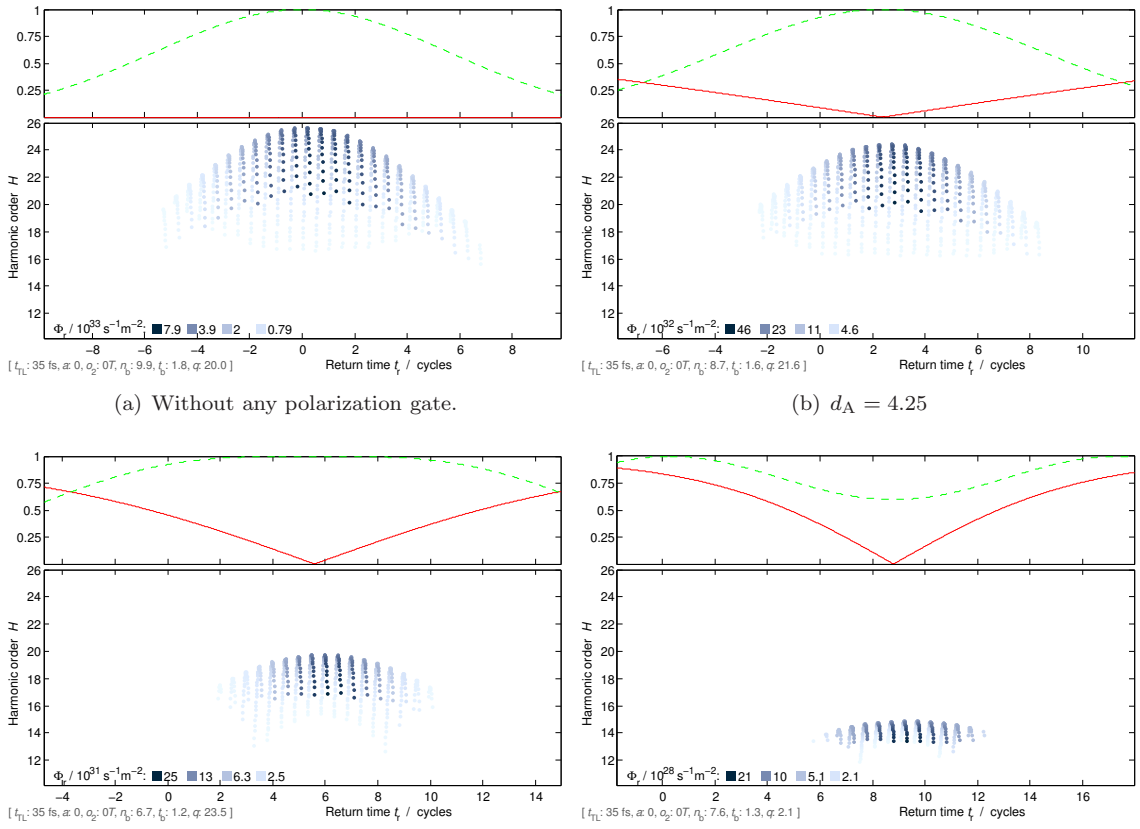


(a) Without any polarization gate.

(b) $d_A = 4.25$

(c) $d_A = 10.25$

(d) $d_A = 16.25$

Figure 4.3: Simulations for the long driving pulse. (a) is the result without any polarization gate. (b)–(d) show a standard gate using different retardations $d_A$, measured in number of optical cycles. The top half of each figure shows the intensity (dashed green) and ellipticity (solid red) of the driving pulse. The bottom half shows a spectrogram of the generated emission, where darker colors represent higher photon flux. Each hill-shape among the points corresponds to a "burst" of photon emission with a wide energy range during a short time.

generation much, the emission is spread over a similarly wide time interval and the weighted number of bursts, $n_\mathrm{b}$ only decreases by 1.2 from the $n_\mathrm{b} = 9.9$ without plates. It is a general result that the ellipticity ($|\varepsilon|$, red line in upper diagram) has a slope similar to the envelope of the pulse (the dashed green line is proportional to $E^2$), so with a long pulse the open part of the gate, where $|\varepsilon| \ll 1$, is also rather long.

When the plate retardation is increased to $d_\mathrm{A} = 10.25$ in (c), the temporal overlap between the fast and slow components of the pulse decreases and the gate occurs where their envelopes are steeper, giving a faster change in $\varepsilon$. The gate becomes more narrow; the weighted number of bursts $n_\mathrm{b}$ decreases from 8.7 to 6.7.

Smaller retardations, give a wider gate, though not displayed here. If the retardation is set too high compared to the pulse length, as $d_\mathrm{A} = 16.25$ in Figure 4.3(d), then the overlap between the fast and slow part of the pulse becomes too low. In this case the peak photon flux has dropped by a factor $5 \times 10^{-5}$ compared to the gate in (b), rendering the decrease in gate width width from $n_\mathrm{b} = 8.7$ to $n_\mathrm{b} = 7.6$ of little interest. The previously mentioned intermediate gate in (c) with $n_\mathrm{b} = 6.7$ is more narrow and does not have quite as low flux, only reduced by a factor $5 \times 10^{-2}$.

### 4.3.2 Adding blue light

Just as expected, it was easy to remove every second burst by adding blue light at the double frequency. In all simulations the ratio between blue and red peak intensity is 5% and their pulse duration is 35 fs. An intensity ratio of 1% is sufficient to see the effect and the exact ratio does not affect the gating performance very much. More important is the time offset between the pulses, $o_2$, for which different values are presented in Figure 4.4. In spectrogram (b) the blue was not sent through the plates, which corresponds to putting the plates in the red interferometer arm. The plate placement makes some difference for $\varepsilon(t)$ and suitable $o_2$-value but similar gate quality is possible with either placement, at least in this case.

Some observations can be made of how the result changes with $o_2$:

- When the peak harmonic order is high, the peak flux is low. This applies to individual bursts as well as to the whole spectrogram.

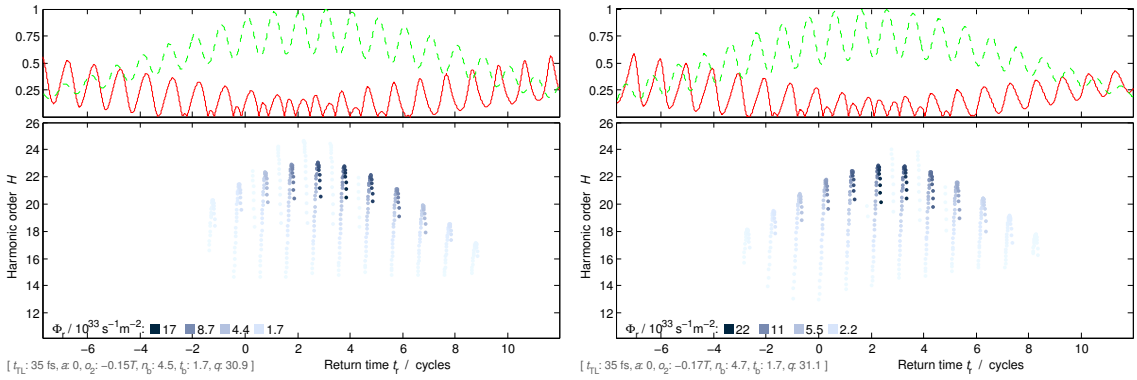


(a) Blue through plates, offset $o_2 = -0.15T$.




(b) Blue skipping plates, offset $o_2 = -0.17T$.

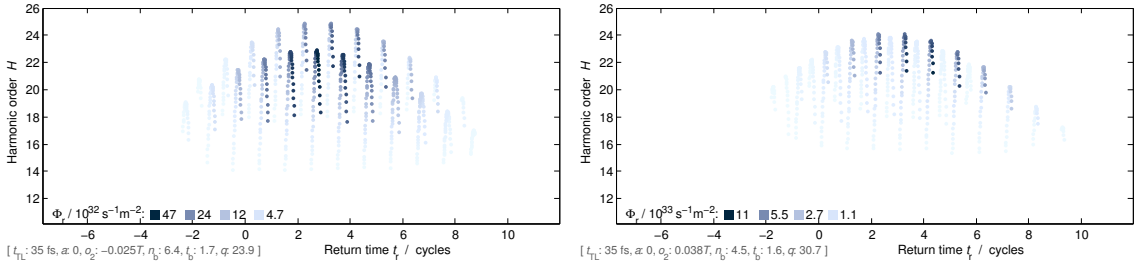


(c) Blue through plates, offset $o_2 = -0.025T$.




(d) Blue through plates, offset $o_2 = 0.038T$.

Figure 4.4: Standard gates with blue light at four different offsets $o_2$. The retardation is $d_\mathrm{A} = 4.25$.

- When $o_2$ is such that every second burst is *not* canceled, *e.g.* Figure 4.4(c), the bursts are alternating at high and low harmonic orders. The peak flux is also at its minimum in this configuration.

- The result is $T/2$-periodic in $o_2$, obviously as that is the period of the blue light. A shift by $T/2$ from a situation like Figure 4.4(c) would flip the high/low energy status of the bursts, as the direction of the blue electric field is reversed.

A conclusion from the simulations with 35 fs input pulse is that there seems to be an optimal retardation somewhere in the range $4.25 < d_\mathrm{A} < 16.25$. But even at this optimum the gate is nowhere near a single optical cycle. Adding the blue light with appropriate delay removes every second burst, but there are still multiple high harmonic bursts emitted so the harmonics may still be rather narrow spectrally.

### 4.3.3 Chirped long pulse

Figure 4.5 shows an example of a setting with non-standard angles outperforming the standard gate, with the long infra-red and blue pulses of transform limit 35 fs chirped to 49 fs actual duration. The improvement when comparing both gates in this figure to Figure 4.4(b) is not mainly caused by the chirp, but by the use of a thicker plate, $d_\mathrm{A} = 10.25$.

With the chirped pulse, the custom gate in 4.5(b) has the weighted burst count $n_\mathrm{b} = 3.8$ which is better than the standard gate's $n_\mathrm{b} = 4.6$ in (a). Removing the chirp would give $n_\mathrm{b} = 4.5$ for the custom gate and $n_\mathrm{b} = 3.5$ for the standard, so the best choice of plate settings depends on the chirp. The offset of the blue pulse is also important, $o_2$ was adjusted to give good results for each gate. The blue light was not sent through the plates. As the number of bursts is not very high, control over carrier-envelope phase also starts to matter.

One aspect that was not taken into account in the simulations is that if the 49 fs pulse is achieved by stretching the transform limited 35 fs pulse, then the pulse intensity would decrease. It would lower the simulated peak energy by about one harmonic order, which is not essential for the discussion above.

Quite a number of non-standard angles, some which would require a certain chirp value and some that were as robust to chirp-variation as the standard setting, were selected from simulations and tried experimentally. One such result is presented among the experimental spectra on page 47.

Also the plate thicknesses can be customized in the program, $d_\mathrm{A}$ and $d_\mathrm{B}$ do not have to be multiples of 0.25. Experimentally it would be more expensive to have custom plates made and there are limitations in the precision and range of thicknesses that manufacturers offer.

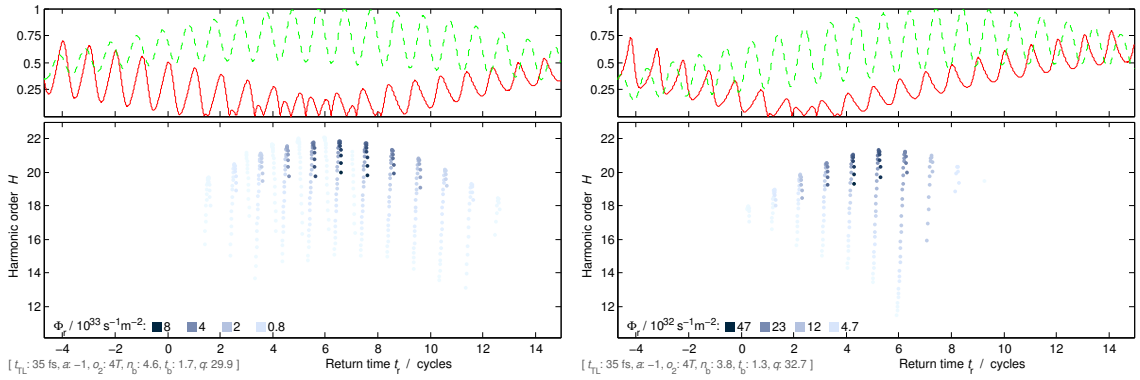


(a) Standard angles $\theta_\mathrm{A} = -45°$ and $\theta_\mathrm{B} = 0°$.

(b) Custom angles $\theta_\mathrm{A} = -60°$ and $\theta_\mathrm{B} = 55°$.

Figure 4.5: With a chirped pulse it is often worthwhile to investigate non-standard plate angles. The angles used in (b) give a narrower gate than the standard setting in (a). Both the infra-red and blue pulses have a transform limit of 35 fs, but are chirped with $a_1 = -1$ to a pulse length of 49 fs.

### 4.3.4 Medium-short pulse, 11.5 fs

The choice of 11.5 fs transform limit duration for the pulse here is based on the experimental pulse estimate described in section 4.2 for 549 mbar capillary pressure and should correspond to the experimental results in section 4.4.4. Prior to experiments, simulations of short pulses were usually made with 10 fs or 15 fs duration, which is rather similar. The peak intensity was $1.07 \times 10^{18}$ W/m$^2$ in these simulations, which was selected to give similar cutoff energy as in the experiments without plates.

A positive chirp $a_1 = 1.13$ reduces the gate performance, as seen when comparing Figure 4.6(a) with (b). The weighted burst count $n_\mathrm{b}$ increases from 2.5 to 4.5. A negative chirp of the same magnitude is not as bad, it gives $n_\mathrm{b} = 3.4$.

The gate in Figure 4.6(c) is not better than the standard gate, but not much worse either. With $a_1 = 1.13$ it has $n_\mathrm{b} = 4.7$ instead of the standard $n_\mathrm{b} = 4.5$. A possible improvement is that the cutoff energy is one harmonic order higher and that there is only one strong burst in a range around the 21st harmonic when this gate is used. In an experimental spectrum this result would correspond to a broadening or increased background around harmonic 21.

Changing to the thin plate, $d_\mathrm{A} = 1.75$, the weighted burst count of the standard gate remains at 4.5 with $a_1 = 1.13$ and only increases from 2.5 to 2.6 if transform limited pulses are used. The thin plate increased the maximum flux by 58%, so overall it may be preferable. A much thicker plate would not suitable for this short pulse, $d_\mathrm{A} = 4.25$ reduces the flux by 78% and also makes the gate wider.

With blue light added the gate can become very good. The result in Figure 4.6(d) has only one dominant burst. The second strongest burst is the on the right side, which occurs at low energies and has an intensity below a quarter of the main burst's. The weighted burst count is $n_\mathrm{b} = 1.3$. A spectrum of this almost single attosecond pulse should have a decreased modulation depth, or at least very wide peaks.

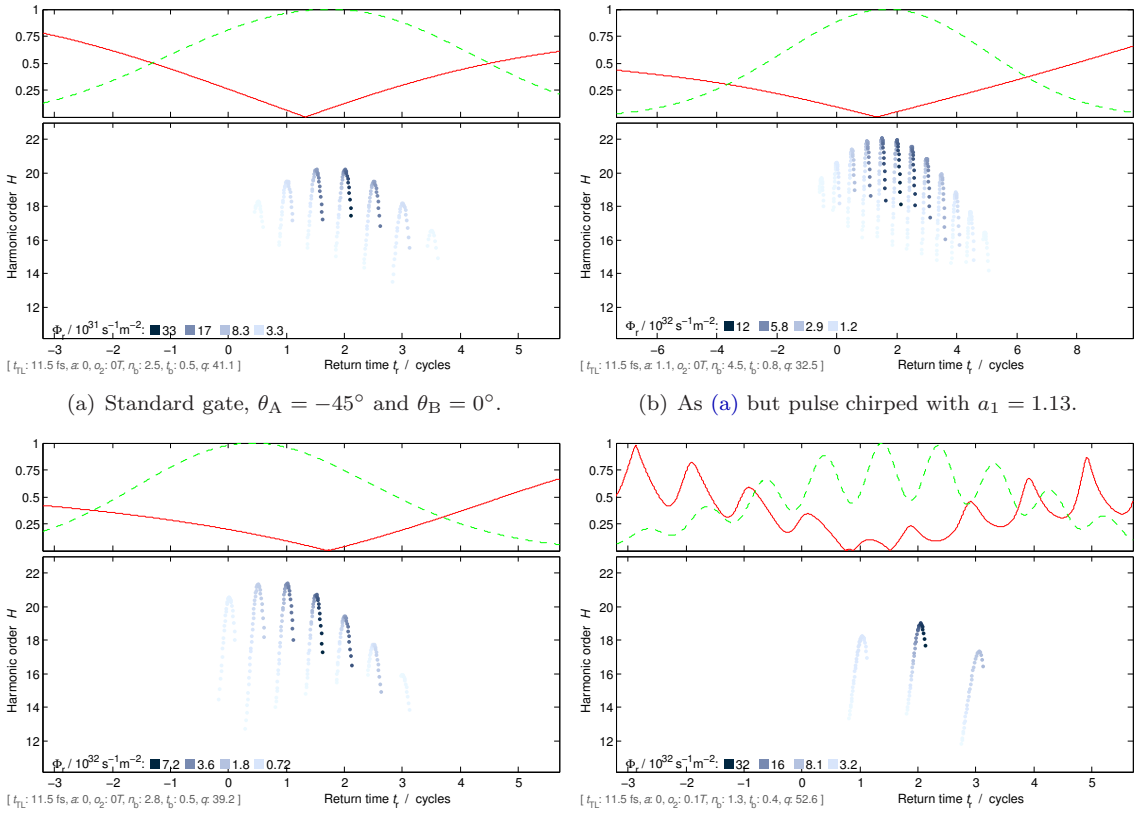


(a) Standard gate, $\theta_\mathrm{A} = -45°$ and $\theta_\mathrm{B} = 0°$.

(b) As (a) but pulse chirped with $a_1 = 1.13$.

(c) A gate with $\theta_\mathrm{A} = -21°$, $\theta_\mathrm{B} = 45°$.

(d) As (a) but with a blue pulse at $o_2 = 0.10T$.

Figure 4.6: Simulations for pulse with 11.5 fs transform limit and $d_\mathrm{A} = 2.5$. In (b) the pulse is chirped to 17.4 fs duration.

Without blue, the second plate can be turned from $\theta_B = 0°$ to 90° with practically identical results, the upper part which shows the ellipticity would look as if the time axis was mirrored in the gate center.

### 4.3.5 Short pulse, 7.88 fs

The short pulse means that the dispersion of the plates increase the chirp parameter of the pulse passing through. $d_A = 1.75, d_B = 0.25$ increases the pulse with transform limit 7.88 fs from chirp $a_1 = 1.29$ (duration 12.9 fs) to $a_1 \approx 1.9$ (duration 15 fs). Figure 2.2 shows how the output duration depends on plate thickness. If the input chirp is negative the pulse becomes shorter, but that change was not as large.

The difference in shape of the spectrogram caused by this chirp increase from dispersion is not interesting enough to illustrate, but the consequences for weighted burst count will be mentioned here. Without plates, the sign of the pulse chirp does not matter much, $n_b \approx 3.5$ when $a_1 = \pm 1.29$. Using the plates $d_A = 1.75$ and $d_B = 0.25$ at angles to not cause any gate, the weighted burst count $n_b$ varies between 4.1 when $a_1 = 1.29$ to 2.9 when $a_1 = -1.29$ because of the dispersion. The transform limited pulse ($a_1 = 0$) is not affected much by these plates, $n_b = 2.1$ both with and without them.

Figure 4.7 shows simulations for the standard gate on the left side and the same custom gate that has been used in previous simulations on the right side, all using $d_A = 2.5$. The top spectrogram is for a pulse without chirp and the bottom spectrogram has the chirp $a_1 = 1.29$.

For the transform limited pulse, the standard gate in (a) has the weighted burst count $n_b = 1.7$ while the non-standard angles $\theta_A = -21°$, $\theta_B = 45°$ in (b) give $n_b = 1.9$. The chirped pulse increases the burst count, yielding $n_b = 3.7$ and $n_b = 3.6$ respectively, but also increases the peak flux 16 respectively 4 times. The standard gate had a particularly low flux without chirp which means it could require a long integration time in experiments. In each case the best carrier-envelope phase, $\Delta_{CEP,1}$, with respect to burst count was selected.

Simulations using the thin plate $d_A = 1.75$ for the the standard gate give no consistent decrease in burst count compared to $d_A = 2.5$, both increments and decrements of 0.3 are easily found. The general trend that a shorter pulse needs a lower $d_A$ may seem weakened, but looking at the photon flux too, its support is restored. The thin plate often has 3 to 9 times as high flux and it was just noted that the thick plate had a rather low flux. As the change in flux rate does not affect the general shape of the spectrograms only the $d_A = 2.5$-plate is presented here.

By adding blue light, sent through the plates with the time offset $o_2 = -0.04T$, an *isolated burst* having $n_b = 1.0$ and $t_b = 0.1T$ is obtained in Figure 4.7(e). Without the plates, the short pulse and blue is enough to give Figure 4.7(f) with $n_b = 1.1$ and $t_b = 0.3T$, which is still close to a single burst.

In the introduction it was stated that being able to select the separation between two or three bursts could also be useful. That aim was not a high priority, and polarization retarder plates alone do not seem to be sufficient to reach that aim. In a short gate that uses blue light, such as Figure 4.7(e), the offset of the blue pulse can determine if one or two strong bursts are generated. A different result is obtained with a strongly chirped pulse, then the polarization state can be made elliptic several times within the pulse envelope, as illustrated in Figure 4.8(a) on page 44. The angles are $\theta_A = -42°$, $\theta_B = 51°$ and the plates are still $d_A = 2.5$, $d_B = 0.25$.

Having several bursts in each gate opening is not ideal, but with blue light it can almost be fixed. Figure 4.8(b) can be said to have one dominant burst per opening. The delay between these openings is not fully adjustable, but with some luck other plate angles and pulse chirps may allow it to be increased or decreased a few multiples of $T/2$. If this would be realized experimentally, it should give a fast modulation on the spectrum because a long burst separation in time is Fourier transformed to a small separation between peaks in energy.

Simulations in this section were made with a peak intensity of $1.03 \times 10^{18}$ W/m$^2$, selected to give similar cutoff energy as in experiments at 803 mbar without plates.

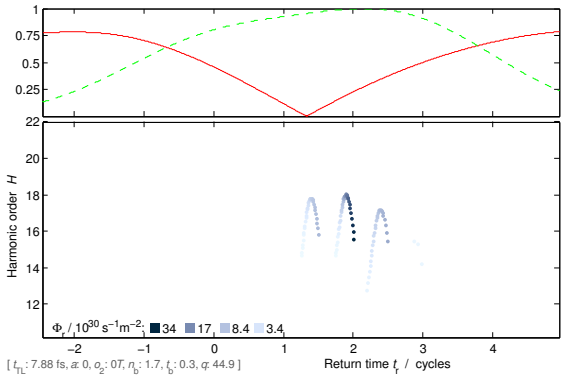


(a) Standard gate with $\theta_A = -45°$, $\theta_B = 0°$ and the best carrier-envelope offset, $\Delta_{CEP,1} = 0.1T$.

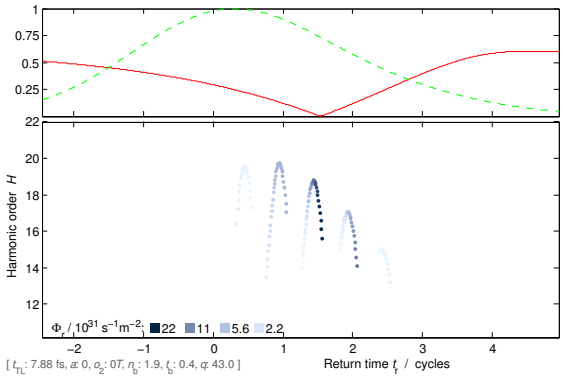


(b) A non-standard gate with $\theta_A = -21°$, $\theta_B = 45°$ and $\Delta_{CEP,1} = 0.06T$.

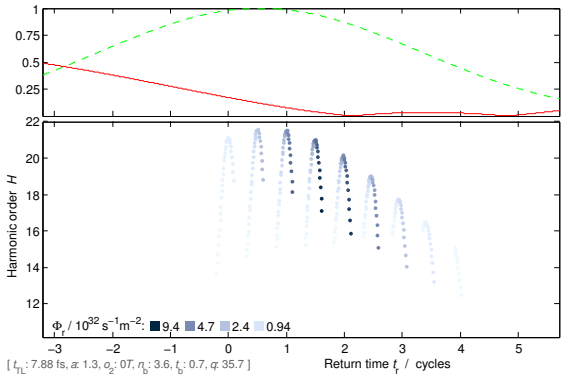


(c) Gate as in (a) but chirped pulse and $\Delta_{CEP,1} = 0$.

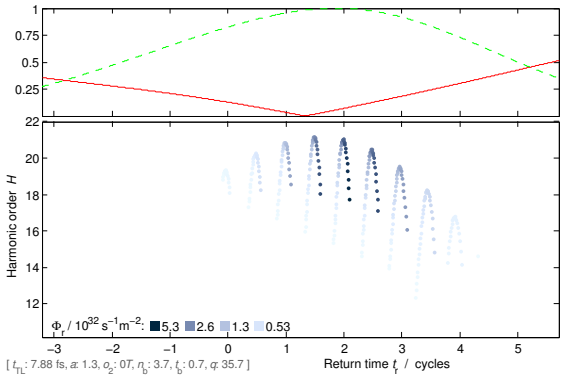


(d) Gate as in (b) but chirped pulse and $\Delta_{CEP,1} = 0$.

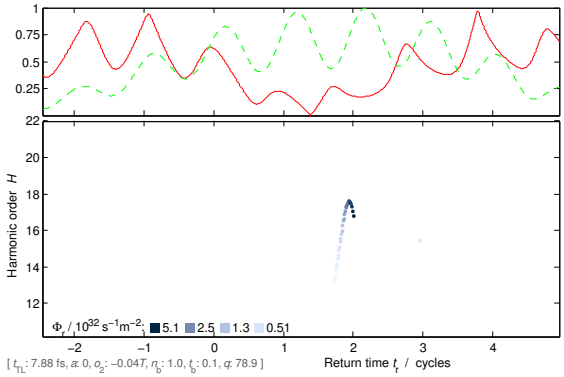


(e) Gate as in 4.7(a) but with blue.

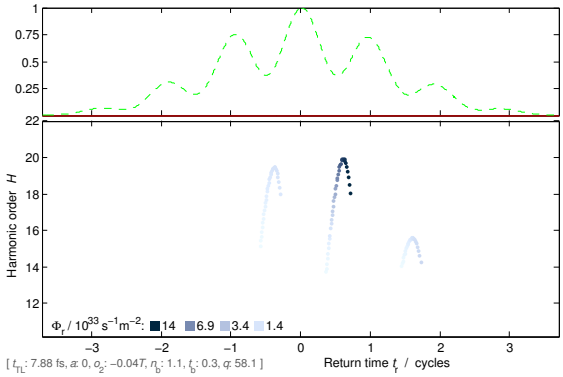


(f) Without plates, thus no polarization gate.

Figure 4.7: Pulse of 7.88 fs transform limit sent through different kinds of gates with $d_A = 2.5$, except (f) which is without plates.
In (c) and (d) the pulse is chirped with $a_1 = 1.29$ which gives a duration of 12.9 fs.
The single bursts obtained in (e) and (f) use a blue pulse at the time offset $o_2 = -0.04T$.

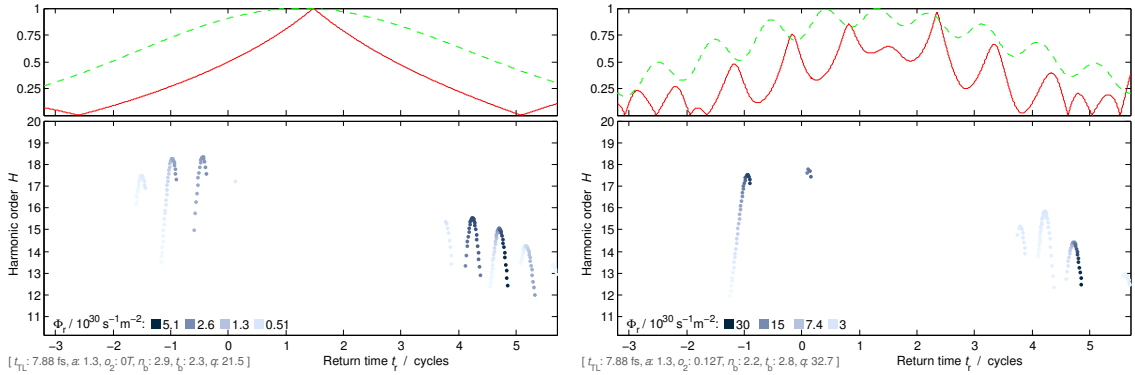


(a) Without blue there are several bursts in each gate opening.

(b) Adding blue light, at $o_2 = 0.12T$ makes one burst dominate in each opening.

Figure 4.8: A double gate can be created with carefully selected parameters and chirp. In this case $a_1 = 1.29$ and 7.88 fs transform limit was used for the pulse.

## 4.4 Experimental use of the plates

### 4.4.1 Calibration

Each spectrum has a number, written after a #-symbol in the figure. The measurements were made on four days, with the first number on each day being #1, #18, #54 and #119. Number #1–53 use the same calibration for the ScanAnalysis program that converts the MBES flight times to an energy scale; the spectral peak positions were similar both days so it seemed appropriate. The wavelength $\lambda_1 = 800$ nm was used for the calibration, although spectra like that of Figure 4.1 often show a local peak more close to 805 nm. Since even the 35 fs pulse corresponds to a spectral width of 27 nm the exact central wavelength was not assumed to be important, mostly the relative energy unit $hc/\lambda_1 = 1$ harmonic order is used anyway but at least in formulas for ionization probability and normalization of the spectrum, an incorrect energy unit will give some error.

Number #54–118 use a new calibration, as the vacuum chambers had been opened, things had been moved and an electronic trigger had been replaced. Measurement number #119 and later were made with the gas capillary and chirped mirrors to get compress the driving pulses. As the SPM-process in the capillary gives a very wide spectrum, it did not seem appropriate to use any of those measurements for calibration, so the same calibration was used here too. The spacing between peaks is typically smaller in these short-pulse measurements, but it fluctuates more within the day than it did when using the long pulse. Whether it would be appropriate to use a different energy calibration for these measurements will be discussed on page 54.

### 4.4.2 Long pulse, no blue

The "long" pulse is the direct output from the laser system, which has a transform limit of about 35 fs. If a single quarter wave plate is placed at $d_A = -45°$ the driving pulse should be circularly polarized (CP) and give no HHG output. Two of the three CP measurements made really gave zero counts on the spectrometer during 15 seconds, in the third there were 23 counts in 50 seconds, which still is a count rate of only $10^{-3}$ times that in Figure 4.9(d). This demonstrates the total reduction of HHG output caused by circular polarization that was earlier claimed using Figure 2.5 on page 26.

Some notes regarding the results in Figure 4.9:

- The widest peaks are found in Figure 4.9(c) and (a). The singleness-value[3] is better for (a), but visually I think the peaks and background in (c) look a little better.
- Nevertheless, the difference is rather small between the four spectra presented here.

[3] See section 3.5 for the definition of $s$ and other result properties.

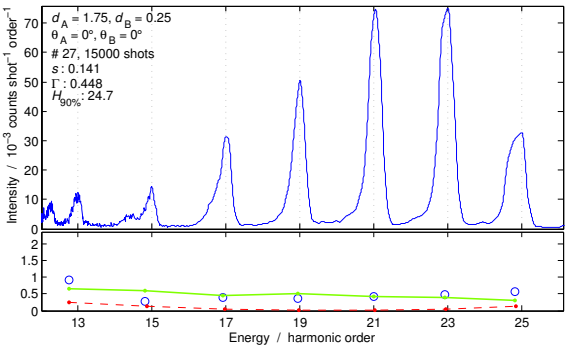


(a) Plates oriented to not cause any polarization gate, $\theta_A = \theta_B = 0°$.

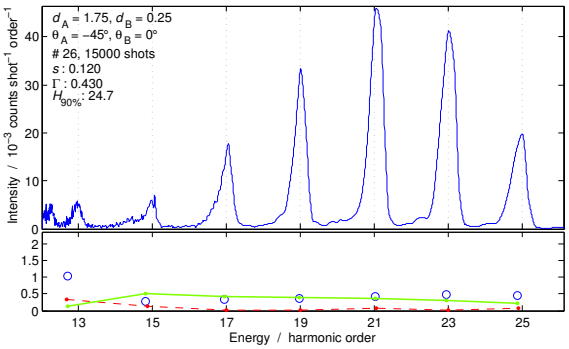


(b) Standard gate with the thin plate, $d_A = 1.75$.

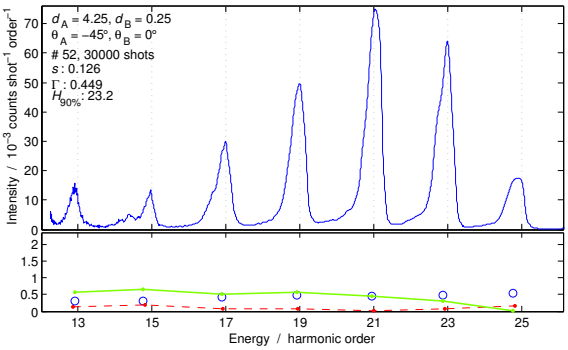


(c) Standard gate with the thick plate, $d_A = 1.75$.

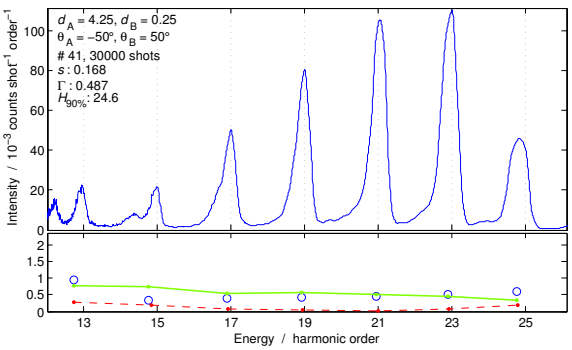


(d) $\theta_A = -50°$, $\theta_B = 50°$ and $d_A = 4.25$ gives good intensity and peak width.

Figure 4.9: Spectra for the long pulse, without blue light. The diagram below each spectrum contains information about the peaks, derived from the spectrum as defined in section 3.5:

- ○ Full width at half max of each peak, $\gamma$ / harmonic order.
- —•— Background level[2]around each peak, $2.9 \times \sqrt{\beta_v}$ [dimensionless].
- – •– Absolute deviation in peak position, from expected (odd) integer, $|\xi|$ / harmonic order.

The aim is to have large width and high background level. The deviation is expected to be zero if the wavelength and calibration are correct.

- Also among the non-displayed spectra, the relative peak width did not get wider than displayed here and not much narrower either. On the other hand, it was possible to find settings where the entire spectrum decreased in intensity, and therefore got more noisy.

- By moving the compressor grating in the laser system, the chirp of the input pulse can be adjusted. It was found that this parameter both affects the general intensity and the distribution among the peaks, seemingly altering the cutoff order. A change in laser intensity would probably also have this effect, so it is possible that we were partly just observing that a misaligned grating makes the laser pulse weaker.
  Up to spectrum number #17, the setting 13.85 mm was used[4], while the best focus in air was obtained with 13.77 mm. The next day 0.10 mm steps between 13.35 and 14.15 mm were tried and 13.65 mm was found to be the best, in a few cases rivaled by 13.75 mm. Since then mainly 13.65 mm was used for the remaining long pulse experiments, and to make figures comparable mostly such spectra are displayed here.

- $\theta_A = -50°$, $\theta_B = 50°$ in Figure 4.9(d) turned out to work well. The singleness-value 0.168 is the highest among the results for long pulse without blue, and the peak widths are equally high as in 4.9(a) and (c). The agreement with simulations is questionable in

[4]The grating position is set via a millimeter screw. As the corresponding chirp is not known, the unit "mm" is kept.

detail, because in simulations the standard gate is more narrow than the gate created by $\theta_A = -50°$, $\theta_B = 50°$ and was therefore expected to have a higher singleness value. On the other hand simulations show 10 times as high peak photon flux with the non-standard setting and a difference in that direction was observed experimentally, although the experimental increase in peak intensity was a more modest 45%.

- The conclusion from simulations that the standard angle pair $(\pm 45°, 0°)$ is not the only possibility to get reasonable results may still be valid, but experimentally no significantly better setting was noted with the long pulse.

### 4.4.3 Long pulse, with blue

#### Introduction

Results obtained when using both the fundamental and a frequency doubled, blue pulse are shown here. After the interferometer (see section 3.3.2) the polarization axis of the blue was $\theta_2 = 0°$, just as for the red. The plates were either placed after the interferometer, so that both pulses passed through them, or placed in the red interferometer arm to avoid altering the blue pulse.

By sweeping the delay of the interferometer one should be able to make the height of the spectral peaks at even orders oscillate, as hinted by the varying number of bursts in Figure 4.4. Results for such scans over $o_2 - o_1$ to compare with the fine tuning in simulations will not be reported, the few measurements that were made were not strongly modulated and the first priority was to see if the gating would work, before trying to compare the details with simulations.

The delay was set to give strong even-order peaks, possibly also preferring a high cutoff, when the plates were set to not alter the polarization. As the plates were in place, this ensured that the overlap existed in the generation chamber (*i.e.* correcting for difference in group velocity for the two colors). It was necessary to keep the plate surfaces normal to the beam, sometimes when the plates had been rotated to change $\theta$ small changes in other rotation directions needed to be corrected to keep the blue overlap good.

To measure the chirp and duration of the fundamental pulse a "Grenouille" instrument [33] was used. We did not seem to get it to function properly, and it seldom gave any reasonable value. Eventually we got some values between 40 fs and 50 fs (transform limited) which would mean that the fundamental pulse was longer than the expected 35 fs. As the Grenouille did not seem reliable, and the difference suggested is not enormous, the theoretical 35 fs value is still used for simulations concerning the long pulse.

#### Results and comments

In Figure 4.10 (the left column) both the red and blue pulses are sent through the retarder plates and in Figure 4.11 (the right column) only the red was sent through the plates.

Figure 4.10, with both pulses trough plates, will be presented first. The ratio of blue and red mean pulse energy was kept at the maximum, 0.31 mJ/2.16 mJ $\approx$ 14% before the retarder plates. As the pulses probably have different duration and focusing characteristics, the latter due to their different wavelength, it is not obvious what the intensity ratio will be in the focus where harmonics are generated. 10% as intensity ratio at focus generally would be considered a high value according to previous work at the department and in my simulations more than 5% usually did not improve the temporal confinement.

The use of maximum experimental blue ratio was decided experimentally because it made the even order peaks almost as high as the odd, indicating that only one burst was generated per cycle. Limiting the blue beam (and pulse energy) with an iris made the even peaks lower, which is interpreted as generating an undesired weak burst also in the other half of each optical cycle. Due to the simulations where 5% intensity was sufficient to eliminate every second burst, it seems the experimental intensity ratio in focus was much lower than the 14% energy ratio before the plates.

[4] After taking the square root and rescaling to fit in the same diagram. Using the square root helps make differences visible among the many results where $\beta_v$ is small.

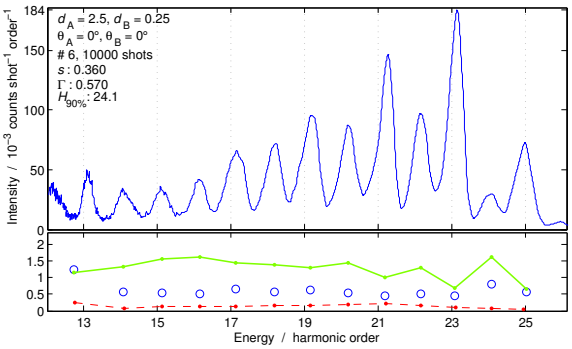


(a) No polarization gate, $d_A = 2.5$.

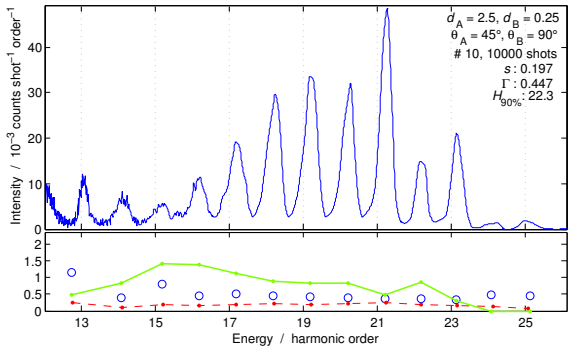


(b) Standard-like polarization gate with $\theta_B = 90°$ and $d_A = 2.5$.

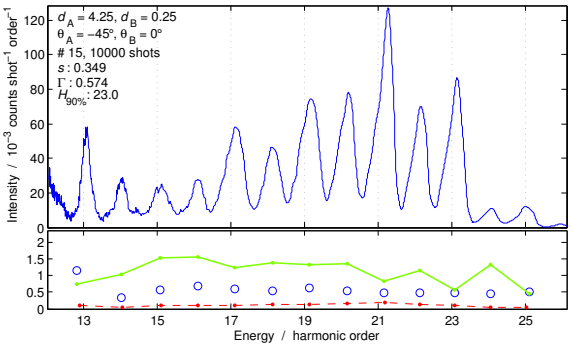


(c) Standard gate with $d_A = 4.25$.

Figure 4.10: With red and blue pulses, both sent through the retarder plates.

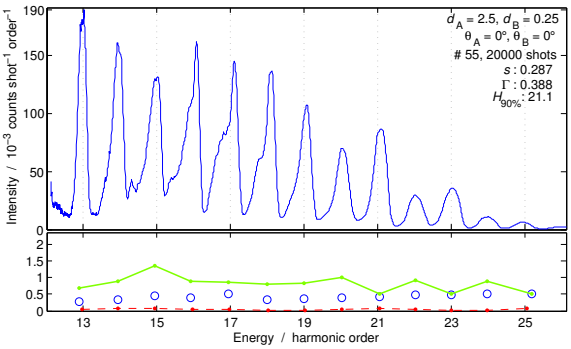


(a) No polarization gate, $d_A = 2.5$.

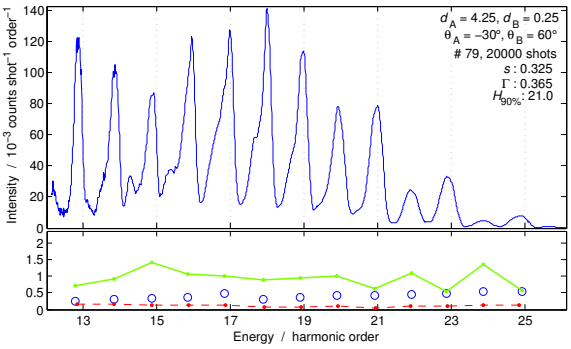


(b) Plates oriented at $\theta_A = -30°$ and $\theta_B = 60°$, with $d_A = 4.25$.

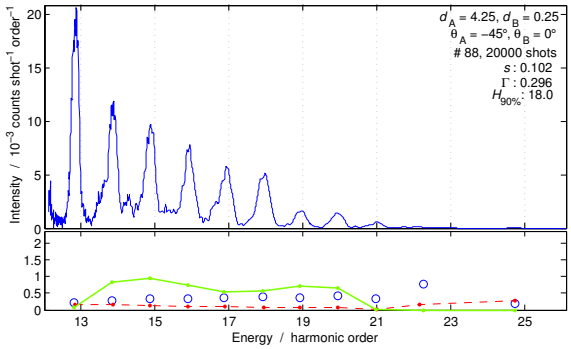


(c) Standard gate with $d_A = 4.25$.

Figure 4.11: With red and blue pulses. Only the red was sent through the retarder plates.

Observations concerning Figure 4.10:

- Although no spectrum without plates is presented, it was very similar in shape to Figure 4.10(a) where the plates are oriented to not alter the polarization state. Regardless of their orientation the plates give dispersion, but it seems to be negligible with the long pulse.

- Figure 4.10(c) has slightly wider peaks, $\Gamma = 0.574$ harmonic order compared to 0.570 order without gating in Figure 4.10(a). 4.10(a)

- Looking at the background ratio or "singleness" $s$ (which also weighs in the widths of peaks), Figure 4.10(a) without any gating of the field (LP all the time) has the highest value presented, better than the standard gate at either plate thickness.

- The spectrum[5] with the best values for both properties, $\Gamma = 0.584$ order and $s = 0.389$, did use a gate like that in Figure 4.10(c) except that $\theta_B = 90°$. The differences caused by gating here is is near the level of the uncontrolled variation, so not much conclusions can be drawn, except that far more than one burst is generated regardless of these gates.

- The lower background between peaks in Figure 4.10(b) is reduced compared to the other two spectra presented, as is the peak width. For harmonic order 19 and above the change seems significant compared to the random variations, which would mean that the gating works better with $d_A = 4.25$ than with $d_A = 2.5$.

- The peaks appear *asymmetric*, with a tail towards low energy. They clearly have a less steep descent on the low-energy side than on the high-energy side. The reason for this is unknown, but one hypothesis is that it is an artifact from the electron counter in the spectrometer, where it would mean that the rise-time is shorter than the fall-time in the current given by the multichannel plate or the detector.

By placing the retarder plates in the red arm of the interferometer, so that the blue pulse was undisturbed, the results in Figure 4.11 were obtained. These spectra were collected another day, with slightly different generation and detection pressures, so comparisons should not be made to Figure 4.10 regarding absolute intensity or cutoff order (measured as $H_{90\%}$).

The energy ratio between blue and red in Figure 4.11 was about 0.23 mJ/1.82 mJ $\approx$ 13% before the retarder plates, which is still similar to the 14% in Figure 4.10. A measurement was also made after the plate, yielding 0.22 mJ/1.14 mJ $\approx$ 19% when oriented to not cause any gating. The large loss of red energy with the plates is probably caused to a large degree by the transparent part of the plates being 9 mm in diameter, and due to tight space not fully centered when the plates were put inside the interferometer, while the red beam probably had energy outside that area too.

Concerning Figure 4.11, the following can be noted:

- The asymmetric shape of peaks is even more pronounced than in Figure 4.10.

- Here the spectrum of Figure 4.11(a), without gating, is much better than the standard gate in (c). None of the attempted standard gates gave good results, however, by changing (c) to use $\theta_B = 20°$ the background level and peak widths were about 85% of the values in (a), while the intensity was 32%. Changing the compressor grating angle did not help.

- By using a non-standard set of angles in 4.11(b), $\theta_A = -30°$ and $\theta_B = 60°$ which was one of the suggestions from simulations, the peak widths dropped by 6% compared to (a), which was not intended, while the singleness value (mostly based on background ratio) increased by 13%. It is still dubious whether this is a significant improvement over the non-gating setup, but it is certainly an improvement over the standard gate with the same plate thickness. As the polarization gate from these plate angles is not particularly narrow in simulations, it is possible that some of the improvement comes from other factors, such as the blue pulse offset which is affected by the plate positioning but not precisely controlled.

### Offset of the harmonics

The peaks in spectra number #1–15, including Figure 4.10, were offset by on average +0.13 harmonic order (standard deviation 0.08) from integers in the calibration used. The red points and dashed lines below spectrum figures show the absolute value, $|\xi|$, of these deviations. Spectra #16-18 taken with $d_A = 4.25$ and $d_A = 0$, without the blue pulse overlapping, does not show this shift so either it disappeared before the end of that day or it was related to the blue light. As these spectra use the calibration from the second day, the offsets there were checked and found to be −0.11 order (standard deviation 0.07) but without the blue pulse. The third day, with blue and another calibration, the offsets were smaller.

[5]That spectrum is not displayed, due to high similarity with Figure 4.10(c). It was deemed more interesting to keep Figure 4.10(c) for comparison with 4.11(c).

As the offsets seem independent of energy in spectra where they are visible, it does not indicate the use of an incorrect fundamental wavelength for calibration or that the time spacing between bursts would have changed. Either it is some other calibration artifact or it is a real result, perhaps from the asymmetric nature of the spectral peaks when using blue. A changed carrier-envelope offset between attosecond bursts could give such a shift, see section 3.4.2, but as the laser is not phase-stable it seems unlikely that the effect could be observed if it was related to carrier-envelope offset.

### 4.4.4 Medium-short pulse, 549 mbar

The output of the SPM-capillary that gives the shorter pulses always fluctuated quite a lot. By turning off the air conditioning and shielding parts of the beam path leading in to the capillary from air flow, the stability increased but was still rather low.

The highest count rates when not using any retarder plates was found for pressures about 530 mbar to 670 mbar. These are also the pressures where the capillary output reached the peak energy of 0.60 mJ/pulse. The five chirped mirrors that reduce the chirp to actually achieve the compression are positioned after the place where the mean pulse energy was measured. Because of low reflectivity, the energy dropped by about 40% after the mirrors when the pressure was 803 mbar. The decrease may have been a bit less for 549 mbar which has a narrower spectrum, but no comparable measurement was made there.

It was found that a compressor grating setting of 13.50 mm gave high power and a "good" SPM-spectrum from the capillary, but also that changing the laser compressor was too coarse to fine tune the spectrum and probably the chirp. At the higher pressure, 803 mbar, the chirp in the "Dazzler" acousto-optic pulse-shaper, placed early in the laser system, was found useful to tune the output. For 549 mbar pressure the default Dazzler setting was used, so it is not known if these results could have been improved by tuning the chirp.

From section 4.2, the transform limit duration of the input pulse is estimated to be between 10 and 15 fs. The simulation uses 11.5 fs and the chirp $a = 1.13$ (chirped pulse duration 17 fs), which are the values of the curves that were fitted to measurements there.

- In all measurements where the capillary was used, the spacing between peaks is decreased and peaks not occur at odd integer harmonic orders – compare Figure 4.12 to 4.9. The offset from integer orders, $\xi$, thus follows an approximately linear trend towards more negative values. As it is positive for low orders, the absolute value $|\xi|$ shown with the red points below each spectrum has a V-shape. The linear trend indicates that the spacing is constant, although smaller than the expected 2 harmonic orders. Possible causes are discussed on page 54.

- The three gates used in Figures 4.12(b)–(d) all have narrower peaks and lower background than the non-gated version in 4.12(a). The difference in peak width is not very large, but this is still contrary to the desired effect of polarization gating.

- An even better result was obtained with $d_A = 2.5$ about an hour before the spectrum of Figure 4.12(a) was recorded, having a singleness-value of 0.435 instead of the 0.254 shown here with the plate $d_A = 1.75$. The reason for not using the best spectrum for comparisons in this report is that the alignment of the laser beam into the capillary had been changed in between[6] it and all other spectra presented. The very good performance in the omitted spectrum may have to do with a different pulse duration, chirp or energy in the SPM-compressed pulse if not caused by the choice of plates. The experience from longer and shorter pulses is that this change in plate thickness, without gating, should not alone cause such different spectra.

- Among the gates, the non-standard setting $\theta_A = -21°$, $\theta_B = 45°$ and $d_A = 2.5$ which was attempted based on simulations has higher cutoff energy $H_{90\%}$, somewhat higher background ratio (green line below spectra) and almost as wide peaks as the standard gate in (b). This is in agreement with the simulation in Figure 4.6(c) and the remark on page 41.

- No major difference was noted between having $\theta_B = 0°$ or 90° in the standard gate with $d_A = 2.5$, which agrees with the simulation remark on page 42. Figure 4.12(c) shows the latter case.

[6] The beam pointing was changed in the process of fixing a problem with the program that corrected for slow beam drifts.

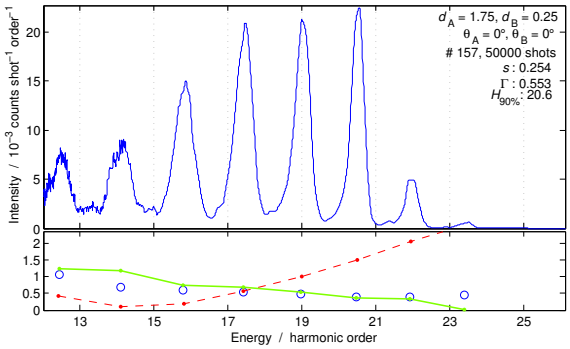


(a) No polarization gate, $d_A = 1.75$.

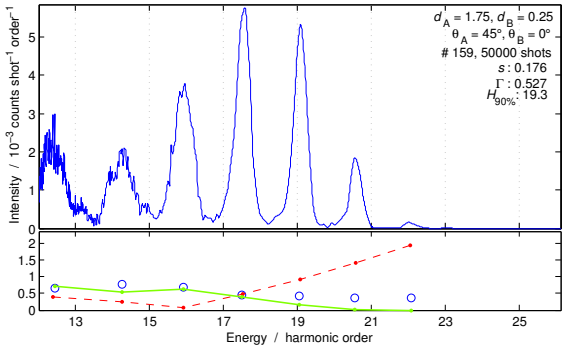


(b) A standard gate with the thin plate, $d_A = 1.75$.

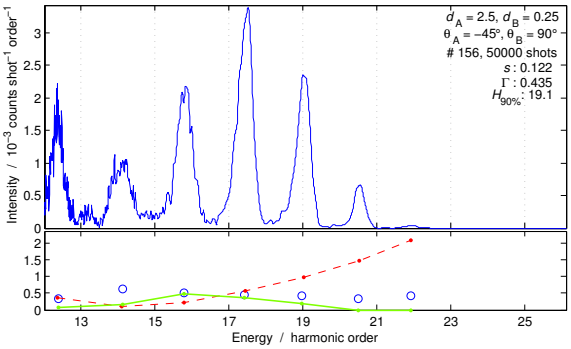


(c) A standard-like gate with $d_A = 2.5$ but $\theta_B = 90°$.

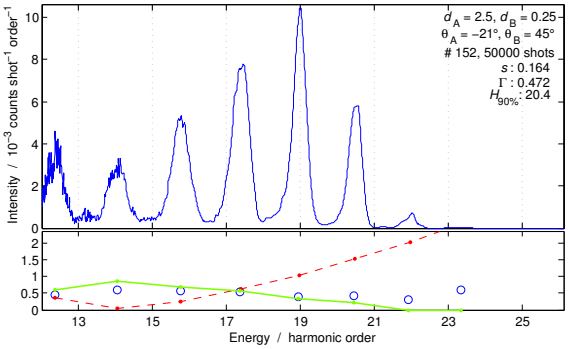


(d) Non-standard gate, having $\theta_A = -21°$, $\theta_B = 45°$ and $d_A = 2.5$.

Figure 4.12: Spectra with the driving pulse SPM-compressed at 549 mbar capillary pressure.

### 4.4.5 Short pulse, 803 mbar

The average energy per pulse from the SPM-capillary was a little lower at this pressure, 0.48 mJ to 0.50 mJ, and approximately 40% of that is lost in the chirped mirrors that compress the pulse.

After several spectra had been collected at the pressure 803 mbar, the chirp of the pulse before SPM-compression was adjusted using the "Dazzler" acousto-optic pulse-shaper. It was found that an increase in chirp from 11 538 $\text{fs}^2$ to 12 538 $\text{fs}^2$ made the harmonic peaks wider. The good Dazzler-setting is used for all presented spectra at this pressure, while a spectrum where the old value was used is shown with dashed lines in Figure 4.13(a).

The transform limit duration of the pulse at this pressure is 5.7 fs if the spectral full-width at half-max of Figure 4.1(b) is used and the pulse is assumed to be Gaussian in time and energy. As the SPM-spectrum is not at all Gaussian, that estimate is not valid. By fitting a curve to estimates using the SPIDER-measurements and other methods at several pressures in section 4.2, another estimate is found. The transform limit from this fit is 7.88 fs and the chirp parameter is 1.29 (in absolute value), which means the chirped pulse has a duration of 12.9 fs. Note that all digits given here are not significant, the variation in these measurements is large as seen in Figure 4.2. The latter estimate was used when making simulations for conditions that should correspond to the experiment.

- Also at this capillary pressure, the energy spacing between harmonics is less than the expected $2\hbar\omega_1$. See page 54 for the interpretation.
- As seen when Figure 4.13(a) is compared to 4.12(a) and 4.9(a), the use of a shorter pulse is enough to widen the peaks quite a lot even without plates.
- Plates $d_\text{A} = 1.75$ and $d_\text{B} = 0.25$, oriented to not form a polarization gate are inserted in Figure 4.13(b), which further improves the spectrum. This setting has given the three spectra with the widest peaks, as measured by $\Gamma$ and $s$, among all collected spectra. $\Gamma = 1.553\hbar\omega_1$ is a dramatic improvement over $\Gamma = 0.553\hbar\omega_1$ in Figure 4.12(a) which has identical settings, except for the Dazzler chirp and the capillary pressure.
- If the $d_\text{A} = 1.75$-plate is turned to form a standard gate, as in Figure 4.14(a), the peak width average decreases to $\Gamma = 1.263$ and the total intensity is reduced to a third.
- With $d_\text{A} = 2.5$ instead, and the angles that should make this half wave plate work like a standard gate, the result seen in Figure 4.14(b) is worse than for the previously mentioned gate. Particularly, the cutoff energy $H_{90\%} = 17.7\hbar\omega_1$ is low.
- The non-standard angles $\theta_\text{A} = -21°$, $\theta_\text{B} = 45°$ in Figure 4.14(c) give a significant improvement over the standard-like gate in 4.14(b) that used the same plate thickness. It is also better than any fully standard gate (that has $\theta_\text{B} = 0°$). According to the values $s = 1.224$, $\Gamma = 1.432$ and $H_{90\%} = 19.0$ it is not as good as 4.13(b), and the intensity is only about a sixth, but visually I think it looks more like continuum spectrum (less modulated) than 4.13(b).
- After having acquired a spectrum with the plates at different angles and returned, a repeated measurement with $\theta_\text{A} = -21°$, $\theta_\text{B} = 45°$ was made. It is shown with dashed lighter lines, overlaid in Figure 4.14(c). The reproducibility is surprisingly high with respect to the noisy look of the spectra, but the long acquisition time (2–2.5 minutes), that was necessary to get sufficient signal, may contribute to the high background and reproducibility via averaging effects.
- In simulations on page 42 it was mentioned that the standard gate gives 3 to 9 times as high peak flux with $d_\text{A} = 1.75$ as with $d_\text{A} = 2.5$. Experimentally, the intensity has dropped approximately 5 times between Figure 4.14(a) and (b) which is in good agreement.

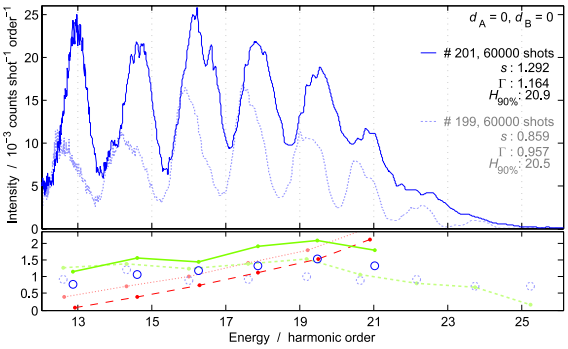


(a) The optimal Dazzler setting (solid, dark lines) compared to the suboptimal setting (dashed, faint lines), in both cases without plates. The modulation around harmonic order 23 practically disappears with the optimal setting.

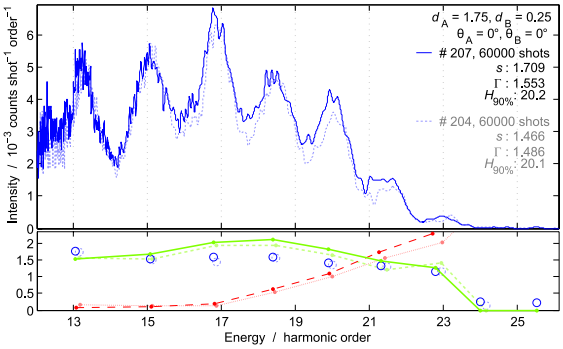


(b) Plates oriented such that they should not cause any gate, $\theta_A = 0°$, $\theta_B = 0°$. A second measurement is overlaid with faint colors to indicate the reproducibility.

Figure 4.13: Spectra without polarization gating at 803 mbar capillary pressure.

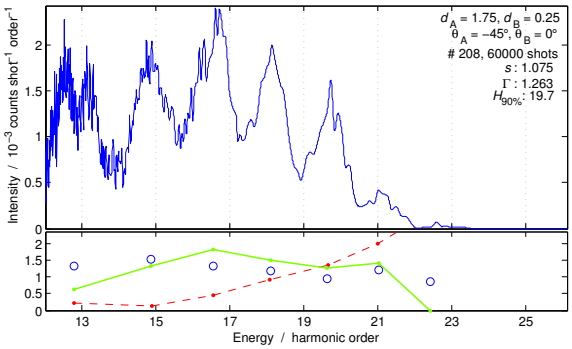


(a) Standard gate with $d_A = 1.75$.

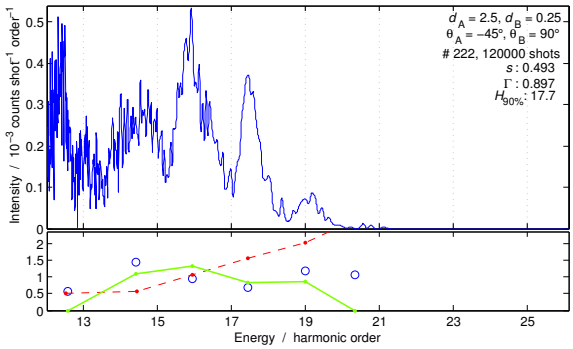


(b) Standard-like gate with $d_A = 2.5$ and $\theta_A = 90°$.

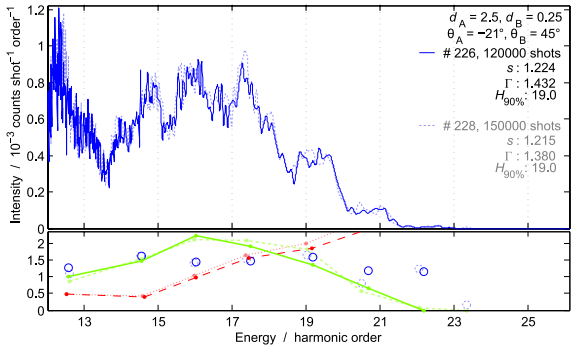


(c) A non-standard gate, $\theta_A = -21°$, $\theta_B = 45°$ and $d_A = 2.5$. To allow the reproducibility to be judged, a second measurement is overlaid with dashed lines and faint colors.

Figure 4.14: Spectra with polarization gating at 803 mbar.

# Chapter 5

# Discussion

## 5.1 Wavelength of the input pulse

Figures 4.12–4.14 show clear trends in the peak position deviations from odd integer orders. A new energy scale corresponding to this changed spacing would still put the peaks at odd integers, but as a calibration based on 800 nm light from the day before short pulses was used the peaks have a different spacing and position. From the MBES-spectra, the energy spacing is found to be lower, corresponding to longer temporal spacing and longer wavelength if the calibration is correct. The reason for a different temporal spacing could either be that the wavelengths hitting the gas are longer or some effect occurring with short pulses as suggested on page 33.

Assuming that it was a different fundamental wavelength that caused the shift, and that the calibration is correct for 800 nm, then the wavelength causing the harmonic generation is longer than 800 nm, as concluded previously, between 960 and 1010 nm (average 983 nm) judging by the spacing in MBES-spectra for capillary pressure 549 mbar. Looking at the spectrum of the driving pulse in Figure 4.1(a) at the same pressure, the dominating wavelength is actually lower than 800 nm. There is also some energy above 800 nm, but not above 950 nm, which makes this explanation inconsistent.

A completely different explanation is that as the MBES-calibration comes from a different day and the setup had been re-aligned between them, the calibration does not apply. If a calibration is made from results with short pulses at the lowest pressures (387 and 507 mbar), then the peaks for 549 mbar fit nicely to odd integers, the estimates based on peak positions give 780 to 850 nm and an average of 800 nm, *i.e.* no shift on average although some unexplained variation. For spectra using 803 mbar the shifts are not as high as with the old calibration, but still deviate considerably from odd integers.

This suggests that the effect, at least for the pulses produced with 549 mbar, was caused at least partly by a calibration error. It is quite possible that some distance changed when the experiment setup was re-aligned between the calibration and the use of short pulses. Thus the energy scale and peak width measurements should not be compared with those from long pulses.

It would of course have been better if a calibration measurement with the MBES had been made without the capillary or with the capillary pressure even lower, while keeping the same alignment and MBES position as used for short pulses. The lowest pressure that a MBES-spectrum was saved for is 387 mbar but it does not have well-defined peaks above order 18 and looks noisy overall, so with the existing measurements it is not possible to do a truly low-pressure calibration for the capillary setup. Using a higher pressures means the fundamental pulse has a very high bandwidth, more than 60 nm, and irregular spectral profile. With such a spectrum it is not obvious what nominal wavelength should be used for the calibration and definition of harmonic order, which makes the precision and usefulness of a high-pressure calibration questionable.

The aim of this project was to reduce the number of bursts in the attosecond pulse train, which is judged by looking at how narrow the peaks are or how deeply the MBES-spectrum is modulated. That judgment can be made equally well even if the energy calibration is

wrong, so it was not deemed necessary to present spectra with the alternative calibration too.

## 5.2 Reproducibility

There are several factors in the experiments, such as the exact generation and detection pressures which were not controlled to more than about one significant digit and differed some between hours and days, that make most comparisons a bit uncertain.

With the high number of cases that was tested, and probably was necessary to find out how the plates behave in different configurations, there was not time to check the reproducibility of every spectrum. Some of the best overall results, *i.e.* Figures 4.13(b) and 4.14(c), were measured three and two times respectively and showed good reproducibility. It could be caused by the long acquisition times (1 to 2.5 minutes, $60 \times 10^3$ to $150 \times 10^3$ shots) that will average over much of the fluctuations of the capillary and perhaps not really represent a single shot spectrum.

## 5.3 Simulations

As illustrated in Figure 4.7 the chirp and its sign will matter for the gating quality, but in section 4.2 only a very rough estimate was made, without sign. As the simulation results will differ substantially depending on what chirp and intensity you use, while these properties were not well determined experimentally it is not relevant to compare details of the short pulse simulations with experiments.

Regarding the long pulse, the random variations were smaller between experiments, but the peak widening possible to achieve was also very small which makes it hard to distinguish from noise. At least some basic properties such as higher $d_\mathrm{A}$ being better for a longer pulse seems to agree between simulation and experiment, but the maximum $d_\mathrm{A} = 4.25$ that was possible with the plates used (selected aiming at short pulses) is still far below the $d_\mathrm{A} \sim 10$ that seemed good in simulations, so the small effect of the plates was not totally unexpected.

## 5.4 Short pulses

With short pulses things started happening in experimental spectra, and at least some observations that agreed with details of the simulations were observed, *e.g.* the increased cutoff order with a particular kind of gate mentioned on page 50.

The peaks got much wider when the capillary pressure was 803 mbar and the Dazzler setting was optimized. Presumably this means that the number of emitted bursts has been reduced, though there could be averaging effects that cause smoothing if the SPM-spectrum fluctuates much on the millisecond timescale, which is not avoidable with the experimental setup used. See section 3.4.2 for the explanation of this effect.

The main issue with averaging is that when the driving pulse is very short, certainly when less than three optical cycles (8 fs), an extra broadening and background in spectra could be produced. As the amount of broadening has not been calculated for our experimental setup or for the use of a polarization gate, is is unknown.

Even with fluctuations I think the most probable explanation is that some significant, real temporal confinement of the high harmonic generation was achieved, although questionable how much the polarization gate contributed. In the best results the background level is above 50% around some harmonic orders and about 40% when averaged for all orders. If Figure 4.13(b) which used the short pulse but plates oriented to not make a gate represents the ordinary background level including averaging effects, then the much less modulated spectra in Figure 4.14(c) where a gate was used seem to have produced even fewer bursts. Those gate spectra are quite noisy as the count rates are low. The long acquisition time may be a reason to be moderate in the interpretation. It is likely that the individual shots varied in intensity, because such fluctuation was often observed with the bare eye which averages over a shorter time than the acquisition times used for the MBES.

There are other good spectra which have much higher count rate, and show very little noise. Among the short pulse spectra Figure 4.13(a) is the best such example. The background level averaged by peak area is 33% and the modulation that exists has wider peaks than in the completely artificial spectrum of Figure 3.4 where three bursts were used. A very generous interpretation would then be that there were on average less than three bursts generated, and that 33% of the shots gave only a single burst (the continuum background). As previously mentioned, because of averaging there may have been a few more bursts in reality.

The interesting, single-burst like results, with blue light that were possible in simulations even using pulses corresponding to the low capillary pressure were never observed experimentally. To make sure that the short pulses were as intense and undispersed as possible, the beam had not been sent through the interferometer when post-compression was used. There was not time to re-align everything through the interferometer when finally attempting to use blue light in combination with the post-compressed pulses, so only a few attempts were made by putting the KDP-crystal that gives the blue light directly in the beam before the plates. Without the interferometer to turn the blue polarization it would have $\theta_2 = 90°$, which according to simulations should be usable too. As the alignment and temporal overlap possibilities of the interferometer were missing it was difficult to search for an overlap between red and blue, and we did not seem to find it.

Revised measurements of transmission through the interferometer and chirped mirrors showed that most of the loss was in the mirrors, which are necessary to compress the pulse, so it may well have been possible to also use the interferometer an thereby increase the chance of using blue together with short pulses.

## 5.5 Conclusions

For the long input pulse, the polarization gating hardly made any improvement. At least no improvement significantly above the unexplained or random variations between measurements. This agrees with simulations, where the used plates do not give any dramatic temporal confinement of the high order harmonic generation. A thicker retardation plate than $d_A = 4.25$ would be necessary to make notable gating with the long pulse.

The simulations showed some possibilities of getting down to a few bursts with long pulses if high retardations and precisely selected chirp were used, but it then meant that a lot of the intensity would be lost. Considering the experimental limitations in peak intensity and chirp control it was decided to try to use shorter pulses instead.

In experiments using blue light with the long pulse there was some support for the hypothesis that higher $d_A$ gives a more narrow temporal gate, but the spectral differences caused were still near the noise level. The hypothesis can at least not be falsified from these experiments.

The simulations, and to some extent experiments, have shown that the plate retardation $d_A$ need not be a quarter wave plate, which seems to have been assumed in previous work. Half-wave plates and intermediate retardations also work, but are believed to give different polarization directions for the generated bursts. In the experiments, except for the very shortest pulses, the standard setting was the best or among the best, so it does not seem revolutionizing to use other retardations or angles.

As we seldom got stable SPIDER measurements of the chirp when using short pulses there are still large uncertainties about what transform limit and initial chirp the pulses had, so it has currently not been meaningful to design plates or angles overly detailed in theory. Though a list of settings to try was decided based on simulations, it seems it could have been almost as rewarding experiment-wise to just turn the plates step by step and observe the results. That would of course have been even more time consuming and not very informative if the random fluctuations were high. The empirical work did eventually show that the configuration $d_A = 2.5, d_B = 1.75, \theta_A = -21°, \theta_B = 45°$, which was on the list of simulated suggestions, gave a spectrum with very little modulation (high background level), which was the aim.

For the short pulses, the peaks are wide and the background high even without plates and with plates that should not alter the polarization state. It seems that using a short

input pulse is the most efficient way to reduce the number of bursts in the attosecond pulse train, but some extra widening was observed when using some of the gates. However, the gates also reduce the observed intensity much, especially with the shortest pulses. A guess is that the number of bursts was below three on average, and approximately one for 10% to 33% of the shots in the best measurements, if it is at all possible to draw conclusions from these spectra averaged over rather long time with a phase-unstable laser.

The best MBES-spectra show continuum background levels similar to that in a previous work where a 5 fs driving pulse without polarization gating was used to get a single or double burst [20, fig. 3], but the noise is higher in our spectra and our laser does not have a stable carrier-envelope phase.

There seems to be some correlation between simulations and experiments in several aspects of gate properties, such as when large or small $d_{\mathrm{A}}$ is suitable, cutoff energy and flux reduction in some gates, but the agreement is nowhere near complete. Several custom gate designs that appeared decent in simulations did not give any notable widening of harmonics in experiments, but as there were several uncontrolled parameters and the experimental input pulses were not completely characterized it is not reasonable to expect perfect agreement.

No results were obtained with blue light at $\theta_2 = 90°$. A few attempts were made, but probably not given enough time. With $\theta_2 = 0°$ the possibility to put plates in the red arm of the interferometer was investigated, compared to put the plates after the interferometer. The widest peaks were measured with the plates after the interferometer, but as the measurements were made on different days, separated by at least one re-alignment of the generation and spectrometer, it is questionable to draw conclusions from this. The peak count rates on both days were similar which indicates that the conditions were not too different and that it may not have been worth the effort of making the plate holder fit inside the interferometer. Even in the simulations, the plate placement does not make an enormous difference, an example is to compare Figure 4.4(a) and (b). It is mainly if very precise control of the pulse properties is ever available, with low random fluctuations, that it could be worthwhile with the option to put plates in the interferometer.

# Chapter 6

# Outlooks and suggestions

## 6.1 Plates and transmission

The Brewster window and toroidal mirror shown in Figure 3.3 are positioned between the retarder plates and the spectrometer. It seems likely that these components have polarization-dependent transmittance that will affect the measured spectrum. As the plate thicknesses and angles are varied the direction of the polarization axis in the linearly polarized part of the pulse changes, which is described on page 23 for a standard gate. It seems likely that the polarization axis of the light emitted by recombining electrons should also change, thus a mirror which is mainly sensitive for the usual polarization direction will be a source of measurement error by giving too low intensity for generation which happens to occur with a different polarization direction.

The transmittance of different polarization directions through these components has not been measured yet. It should be rather simple to do when the vacuum chambers are open, or even with similar components that are not currently in use. In case the parallel or perpendicular polarization direction has notably lower transmittance than the other it will be necessary to take that into account when designing or simulating the gate, unless it is possible to change the experimental setup.

Retarder plates are typically not broadband, as the phase retardation is intrinsically related to the wavelength and refractive index. However, by combining two or more materials with different dispersion, the refractive indices curves can be matched to produce the same number of cycles retardation over a wider range of wavelengths, known as an "achromatic" retarder. The plates that were used are not achromatic and the simulation program is designed to take that into account, but only using first and second order corrections with group delay and linear chirp. The anti-reflection coating of the plates is unknown and excluded from the analysis.

Before deciding if achromatic plates would be better for the very shortest pulses, one should probably use a more broadband plate simulator that works in the frequency domain and uses the correct phase velocity for each frequency component. As the program developed during this project did not even use the chirp filter correction when the plates were ordered, it was decided to not buy the more expensive achromatic plates, which also would have had a longer delivery time, but to first test using regular plates. As the best results were obtained with short pulses it does not seem that these plates were that bad even with broadband light.

## 6.2 Improved experiments

It would be interesting to use some other experimental technique, perhaps involving autocorrelation or streaking, to try to characterize the burst produced by the previously mentioned configuration. The low spectral modulation could partly be an averaging effect, so it would good to obtain some measurement on single shot basis, or which gives a secondary signal that can then be averaged without being prone to exactly the same kind of averaging ambiguities as the MBES-spectrum.

Had more time been available it should not have been to difficult to use the interferometer also with short pulses, and try one more time to combine them with blue light. The few attempts made failed as explained on page 56, but with the interferometer more control is available. If blue can be used together with short pulses, forming a Double Optical Gate, the shortness requirement for the driving pulse could be relaxed a little and maybe allow the capillary pressure to be reduced. It seems a lower pressure in the capillary would give less fluctuations. One should also try to optimize the capillary output using the Dazzler pulse-shaper at lower pressures, which was only made at 803 mbar pressure in this project. When it was made it gave a rather dramatic improvement, whereas optimizing by turning the compressor grating which was attempted at low pressures was not as successful.

A wider capillary could probably let through more power and allow shorter acquisition times to be used with the short pulses. Currently 70%–80% of the power is split away or lost when using the capillary, and on top of that about 40% in the chirped mirrors afterwards. This very energy-inefficient compression is probably the main cause to why long acquisition times are needed. If it could be fixed then the shorter averaging times would dispel some of the doubts regarding if the continuum-like spectra are partly caused by averaging effects.

It would also be nice with better expression for the pulse after the SPM compression to use in the input field before the plates in simulations. Attempts to experimentally determine the properties of SPM-pulses using the SPIDER-analyzer were not very reliable but indicate that the pulse properties fluctuate a lot. Thus one would still not know what parameters to use for a more accurate simulation with short pulses and it would not be worth the effort yet.

Initially it was stated that one aim of the project was the ability to create one or a few bursts and ideally adjust the separation between these bursts. To obtain any temporal confinement at all, as close to a single pulse as possible, has been given priority as it seems easier to strive towards and evaluate with the measurement method used. The simulations in Figure 4.8 show that a chirped[1] pulse can give gates that recur several times within the envelope of the pulse. This could be a building block to allow two or three bursts to be selected with a few optical cycles separation, if the chirp and pulse shape are well known and does not fluctuate much. There does not seem to be much previous work made with this kind of gate, but as it may be less tolerant to experimental variations and perhaps not be immediately useful that is understandable.

## 6.3 Simulations

In section 2.3.4 several ways of determining the return probability of an electron trajectory are mentioned. Most of the previous theoretical work that was found concerned driving pulses with zero or constant ellipticity, and it was hard to find published models for recombination probability that support the conditions of this project, with a time-dependent ellipticity. The mainly used $\eta_{\text{diffusion}}$ could probably be improved, either by better estimates of initial electron wave packet size (instead of $r_{\text{th}}$) or by using a completely different model.

As explained on page 30, it is possible that the distance-based return selector with the current settings over-estimates the return flux of long trajectories. As $\eta$ is one factor in the flux definition, this may be connected to the choice of $\eta$-model. No better value for $r_{\text{th}}$ was found when requiring agreement between $\eta_{\text{diffusion}}$ and $\eta_{\text{ellipticity}}$ for fields with constant ellipticity, but further investigations of this or a switch to a more directly quantum mechanical simulation method than the semi-classical Three step model may be necessary for better simulations.

A perhaps simpler approach, worthy of examination, would be to include the force of the ion on the electron; especially at low instantaneous optical field the current approximation that neglects the electric field of the ion does not seem well-motivated. In the traditional case with only linear polarization, the electron will always pass the ion and only the return time and energy would be affected by an error, but when elliptic polarization states are used the return probability $\eta$ will be affected by transverse acceleration. I expect the use of any nonzero ionic force to make $\eta$ depend also on the speed of the returning electron and affect

[1] $|a| \gtrsim 2$ may be good, but 1.29 worked with the short pulse. The sign is not critical, but maybe negative is preferable.

what values for $r_{\mathrm{th}}$ are suitable. If the Coulomb potential of a point charge is used in the classical trajectory simulation it will be necessary to let the electron start at some finite distance from the ion, to avoid an infinite initial force. Perhaps a suitable, approximative potential should have a "soft core", *e.g.* the potential of a uniformly charged solid sphere of some radius representative of the ion.

The results from the simulation program are currently mainly evaluated as spectrograms or in diagrams where photon flux is shown on the vertical axis instead of as color in the spectrogram. The experiments on the other hand produce spectra of intensity per energy, measured after photons have interfered coherently. It is not possible to compare simulation with experiment in the same domain currently, the simulation gives a result in the time domain while the experiments give the Fourier transformed version, where the main axis is energy or frequency.

To calculate the pulse shape of the emitted high harmonics from simulations, the electronic phase picked up during the trajectory, relative to the atomic phase, should be included as well as the phase of emitted photons. Perhaps there are formulations where this is possible also in models with discrete trajectories, using Lagrangian action- or Feynman path integral-formulations [25].

If the program could produce a regular spectrum, where the complex phase is included so that photons emitted at different times may interfere "correctly", it would be easier to compare and see how much the harmonic peaks widen in simulations versus in experiments. As mentioned on page 25 the current histogram-spectrum, which does not handle interference and therefore was not used, is dominated by the low or the high harmonic orders, depending on which return selection algorithm is used. If the cause for this could be explained then perhaps a correction factor could be introduced, unless the energy-based return selector which makes the low orders dominate is sufficient. One idea would be to not use a histogram where the sum of flux is used, but to use the average flux in each energy interval. Both return selection methods produce an uneven density of points in the spectrogram, and using the average rather than the sum would reduce the bias from the density variation.

The effect of carrier-envelope phase variations [31] and averaging of spectra, need to be investigated for the case of varying ellipticity in argon, at least unless the laser system is made phase-stable. Otherwise it will be impossible to draw precise conclusions about the number of bursts being generated.

The simulations suggest that blue light in combination with 7.88 fs pulses could give an almost isolated pulse in the attosecond-regime, even without the use of retarder plates. As the plates reduced the generated intensity much when short pulses were used but the use of blue may increase it, I recommend that a second attempt is made to get overlapping blue light in experiments with short pulses.

# Bibliography


[1] B. E. A. Saleh and M. C. Teich, *Fundamentals of Photonics*, second edition ed. (John Wiley & Sons, Inc., Hoboken, New Jersey, 2007).

[2] G. Kristensson, *Elektromagnetisk vågutbredning* (Studentlitteratur, Lund, 1999).

[3] P. Johnsson, Ph.D. thesis, Faculty of Engineering LTH, Lund University, 2006.

[4] M. Lewenstein, P. Balcou, M. Ivanov, A. L'Huillier, and P. B. Corkum, *Theory of high-order harmonic generation by low-frequency laser fields*. Phys. Rev. A **49**, 2117 (1994).

[5] E. Seres, J. Seres, F. Krausz, and C. Spielmann, *Generation of Coherent Soft-X-Ray Radiation Extending Far Beyond the Titanium L Edge*. Phys. Rev. Lett. **92**, 163002 (2004).

[6] P. B. Corkum, N. H. Burnett, and M. Y. Ivanov, *Subfemtosecond pulses*. Opt. Lett. **19**, 1870 (1994).

[7] K. C. Kulander, K. J. Schafer, and J. L. Krause, in *Super-Intense Laser-Atom Physics* (Plenum Press, New York, 1993).

[8] P. B. Corkum, *Plasma perspective on strong-field multiphoton ionization*. Phys. Rev. Lett. **71**, 1994 (1993).

[9] R. López-Martens, K. Varjú, P. Johnsson, J. Mauritsson, Y. Mairesse, P. Salières, M. B. Gaarde, K. J. Schafer, A. Persson, S. Svanberg, C.-G. Wahlström, and A. L'Huillier, *Amplitude and Phase Control of Attosecond Light Pulses*. Phys. Rev. Lett. **94**, 033001 (2005).

[10] N. Ben-Tal, N. Moiseyev, and A. Beswickt, *The effect of Hamiltonian symmetry on generation of odd and even harmonics*. J. Phys. B **26**, 3017 (1993).

[11] G. Sansone, E. Benedetti, F. Calegari, C. Vozzi, L. Avaldi, R. Flammini, L. Poletto, P. Villoresi, C. Altucci, R. Velotta, S. Stagira, S. D. Silvestri, and M. Nisoli, *Isolated Single-Cycle Attosecond Pulses*. Science **314**, 443 (2006).

[12] Y. Xiang, Y. Niu, and S. Gong, *Control the high-order harmonics cutoff through the combination of chirped laser and static electric field*. Manuscript (probably not reviewed) (2008), retrieved from http://arxiv.org/abs/0809.2191, January 6, 2009.

[13] R. López-Martens, J. Mauritsson, P. Johnsson, A. L'Huillier, O. Tcherbakoff, A. Zair, E. Mevel, and E. Constant, *Time-resolved ellipticity gating of high-order harmonic emission*. Phys. Rev. A **69**, 053811 (2004).

[14] P. Tzallas, E. Skantzakis, C. Kalpouzos, E. P. Benis, G. D. Tsakiris, and D. Charalambidis, *Generation of intense continuum extreme-ultraviolet radiation by many-cycle laser fields*. Nature Phys. (2007).

[15] V. T. Carlo Altucci, Rosari Esposito and R. Velotta, *Single isolated attosecond pulse from multi-cycle laser pulse*. Optics Letters **33**, 2943 .

[16] J. Mauritsson, P. Johnsson, E. Gustafsson, A. L'Huillier, K. J. Schafer, and M. B. Gaarde, *Attosecond Pulse Trains Generated Using Two Color Laser Fields*. Phys. Rev. Lett. **97**, 013001 (2006).

[17] H. Mashiko, S. Gilbertson, C. Li, S. D. Khan, M. M. Shakya, E. Moon, and Z. Chang, *Double Optical Gating of High-Order Harmonic Generation with Carrier-Envelope Phase Stabilized Lasers*. Phys. Rev. Lett. **100**, 103906 (2008).

[18] CVI Melles Griot, Dispersion Equations, Published January 25, 2008. Retrieved from http://www.cvilaser.com/Common/PDFs/Dispersion_Equations.pdf, July 7, 2008.

[19] DayOptics Inc., Birefringent Crystals, Published January 25, 2008. Retrieved from http://www.dayoptics.com/products/material/biref_crystals/biref_crystals.htm and subpages for each material, July 7, 2008.

[20] I. J. Sola, E. Mével, L. Elouga, E. Constant, V. Strelkov, L. Poletto, P. Villoresi, E. Benedetti, J.-P. Caumes, S. Stagira, C. Vozzi, G. Sansone, and M. Nisoli, *Controlling attosecond electron dynamics by phase-stabilized polarization gating*. Nature Phys. **2**, 319 (2006).

[21] C. Z. Bisgaard and L. B. Madsen, *Tunneling ionization of atoms*. Am. J. Phys. **72**, 249 (2003).

[22] X. M. Tong and C. D. Lin, *Empirical formula for static field ionization rates of atoms and molecules by lasers in the barrier-suppression regime*. J. of Physics B **38**, 2593 (2005).

[23] X. M. Tong, Z. X. Zhao, and C. D. Lin, *Theory of molecular tunneling ionization*. Physical Review A **66**, (2002).

[24] P. B. Corkum, N. H. Burnett, and F. Brunel, *Above-Threshold Ionization in the Long-Wavelength Limit*. Phys. Rev. Lett. **62**, 1259 (1989).

[25] J. M. Dahlström, *Strong Field Approximation for High Order Harmonic Generation with $\omega/2\omega$ Laser Fields*, Vol. 381 of *Lund Reports on Atomic Physics (LRAP)*. Master's thesis, Lund University, 2007.

[26] K. S. Budil, P. Salières, A. L'Huillier, T. Ditmire, and M. D. Perry, *Influence of ellipticity on harmonic generation*. Phys. Rev. A **48**, R3437 (1993).

[27] P. Dietrich, N. H. Brunett, M. Ivanov, and P. Corkum, *High-harmonic generation and correlated two-electron multiphoton ionization with elliptically polarized light*. Phys. Rev. A **50**, 3585 (1994).

[28] Y. Zhang and Z. Xu, *Atomic radii of noble gas elements in condensed phase*. American Mineralogist **80**, 670 (1995), table 1 gives non-condensed state values too.

[29] E. Mansten, J. M. Dahlström, P. Johnsson, M. Swoboda, A. L'Huillier, and J. Mauritsson, *Spectral shaping of attosecond pulses using two-colour laser fields*. New. J. Phys. **10**, 083041 (2008).

[30] D. Walter, Ph.D. thesis, Bayerischen Julius-Maximilians-Universität, Würzburg, 2006.

[31] A. Baltuška, T. Udem, M. Uiberacker, M. Hentschel, E. Goulielmakis, C. Gohle, R. Holzwarth, V. S. Yakovlev, A. Scrinzi, T. W. Hänsch, and F. Krausz, *Attosecond control of electronic processes by intense light fields*. Nature **421**, 611 (2003).

[32] C. Iaconis and I. A. Walmsley, *Spectral phase interferometry for direct electric field reconstruction of ultrashort optical pulses*. Opt. Lett. **23**, 792 (1998).

[33] P. O'Shea, M. Kimmel, X. Gu, and R. Trebin, *Highly Simplified Device for Ultrashort-Pulse Measurement*. Opt. Lett. **26**, 932 (2001).